IUL School of Technology and Architecture
Department of Information Science and Technology

APPROACHING UNIVERSAL FREQUENCY REUSE THROUGH BASE STATION COOPERATION

FILIPE JORGE BOLAS CASAL RIBEIRO

Thesis specially presented for the fulfilment of the degree of Doctor in

Information Science and Technology

Jury:

Doctor Américo Manuel Carapeto Correia, Full Professor, ISCTE-IUL

Doctor Marco Alexandre Cravo Gomes, Assistant Professor, FCTUC

Doctor Paulo Gustavo Martins da Silva, Assistant Professor, UAlg

Doctor João Francisco Martins Lêdo Guerreiro, Assistant Professor, UAL

Doctor Pedro Joaquim Amaro Sebastião, Assistant Professor, ISCTE-IUL

Doctor Francisco António Bucho Cercas, Full Professor, ISCTE-IUL

October, 2017

Dedication

To my family and friends

Abstract

Base Station (BS) architectures are a promising cellular wireless solution to mitigate the interference issues and to avoid the high frequency reuse factors implemented in conventional systems. Combined with block transmission techniques, such as Orthogonal Frequency-Division Multiplexing (OFDM) for the downlink and Single-Carrier with Frequency-Domain Equalization (SC-FDE) for the uplink, these systems provide a significant performance improvement to the overall system. Block transmission techniques are suitable for broadband wireless communication systems, which have to deal with strongly frequency-selective fading channels and are able to provide high bit rates despite the channel adversities. In BS cooperation schemes users in adjacent cells share the same physical channel and the signals received by each BS are sent to a Central Processing Unit (CPU) that combines the different signals and performs the user detections and/or separation, which can be regarded as a Multi-User Detection (MUD) technique. The work presented in this thesis is focused on the study of uplink transmissions in BS cooperations systems, considering single carrier block transmission schemes and iterative receivers based on the Iterative-Block Decision Feedback Equalization (IB-DFE) concept, which combined with the employment of Cyclic Prefix (CP)-assisted block transmission techniques are appropriate to scenarios with strongly time-dispersive channels. Furthermore, the impact of the sampling and quantization applied to the received signals from each Mobile Terminal (MT) to the corresponding BS is studied, with the achievement of the spectral characterization of the quantization noise. This thesis also provides a conventional analytical model for the BER (Bit Error Rate) performance complemented with an approach to improve its results. Finally, this thesis addresses the contextualization of BS cooperation schemes in clustered C-RAN (Centralized-Radio Access Network)-type solutions.

Keywords: Matched filter bound, SC-FDE, Frequency-Domain Equalization, Iterative Receivers, IB-DFE, Quantization, C-RAN, Analytical performance.

Resumo

As arquitecturas *BS cooperation* são uma solução promissora de redes celulares sem fios para atenuar o problema da interferência e evitar os factores de reuso elevados, que se encontram implementados nos sistemas convencionais. Combinadas com técnicas de transmissão por blocos, como o *OFDM* para o *downlink* e o *SC-FDE* no *uplink*, estes sistemas fornecem uma melhoria significativa no desempenho geral do sistema. Técnicas de transmissão por blocos são adequadas para sistemas de comunicações de banda larga sem fios, que têm que lidar com canais que possuem um forte desvanescimento selectivo na frequência e são capazes de fornecer ligações com taxas de transmissão altas apesar das adversidades do canal. Em esquemas *BS cooperation* os terminais móveis situados em células adjacentes partilham o mesmo canal físico e os sinais recebidos em cada estação de base são enviados para uma Unidade Central de Processamento (*CPU*) que combina os diferentes sinais recebidos associados a um dado utilizador e realiza a detecção e/ou separação do mesmo, sendo esta considerada uma técnica de Detecção Multi-Utilizador (*MUD*). O trabalho apresentado nesta tese concentra o seu estudo no *uplink* de transmissões em sistemas *BS cooperation*, considerando transmissões em bloco de esquemas mono-portadoras e receptores iterativos baseados no conceito *B-DFE*, em que quando combinados com a implementação de técnicas de transmissao por blocos assistidas por prefixos cíclicos (CP) são apropriados a cenários com canais fortemente dispersivos no tempo. Além disso, é estudado o impacto do processo de amostragem e quantização aplicados aos sinais recebidos de cada terminal móvel para a estação de base, com a obtenção da caracterização espectral do ruído de quantização. Esta tese também fornece um modelo analítico convencional para a computação do desempenho da taxa de erros de *bit* (*BER*), com um método melhorado para o mesmo. Por último, esta tese visa a contextualização dos sistemas *BS cooperation* em soluções do tipo *C-RAN*.

Palavras Chave: Matched filter bound, SC-FDE, Igualação no Domínio da Frequência, Receptores Iterativos, IB-DFE, Quantização, C-RAN, Desempenho analítico.

Contents

List of Figures

List of Tables

Acronyms

3G	Third Generation.
4G	Fourth Generation.
5G	Fifth Generation.
ADC	Analog-to-Digital Converter.
BER	Bit Error Rate.
BS	Base Station.
CDMA	Code-Division Multiple Access.
C-RAN	Centralized-Radio Access Network.
CIR	Channel Impulsive Response.
CP	Cyclic Prefix.
CPU	Central Processing Unit.
CSI	Channel State Information.
DFE	Decision Feedback Equalization.
DFT	Discrete Fourier Transform.
EIRP	Equivalent Isotropic Radiated Power.

FDE	Frequency-Domain Equalization.
FDM	Frequency Division Multiplexing.
FFT	Fast Fourier Transform.
FHSS	Frequency Hopping Spread Spectrum.
FIR	Finite Impulse Response.
IA	Interference Alignment.
IB-DFE	Iterative-Block Decision Feedback Equalization.
IFFT	Inverse Fast Fourier Transform.
ISI	Inter-Symbol Interference.
LLR	LogLikelihood Ratio.
MC	Multi-Carrier.
MFB	Matched Filter Bound.
MIMO	Multiple-Input and Multiple-Output.
MMSE	Minimum Mean Square Error.
MSE	Mean Square Error.
MT	Mobile Terminal.
MUD	Multiuser Detection.
NSR	Noise-to-Signal Ratio.

OFDM	Orthogonal Frequency-Division Multiplexing.
PMEPR	Peak-to-Mean Envelope Power Ratio.
PSD	Power Spectrum Density.
QPSK	Quaternary Phase Shift Keying.
SC	Single Carrier.
SC-FDE	Single-Carrier with Frequency-Domain Equalization.
SIC	Successive Interference Cancelation.
SISO	Single-Input Single-Output System.
SNR	Signal-to-Noise Ratio.
UFR	Universal Frequency Reuse.
ZF	Zero-Forcing.

CHAPTER 1

Introduction

1.1 Motivation and Scope

The ever-increasing demand for wireless services means higher capacity requirements and efficient use of radio resources, with links capacities already close to the fundamental Shannon limit [1, 2]. Therefore, future improvements on wireless systems must be focused on the overall system's capacity. However, the design of future broadband wireless systems presents a big challenge, since these systems should be able to cope with severely time-dispersive channels and are expected to provide a wide range of services (which may involve data rates of several hundreds of Mbit/s) and to have high spectral and power efficiencies. Base Station (BS) cooperation architectures are a promising and logical approach when designing wireless environments in the near future, where the overall system's performance is improved through the cooperation of the network elements.

Unlike BS cooperation architectures, conventional cellular systems adopt different frequencies at different cells, with frequency reuse factors of 3, or even more. Clearly, the overall system spectral efficiency and capacity are conditioned by the frequency reuse factor, typically decreasing linearly with it. Since the spectrum is a scarce and expensive resource in wireless communications, it would be desirable to design systems operating in Universal Frequency Reuse (UFR) (i.e., with frequency reuse factor 1). BS cooperation schemes allow the capacity to mitigate one of the main problems in cellular communication, the interference. In conventional cellular architectures different cells are regarded as separate entities and each Mobile Terminal (MT) is assigned to a given cell (and, consequently, to one particular BS). The MT transmits its signals to the corresponding BS and when this signal is received by another BS it is regarded as interference. In BS cooperation architectures the signals between different MTs and BSs are collected and processed by a Central Processing Unit (CPU) so as to perform the user separation and/or interference

mitigation, where the set of MTs and BSs sharing a given physical channel is regarded as a large-scale Multiple-Input and Multiple-Output (MIMO) system.

Wireless channels are a challenging propagation medium due to multipath effects, where multiple copies of the original transmitted signal with different delays arrive to the receiver. That cause Inter-Symbol Interference (ISI). Moreover, the multipath propagation environment leads to the time dispersion of the transmitted data resulting in frequency-selective fading. To deal with severely frequency-selective channels effects appropriate equalization techniques at the receiver side are mandatory, in order to compensate for the signal distortion and to ensure an adequate performance, as well as to remove the effects of the ISI [1]. Nevertheless, the implementation complexity and power consumption must be kept relatively low, especially at the MTs, since low-cost and relatively long live batteries are pretended. One approach is to combine Single Carrier (SC) [1] modulations with time-domain equalization at the receiver. However, according to [3], the use of time-domain equalization can lead to several hundred multiplication operations per data symbol, proportional to the maximum Channel Impulsive Response (CIR) length. Consequently, the complexity and digital processing required to the equalization process becomes prohibitive and unattractive.

Multi-Carrier (MC) [1] modulation systems employing Frequency-Domain Equalization (FDE) [1] are an alternative to SC schemes, where the most commonly used modulation is Orthogonal Frequency-Division Multiplexing (OFDM) [4], where multiple modulated sub-carriers are transmitted in parallel and each one occupies a small portion of the available bandwidth. For channels with severe delay spread, OFDM employs frequency-domain equalization which is computationally less complex than its corresponding time domain. Because equalization is performed on a block at a time, the operations on this block involve Discrete Fourier Transform (DFT) implemented by an efficient Fast Fourier Transform (FFT) operation and a simple channel inversion operation.

More recently, the attentions have been turned to SC modulations as an alternative to MC [5]. By combining SC schemes with nonlinear equalization through receiver implementation in the frequency-domain, the employment of FFTs allow better performance when compared to the corresponding OFDM, while keeping low complexity of implementation. Besides, OFDM modulations present issues with envelope fluctuations in addition to its higher required transmission power. These reasons led to an agreement on the use of SC modulations for the uplink (i.e., the link from the MTs to the BSs) and OFDM schemes for the downlink (i.e., the link from the BSs to the MTs).

Nonlinear equalization, such as Decision Feedback Equalization (DFE) offers better performance for frequency-selective radio channels than linear equalization with just a small complexity increase. Moreover, SC modulations have shown to be effective as a block transmission techniques employing FDE techniques, where each block includes an appropriate Cyclic Prefix (CP) (i.e., with a size that deals with the maximum channel delay), proved to be suitable for high data rate transmission over highly dispersive channels [3, 6], since they require simple FFT operations and the signal processing complexity grows

logarithmically with the channel's impulsive response length. Hence, the use of the CP gives the transmitted block the appearance of being periodic. This makes the semblance of circular convolution, which is essential to the proper functioning of the FFT operation. Therefore, the combination of block based schemes with DFE, such as Iterative-Block Decision Feedback Equalization (IB-DFE) [7, 8], vahe been shown to be suitable for a proper equalization at the receiving end of the uplink communication, while maintaining the restrictions in designing and employing such systems.

Design complexity and power efficiency are very important, especially at the uplink transmission where low implementation complexity and power consumption at the mobile terminals are crucial to assure efficient battery preservation and the resort to low cost power amplifiers. Therefore, the power amplification complexity and processing charge can be concentrated in the base station, where power consumption and processing complexity are not a restriction.

This thesis focus on the uplink transmission of BS cooperation architectures in wireless cellular communication systems. SC block transmission techniques with cyclic prefix over severely frequency-selective fading radio channels are considered. Moreover, at the receiver end, the BS implements nonlinear iterative receivers based on the IB-DFE concept. These systems are usually evaluated through Bit Error Rate (BER) performance analysis obtained by means of lengthy Monte Carlo simulations, which are compared with the respective Gaussian-based theoretical models. In this work, the signals from different MTs received at a given BS are collected, sampled and quantized by an Analog-to-Digital Converter (ADC), with the objective of decreasing the overall backhaul communication requirements. The analog-to-digital conversion leads to quantization noise that can cause substantial performance degradation. Hence, this thesis presents different methods to obtain the spectral characterization of the quantization noise, allowing the possibility to design robust receivers that can cope with the corresponding degradation.

In the near future, the concept of internet of things and the explosion of connected devices will test the robustness of cellular infrastructures. When compared to current Fourth Generation (4G) systems, it is expected that Fifth Generation (5G) cellular communications can deal with the massive increase of mobile devices, the need for higher data transmissions (such as high quality streaming), spectral efficiency and high-speed mobility users [9]. This will be achieved mainly by combining massive MIMO techniques, small cells and the employment of reduced frequency reuse factors, ideally aiming at a universal frequency reuse. To overcome these issues, this thesis considers Centralized-Radio Access Network (C-RAN) architectures as one of the optimal approaches to enhance the potential of BS cooperation schemes. In C-RAN systems, cloud-based processing clustering solutions are a promising approach for designing transmission schemes for 5G networks.

1.2 Objectives

The work presented in this thesis is mainly focused on the study of the uplink transmission of BS cooperation architectures in cellular wireless communications systems. For that purpose, the main target is to design iterative receivers for the uplink of BS cooperation systems where the transmitters employ SC-FDE schemes. These receivers are based on the IB-DFE concept and are able to approach the Matched Filter Bound (MFB) in many practical scenarios. These systems were evaluated through Monte Carlo simulations, and the obtained results are compared with the corresponding theoretical analysis. Moreover, a simple method for improving the obtainment of the system performance through analytical means is presented. Jointly, this thesis focus on the design and evaluation of BS cooperations systems employing quantization schemes before the user detection and/or separation performed by the central processing unit. The quantization effects are studied with the design of robust receivers that take into account quantization effects in the backhaul links. Finally, this thesis presents the design of low-complexity receivers based on clustered techniques.

1.3 Contributions

The contributions in this dissertation are as follows:

- Development of efficient iterative FDE receivers for the uplink of BS cooperation schemes and analytical performance evaluation of those receivers (conditioned to a given channel realization). The implementation of iterative receivers based on the IB-DFE concept proves that the signals from different users can be separated and/or detected efficiently allowing the possibility of using a unique communication frequency. Moreover, it is presented a method for theoretically obtain the BER performance for the uplink of BS cooperation systems with SC-FDE modulations and IB-DFE receivers. The analytical approach for the BER performance is very accurate for the linear FDE, however, on the remaining iterations there is a non-negligible error. Therefore, in this thesis, it is also presented an approach for estimating and correcting the error of MSE-based BER estimates. The work developed in this topic was published in [10–12].

- Development of robust receivers that take into account quantization effects in the backhaul links. It is presented several approaches for accurately obtain the spectral characterization of the quantization noise, in which the quantization noise can be considered as uniform or it can be a function of each frequency component. The work developed in this topic was published in [10] (when it is only considered uniform quantization effects) and [13–15] (for the more robust receivers case).

- Development of clustered techniques to cope with large cellular scenarios, with the concept of BS cooperation being extended to a clustered 5G C-RAN-type architecture. The work developed in this topic was published in [16–18].

1.4 Thesis Organization

After this introductory chapter, chapter 2 describes the working principles of conventional cellular systems, with the introduction of concepts such as interference and frequency-reuse. Chapter 2 describes how a cellular transmission is affected by fading, with reference to the different types of fading, and provides the modeling of the cellular transmission, emphasizing it to multipath channels. Furthermore, chapter 2 introduces the multi-cell cooperation concept and the compares it with conventional systems. Several approaches for implementing multi-cell cooperation are described, including relay-based architectures, interference coordination (combined with beamforming) and cooperative MIMO techniques.

Chapter 3 characterizes the basic principles of SC and MC modulations, as well as in which terms both schemes are related. OFDM and SC-FDE modulations with linear and nonlinear equalizer receivers, such as IB-DFE, are described, including transmitter and receiver schemes and the signal's representation in time and frequency domain.

Chapter 4 discusses the architecture of BS cooperations schemes with a system overview and an analysis of the computation of all variables in the system. In chapter 4 an analytical approach to the calculation of the BER performance is presented and a comparison to the experimental approach is provided. Moreover, chapter 4 provides an improved method for achieving the BER performance, which is previously described.

Chapter 5 extends the BS cooperation concept to the use of the quantization process on the transmitted signals, and an evaluation of the quantization requirements in BS cooperations systems is performed. Furthermore, chapter 5 proposes the implementation of robust receivers that can take into account the spectral characterization of the quantization noise.

In chapter 6 the connection of BS cooperation schemes with 5G implementation scenarios is performed, such as C-RAN-type systems. This is done by designing low-complexity receivers based on clustered techniques.

Chapter 7 concludes the thesis, with a fair clue on what the continuation work approach must be. As the thesis progresses, several performance results are illustrated to evaluate the corresponding work analysis.

1.5 Notation Aspects

Throughout this thesis, the following notation is adopted: bold upper case letters denote matrices or vectors; $\mathbf{I}_N$ denote the $N \times N$ identity matrix; $\mathbf{x}^*$, $\mathbf{x}^T$ and $\mathbf{x}^H$ denote complex conjugate, transpose and hermitian (complex conjugate transpose) of $\mathbf{x}$, respectively. In general, lower case letters denote time-domain variables and upper case letters denote

frequency-domain letters; $\tilde{x}$, $\hat{x}$ and $\bar{x}$ denote sample estimate, "hard decision"estimate and "soft decision"estimate of x, respectively. The expectation of x is denoted by $\mathbb{E}[x]$.

CHAPTER 2

Digital Transmission in Cellular Systems

This chapter starts with an historical contextualization that aims to ponder the evolution of wireless mobile communications systems, namely the radio access technologies. Chapter 2 also describes the basic components of a conventional cellular system and how the communication between the different network elements is performed. Moreover, the concept of conventional cellular architectures introduces the notion of inherent aspects and techniques, such as interference, electromagnetic spectrum usage and frequency-reuse. This chapter also describes one of the most significant phenomenon that affects a transmission of a given wireless signal: fading. Fading can be classified as large and small scale fading, and depending on the type of fading the communication links are affected differently. Since the wireless channel considered in this thesis is strongly affected by multipath propagations, chapter 2 also models the multipath channel and the transmitted and received signals that are subject to it. Lastly, in this chapter, the concept of multi-cell cooperation is introduced, with the possibility of different approaches being considered.

Chapter 2 is organized as follows: An historical contextualization on the mobile communication systems is given in section 2.1 and section 2.2 provides an overview of the functioning of a conventional cellular architecture. In section 2.3 the phenomenon of fading is explained and the modeling of the multipath channel is provided. Section 2.5 describes the concept of multi-cell cooperation systems.

2.1 Historical Contextualization

From the initial deployment of Third Generation (3G) networks in 2001 until present days many improvements have been implemented in wireless cellular networks. These improvements are about to set the new standards through the Long Term Evolution (LTE)-Advanced as the reference of 4G networks. 3G systems, which use Wideband

Code-Division Multiple Access (W-CDMA) as a radio access technology, are already overwhelmed by the exponential growth of the need for higher bandwidth applications. Pre-4G systems, such as Evolved High Speed Packet Access (HSPA+), can provide higher data rates, lower latencies and significant battery life improvements when compared to the initially implemented 3G networks. However, these improvements are still far from the required technical demand. Commonly branded as a 4G architecture, LTE is based on the Global System for Mobile communications (GSM)/ Enhanced Data rates for GSM Evolution (EDGE) and Universal Mobile Telecommunications System (UMTS)/HSPA family of standards. It was first proposed in 2004 and even though it does not meet the technical criteria of a 4G service, its implementation marked the bridge to the state of the art LTE-Advanced standard. With the arrival of LTE comes the implementation of a new air interface designated Evolved Universal Terrestrial Radio Access (E-UTRA), that replaces the previous ones and it is not compatible with W-CDMA. E-UTRA combines the use of Orthogonal Frequency-Division Multiplexing (OFDM) as a multi-carrier (MC) modulation for the downlink, and Single-Carrier with Frequency-Domain Equalization (SC-FDE) as a single-carrier (SC) modulation for the uplink. Since broadband wireless channels present frequency-selective characteristics, the new air interface allows the system to exploit its properties without complex equalization methods. OFDM and SC-FDE systems do not present significant differences in performance and complexity. Nevertheless, the high Peak-to-Mean Envelope Power Ratio (PMEPR) and the strong envelope fluctuations are the major problems concerning OFDM modulations. Thus, these schemes are revealed to be vulnerable to transmitter nonlinearities, especially power amplification ones. Consequently, the employment of single-carrier schemes is desirable, particularly in the uplink transmission, allowing the user terminals to be cheaper and to have higher-power amplifiers.

2.2 Conventional Cellular Systems

Cellular systems are mobile networks where the communication between network elements is made through the propagation of electromagnetic radio waves. In conventional architectures, the network is distributed over separated land zones, designated as cells, in which each one is served by a BS (Base Station) that can communicate with several MTs (Mobile Terminals) transmitting in the area covered by that BS. Fig. 2.1 depicts a conventional cellular system, with the different elements and the transmission links that constitute the communication architecture. In a typical cellular system the communication between each MT and its corresponding BS in adjacent cells has to be performed in different frequencies (indicated as f_1 and f_2) to avoid mutual interference, caused by users that share the same propagation medium, also known as co-channel interference [19, 20]. Two of the main challenges and consensus in designing mobile communication systems are interference and fading. Generally, fading constrains the point-to-point wireless transmissions and interference affects the usage of the spectrum, restraining the overall spectral efficiency. Since

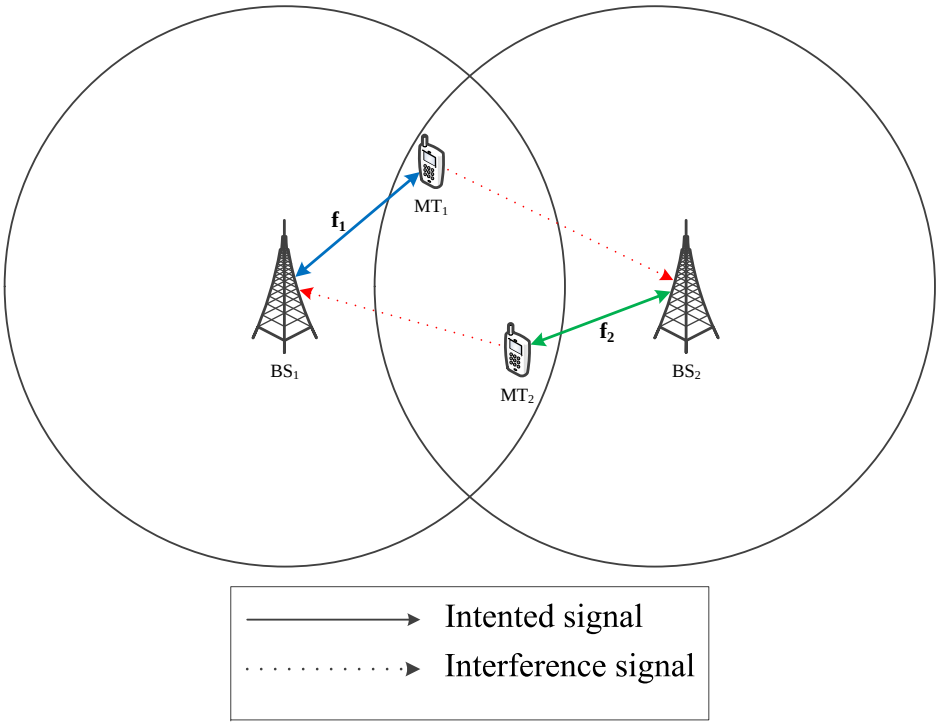

Figure 2.1: Conventional cellular system.

spectrum is a scarce and expensive resource in wireless communications, the different cells adopt distinct frequencies, and depending on the distance between cells, the same frequency can be reused. Fig. 2.2 exemplifies the concept of frequency-reuse, where the reuse distance, denoted as D, is the distance from the centers of cells employing the same frequency. Moreover, $D = R\sqrt{3N}$, where R and N are the cell's radius and the cluster size, respectively. Fig. 2.2 illustrate the most common frequency-reuse distribution in GSM networks, with a frequency-reuse pattern $K = 7$ and a frequency-reuse factor of $1/7$.

2.3 Fading

Fading corresponds to a occurrence affecting the transmission of signals propagating in a wireless communication channel. These occurrences include phenomenas like delay, attenuation and phase shifting. Mainly, the causes of affecting negatively the wireless transmission are the conditions of the environment, such as objects obstructing the path between transmitter and receiver and multipath propagation. Fig. 2.3 illustrates the distinct causes of fading in a wireless propagation environment, in which the scenario corresponds to a typical urban area, where the majority of mobile communications occur. In wireless communications, the transmitted information has more than one path that can be taken until it reaches the receiver. Due to the multipath environment, the received signal can be considered as a sum of distinct copies of the original signal. Moreover, multipath can be also caused by natural formations or man-made constructions, and the

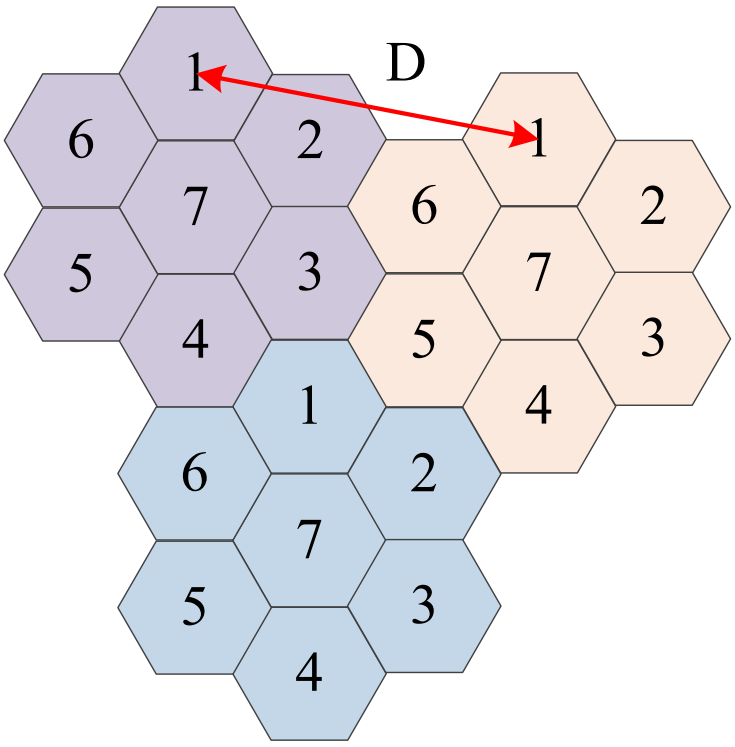

Figure 2.2: Frequency-reuse concept (with frequency-reuse factor of 1/7).

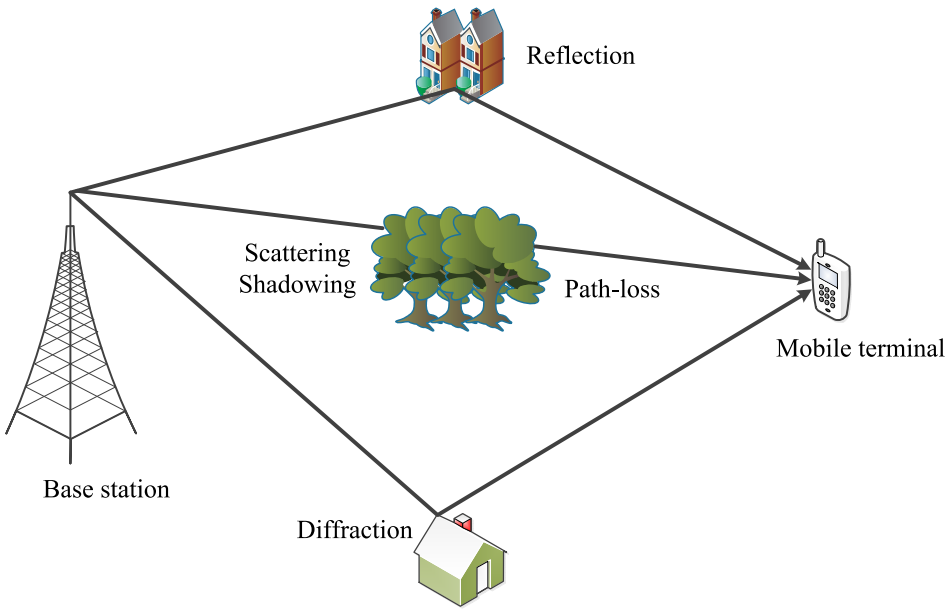

Figure 2.3: Causes of fading in a wireless propagation environment.

mobility of any element in the communication process. This can also cause fading, making the propagation time vary.

Fading can be classified as large-scale (slow) and small-scale (fast). The type of fading depends on the propagation effects and if it is considerably destructive, then the communication can experience deep fading effects.

2.3.1 Large Scale Fading

Large-scale, or slow fading, is defined by minor fluctuations in phase and magnitude of the propagation channel which includes shadowing (caused by large obstructions that attenuate the main signal path) and path-loss. It is basically the result of signal attenuation caused by large distances in the communication path and it occurs when the symbol that is being transmitted is smaller than the channel's coherence time. The coherence time corresponds to the time duration over which the CIR is invariant. Because of this, the amplitude and phase fluctuations caused by the channel can be seen as constant over that period. This section describes the shadowing and path-loss occurrences that lead to large-scale fading.

2.3.1.1 Path-Loss

Path-loss is related to large-scale fading, in which the transmitted signal is affected by the propagating distance between transmitter and receiver, terrain factors, type of environment (urban or rural), location and position of antennas and frequency of the signal. The path-loss channel model can be defined, in linear measures, by the expression

$$P_L = \frac{P_{Tx}}{P_{Rx}}, \tag{2.1}$$

where P_{Tx} and P_{Rx} denote the transmitted and received power in Watts, respectively. In dB, (2.1) can be expressed as

$$P_L = 10\log_{10}\left(\frac{P_{Tx}}{P_{Rx}}\right)(\text{dB}). \tag{2.2}$$

The simplest fading model regarding path-loss is the free-space, where there is no reflection or attenuation between transmitter and receiver. With the increase of the transmission distance, the power radiated by the transmitter dissipates as the signal propagates. The free-space model states that between transmitter and receiver there is a line of sight free from obstructions, and it attempts to predict the received signal strength assuming that power decays as a function of the propagation channel distance. In [21], Friis states the free-space path-loss equation as

$$P_{Rx} = P_{Tx}G_{Tx}G_{Rx}\left(\frac{\lambda}{4\pi d}\right)^2, \tag{2.3}$$

with G_{Tx} and G_{Rx} indicating the antenna gain from the transmitter and receiver, respectively. Moreover, λ is the wavelength in meters and d the distance between transmitter and receiver in meters. The attenuation of the signal due to path-loss (in dB) corresponds

to the difference between the Equivalent Isotropic Radiated Power (EIRP) and the received power, consisting in a measurement for the maximum radiated power available from a transmitter in the direction of maximum antenna gain, as compared to an isotropic radiator. The model for free space path-loss can be expressed as

$$P_L = 10\log_{10}\frac{P_{Tx}}{P_{Rx}} = -10\log_{10}\left[\frac{G_{Tx}G_{Rx}\lambda^2}{(4\pi)^2 d^2}\right]. \tag{2.4}$$

In real cases, where the transmitted signal can be reflected, the power of the signal decay faster as a function of the distance. Then, the average received power, for a distance d between the transmitter and receiver antennas, and with resort to path-loss factor n, which is the rate at which the path-loss increases with distance, is given by [21] as

$$\bar{P_L} = \bar{P_L}(d_0) + 10n\log_{10}\left(\frac{d}{d_0}\right)(\text{dB}), \tag{2.5}$$

where $\bar{P_L}(d_0)$ is the mean path-loss in dB at distance d_0.

2.3.1.2 Shadowing

Shadowing causes fading due to the presence, between transmitting and receiving antennas, of mountains, hills, man-made buildings and other objects. So, the signal is affected and damaged because of diffraction, scattering and absorption.

The parameter d in equation (2.5) indicates an average, however, in shadowing the received power in two different locations at the same distance d may have very different values of path-loss. Therefore, the $\bar{P_L}$ in (2.5) is not indicated. In [22] the path-loss value P_L is described, at a certain distance d, as a random variable characterized by a log-normal distribution about the mean value of P_L. Hence, P_L can be written in terms of $\bar{P_L}$ and a random variable φ [21], as

$$\bar{P_L} = \bar{P_L}(d) + \varphi = \bar{P_L}(d_0) + 10n\log_{10}\left(\frac{d}{d_0}\right) + \varphi(\text{dB}), \tag{2.6}$$

where $\varphi \sim \mathcal{CN}(0,\sigma)$, with zero mean and standard deviation σ. The definition of the path-loss caused by slow fading for a certain distance d, requires the reference d_0 and the random variable φ with its standard deviation σ.

2.3.2 Small Scale Fading

Small-scale (or fast fading) is an occurrence affecting the transmitted signals where fast changes occur in the signal's amplitude and phase shifts over very short variations in time or in the area between the receiver and the transmitter. This type of fading happens when signals are subject to refractions, reflections, diffractions and scattering of the radio waves. There are two main sources [21] of small-scale fading, being multipath propagation and Doppler spread.

2.3.2.1 Multipath

In wired environments transmitted signals only have a single path to propagate between the transmitter and the receiver, whereas in wireless systems there can be several paths to be considered. Multipath propagation scenarios are usually related to urban environments, where the radio channel is influenced by densely positioned structures, such as buildings, cars and others. Moreover, in urban-type environments the line-of-sight component does not usually exists, hence, the communication is only possible due to the influence of propagation mechanisms (diffraction, scattering and reflection), as illustrated in Fig. 2.4. Reflections are the result of the traveling signal encountering a surface that is larger than

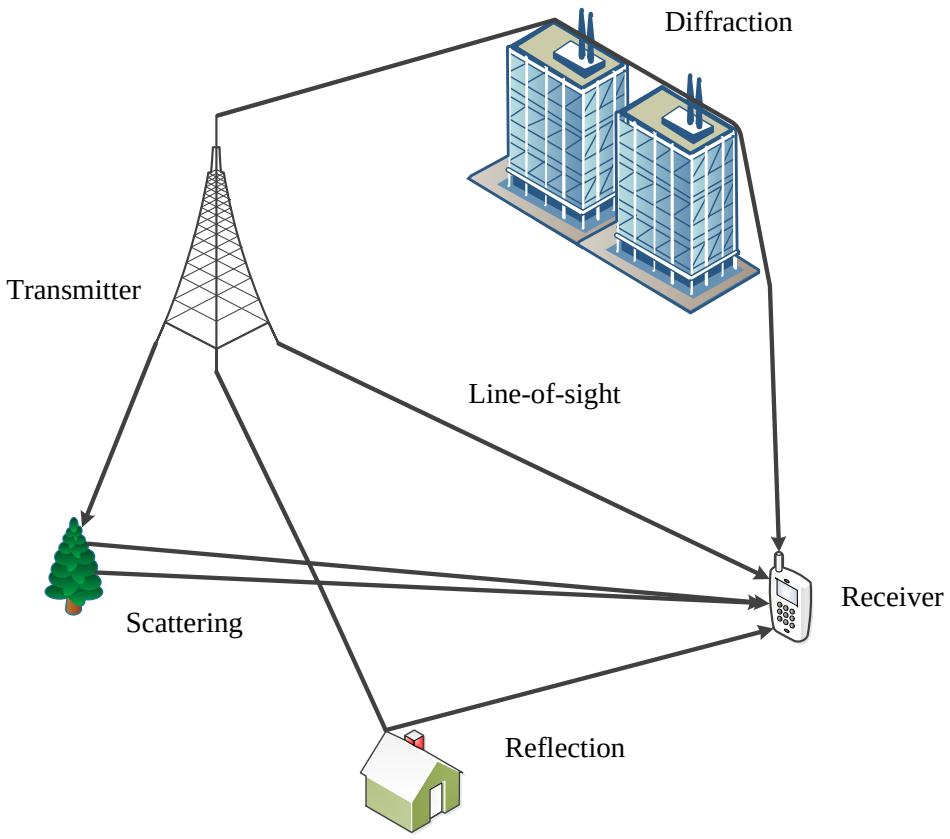

Figure 2.4: Causes of multipath fading.

the wavelength of the propagation wave. One example can be a hill or a building wall. On the other hand, diffraction is the result of an obstruction by an object with larger dimensions than the wavelength of the propagation wave being diffracted on the edges of such objects. These include houses, cars and mountains. In this case the signal travels around the object allowing it to be received. Finally, the fading caused by scattering occurs when the transmitted signal hits an object with size of the signal's wavelength or less.

Due to the fact that in multipath propagation scenarios the incoming multipath components arrive at the receiving antenna by different propagation paths, the difference between the distinct propagation signals leads to fading. Furthermore, the several copies that arrive

to the receiver have different delays and distinct phase factors, adding up constructive or destructive influence. If the multipath fading channel has very long path lengths, then the different signals may be received after one symbol duration, causing ISI, which distorts the signal and induces degradation on the transmission's performance.

In the multipath fading channel, the main components can be described as:

- T_S: the duration of a transmitted symbol;
- T_M: the delay spread, and it defines the difference in time arrivals from the first and the last multipath contributions.

Fig. 2.5 shows the CIR $h(t)$ regarding a multipath propagation channel. The existence of

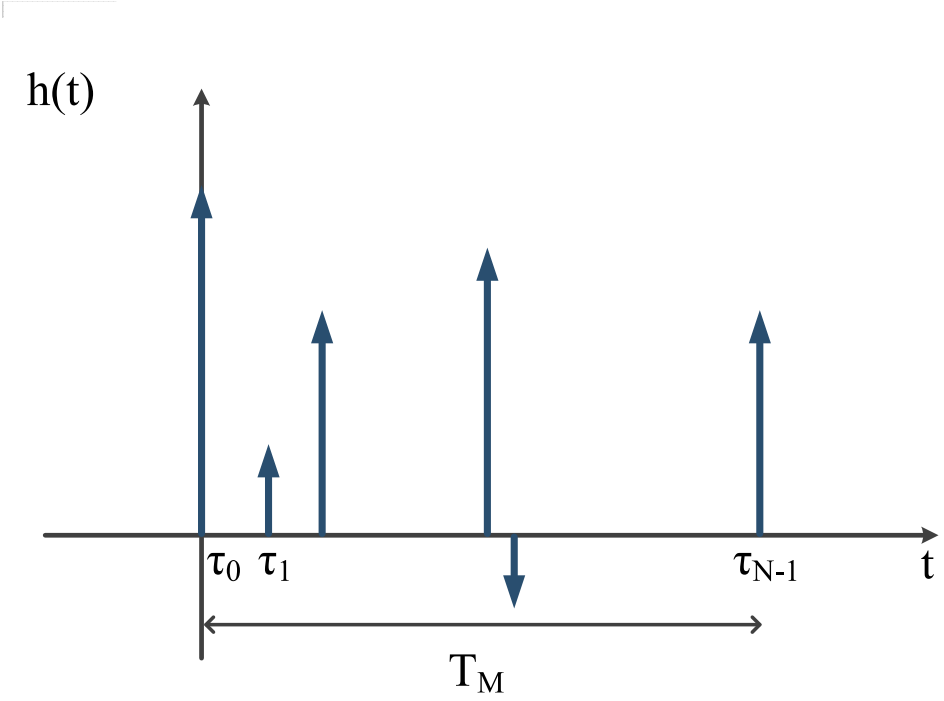

Figure 2.5: Multipath propagation channel impulse response $h(t)$.

multiple paths leads to several copies of the transmitted symbol and thus time spreading of the received symbol. Depending on the relation between symbol's time T_S and delay spread time T_M, the fading caused by multipath propagation can be classified as:

- Flat Fading: The time delay spread T_M is smaller than the symbol's period T_S ($T_S > T_M$). In this case the channel exhibits flat fading and the ISI can be neglected;
- Frequency-Selective Fading: The symbol's period T_S is smaller than the time delay spread T_M ($T_M > T_S$). In this case the channel introduces ISI that must be mitigated.

When flat or frequency-selective fading are considered one must define the coherence bandwidth B_C. The coherence bandwidth is a frequency-domain statistical measure that indicates if the channel characteristics are frequency-selective or flat as:

- Flat fading: If the signal bandwidth B_S is greater than the coherence bandwidth B_C, then the spectral characterization of the transmitted signal is preserved, since the channel bandwidth affects all spectral components with approximately equal gain and phase ($B_S < B_C$);
- Frequency-selective fading: If the signal's bandwidth is greater than the channel coherence bandwidth ($B_S > B_C$), with the different frequency components of the signal experiencing different fading. In this case the distinct multipath contributions that are combined at the receiver arrive outside the symbol duration and causes ISI.

In this thesis a special attention is given to multipath propagation, since it corresponds to the type of fading that is more suitable for the adopted cellular scenario.

2.3.2.2 Doppler Spread

When relative motion between the transmitter and the receiver is considered, the multipath propagation channel becomes variant in time. This way, the channel can be quantified using coherence time T_C and Doppler spread B_D [21] as:

- Coherence time (T_C): Corresponds to the time duration over which the channel impulse response is time invariant. Signals that are separated in time by the coherence time have independent fading;
- Doppler spread (B_D): When a pure sinusoidal tone of frequency f_C is transmitted in a multipath environment, the received signal spectrum, called Doppler spectrum, will have components in the range $f_C - f_D$ to $f_C + f_D$, due to Doppler shift, f_D. The Doppler spread is the width of the Doppler spectrum.

The small-scale fading caused by Doppler spread can be described as slow or fast fading as:

- Slow fading: Slow fading happens when the channel's coherence time T_C is greater than the symbol time duration $T_S (T_C > T_S)$. The channel exhibits slow fading if the CIR changes at a rate much slower than the transmitted symbol time. In the frequency domain, the signal bandwidth is greater then the Doppler spread ($B_S > B_D$), and in that case the effects of Doppler spread are negligible;
- Fast fading: Fast fading occurs when the time duration T_C, in which the channel has a correlated behavior, is shorter than the symbol time duration $T_S (T_C < T_S)$. Therefore, the CIR changes rapidly within the symbol time duration. In the frequency-domain, the signal bandwidth is smaller than the Doppler spread ($B_S < B_D$). The

signal distortion due to fast fading increases with increasing Doppler spread relative to the bandwidth of the transmitted signal. In practice, fast fading only occurs for very low data rates.

2.4 Modeling the Multipath Transmission Scheme

This section provides the modeling of a wireless multipath propagation model, depicted in Fig. 2.6. Since this thesis approaches the uplink transmission in a multipath environment,

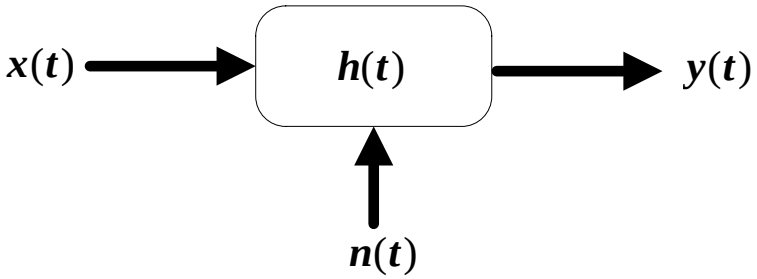

Figure 2.6: Transmission model.

this is the type of channel that requires a detailed attention.

In multipath environment the received signal can be seen as a sum of distinct copies of the transmitted signal with different delays and amplitudes associated to the different paths between transmit and receiving antennas (illustrated in Fig. 2.7). Consequently, the

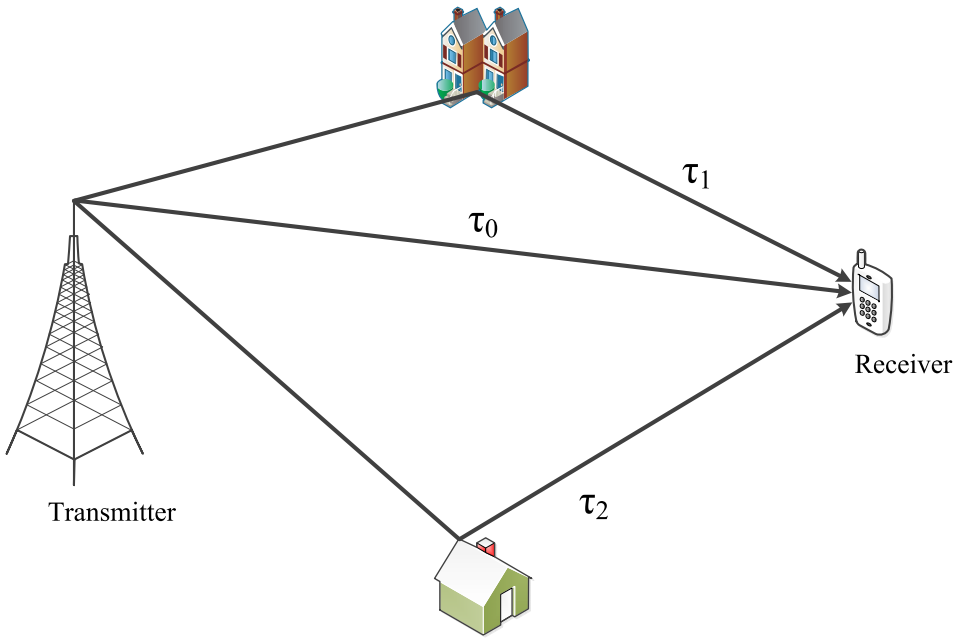

Figure 2.7: Transmission over a multipath channel environment.

received signals can experience ISI and fading, caused by the difference in gains and delays which can have a destructively influence. This thesis considers frequency-selective channels,

which can be characterized by a linear, time-invariant filter with channel impulsive response CIR expressed by

$$h(t) = \sum_{l=0}^{L-1} \alpha_l \delta\left(t - \tau_l\right), \tag{2.7}$$

where α_l and τ_l denotes the complex amplitude and the delay associated to the l^{th} element of the total L multipath component, respectively. Moreover, the different impulse function $\delta\left(t - \tau_l\right)$ simply corresponds to the impulse where the l^{th} multipath component appears, associated to the respective delay. The channel $h(t)$ is therefore modeled as a linear Finite Impulse Response (FIR) filter, where its frequency response corresponds to

$$H(f) = \mathcal{F}\{h(t)\} = \sum_{l=0}^{L-1} \alpha_l \exp\left(-j2\pi f \tau_l\right), \tag{2.8}$$

which indicates frequency selectivity. An example of a channel frequency response with frequency-selective fading is shown in 2.8. As with frequency-selective fading channels, the

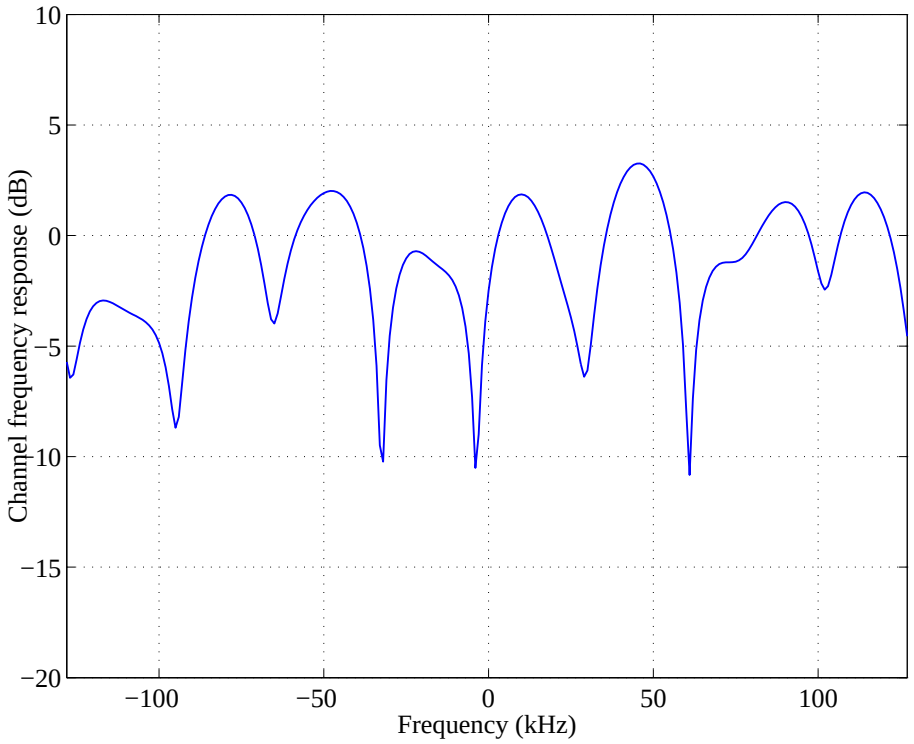

Figure 2.8: Transmission over a multipath channel environment.

bandwidth of the transmitted symbol is greater than the channel coherence bandwidth. Furthermore, coherence bandwidth and the delay spread are inversely related, in which the larger the delay spread, the less the coherence bandwidth.

The transmitted signal corresponds to baseband, or low-pass signal, in the band $[-B, B]$ Hz and zero elsewhere, where B indicates the bandwidth bound. In wireless systems signals are modulated, where the baseband information is upconverted from the carrier component

into higher frequencies. This is performed using a sinusoidal carrier of frequency f_c before transmission, centering the original signal around an appropriate frequency. After this conversion, the transmitted signal is designated as passband, with spectrum between $f_c - B < |f| < f_c + B$, with $f_c >> B$.

One can define a passband signal $s(t)$, transmitted at the carrier frequency, and expressed as

$$s(t) = \mathrm{Re}\{s_b(t)e^{j2\pi f_c t}\}, \tag{2.9}$$

in which $s_b(t)$ is the complex baseband characterization of $s(t)$. Moreover, regarding $s_b(t)$, its real and imaginary parts carry information about the signal's in-phase and quadrature components (the components that are modulating the terms $cos(2\pi f_c t)$ and $sin(2\pi f_c t)$, respectively.

Considering the received signal $y(t)$, this can be considered as a sum of all the contributions that result from the existence of $L-1$ paths. Hence, $y(t)$ can be expressed by

$$y(t) = \mathrm{Re}\{\sum_{l=0}^{L-1} \alpha_l s_b(t-\tau_l)e^{j2\pi f_c(t-\tau_l)}\}, \tag{2.10}$$

and since $e^{j2\pi f_c t}$ is common to all terms, 2.10 can be written as

$$y(t) = \mathrm{Re}\{\left(\sum_{l=0}^{L-1} \alpha_l s_b(t-\tau_l)e^{-j2\pi\tau_l}\right) e^{j2\pi f_c t}\}. \tag{2.11}$$

In 2.11, the inner brackets term consists in a complex baseband received signal, hence it can be expressed as

$$y(t) = \mathrm{Re}\{y_b(t)e^{j2\pi f_c t}\}, \tag{2.12}$$

where its equivalent complex baseband representation is

$$y_b(t) = \sum_{l=0}^{L-1} \alpha_l s_b(t-\tau_l)e^{-j2\pi\tau_l} \tag{2.13}$$

and the equivalent low-pass representation of the channel is

$$y_b(t) = \sum_{l=0}^{L-1} \alpha_l e^{-j2\pi\tau_l}\delta(t-\tau_l). \tag{2.14}$$

The complex baseband received signal at the receiver $h_b(t)$ consists in the sum of L received multipath components, each one having a corresponding attenuation α_l and delay τ_l. The baseband representation of distinct assignments of τ_l is approximately $s_b(t)$, hence 2.11 can be simplified through the narrowband assumption, due to the fact that all values of $s_b(t-\tau_l)$ are approximately equal to $s_b(t)$, as

$$y_b(t) = s_b(t)\sum_{l=0}^{L-1} \alpha_l e^{-j2\pi\tau_l}, \tag{2.15}$$

in which the analytical model of the wireless transmission system can be defined as

$$y_b(t) = h_b(t)s_b(t). \tag{2.16}$$

Regarding the lowpass representation of the channel $h_b(t)$, with τ indicating a certain delay, it is possible to notice the so called phase factor, given by $e^{-j2\pi\tau_l}$. As previously mentioned, the received signal can be regarded as a sum of copies of the original signal where each multipath component induces a different delay. Therefore, the delay related to the l^{th} multipath component $e^{-j2\pi\tau_l}$ is out of phase regarding the delay τ_l. As a result of the several delays, when the multipath components are added, depending on the delays and attenuations, the result can be constructive or destructive interference.

It is possible to statistically analyze the channel's equivalent lowpass representation, that can assume the existence of a large number of independent Gaussian R.V.'s multipath taps, allowing to model the channel impulse response as a Gaussian process as

$$y_b(t) = h_b(\tau)s_b(t) = s_b(t)\sum_{l=0}^{L-1}\alpha_l e^{-j2\pi f_c\tau_l} = s_b(t)\sum_{l=0}^{L-1}\alpha_l cos(2\pi f_c\tau_l) - \alpha_l sin(2\pi f_c\tau_l), \tag{2.17}$$

where the real and imaginary parts of this complex-valued quantity are given by

$$X = \sum_{l=0}^{L-1}\alpha_l cos(2\pi f_c\tau_l) \tag{2.18}$$

and

$$Y = \sum_{l=0}^{L-1} -\alpha_l sin(2\pi f_c\tau_l). \tag{2.19}$$

X and Y can be regarded as random numbers depending on the random quantities given by α_l and τ_l. Analyzing the wireless channel with resort to statistical propagation models, X and Y are the sum of a large number of random components, therefore, assumed as Gaussian random variables. Then, $h_b(\tau)$ can be expressed as

$$h_b(\tau) = X + jY. \tag{2.20}$$

Considering that X and Y are Normal-distributed, then

$$X \sim \mathcal{N}(0, 1/2) \tag{2.21}$$

and

$$Y \sim \mathcal{N}(0, 1/2), \tag{2.22}$$

where X and Y are described as Gaussian random variables of zero mean and variance $1/2$. Assuming that the process has zero mean, then the envelope of the received signal can be statistically described by a Rayleigh probability distribution, with the phase uniformly distributed in $(0, 2\pi)$. Hence, assuming that X and Y are independent R.Vs., then the joint distribution of XY can be expressed by the product of the individual distributions, given by

$$f_X(x) = \frac{1}{\sqrt{2\pi\sigma}}e^{-\frac{(x-\mu)^2}{2\sigma^2}} = \frac{1}{\sqrt{\pi}}e^{-x^2} \tag{2.23}$$

and

$$f_Y(y) = \frac{1}{\sqrt{2\pi\sigma}} e^{-\frac{(y-\mu)^2}{2\sigma^2}} = \frac{1}{\sqrt{\pi}} e^{-y^2}, \tag{2.24}$$

so their joint distribution is given by

$$f_{X,Y}(x,y) = f_X(x)\dot{f}_Y(y) = \frac{1}{\sqrt{\pi}} e^{-\left(x^2+y^2\right)}, \tag{2.25}$$

which allows to obtain the joint distribution of the components of $h_b(\tau)$.

The Rayleigh distribution model is suitable for this multipath environments since there is not a dominant transmission path between the transmitter and receiver antennas and all the multipath components arrive at the receiver with identical signal amplitude. If the channel has a dominant multipath signal component, then the fading can be described by a Rician distribution [23].

2.5 Multi-Cell Cooperation Concept

Multi-cell cooperation systems can significantly enhance the overall network performance by shifting its paradigm of exploiting the inter-cell interference. This can be achieved by allowing the data from users to be together processed by several interfering base stations, much like a big virtual MIMO array. In conventional architectures, the methodology to cope with interference is to reuse communication frequencies. As mentioned in section 2.2, the frequency reuse factor is chosen so that the level of co-channel interference is low. Moreover, the interference is treated as noise at the receiving BS and is dealt with by improving the point-to-point transmission between the MT and the BS mainly through coding techniques [24].

Since frequency-reuse techniques lower the spectral efficiency, it is desirable to operate in full frequency-reuse factors, i.e., to consider a single frequency. This can be achieved through the employment of Code-Division Multiple Access (CDMA) or Frequency Hopping Spread Spectrum (FHSS). Despite of single frequency communications, CDMA and FHSS can have critical interference problems at the cell's edge, significantly affecting the system fairness. Soft-handoff techniques can allow that a MT communicates to several BSs, with diversity being used to select the optimal link, increasing the capacity and coverage. Jointly with power control, it allows for a universal frequency-reuse. However, the capacity in CDMA is restricted by inter-cell interference, and the capacity of a cell in an interfering system is much lower than that of a single isolated cell [25]. Hence, there is the need for different approaches when the aim is to communicate in universal frequency-reuse environments, namely the cooperation of the network elements. Three types of cooperation approaches can be considered in wireless networks, being Relay-based cooperation systems, schemes with interference coordination and MIMO techniques over interfering links.

2.5.1 Relays

In relay-based cooperative systems, a third party (BS or MT) is used to deal with the interference propagation links, as exemplified in Fig. 2.9. Even though cooperation

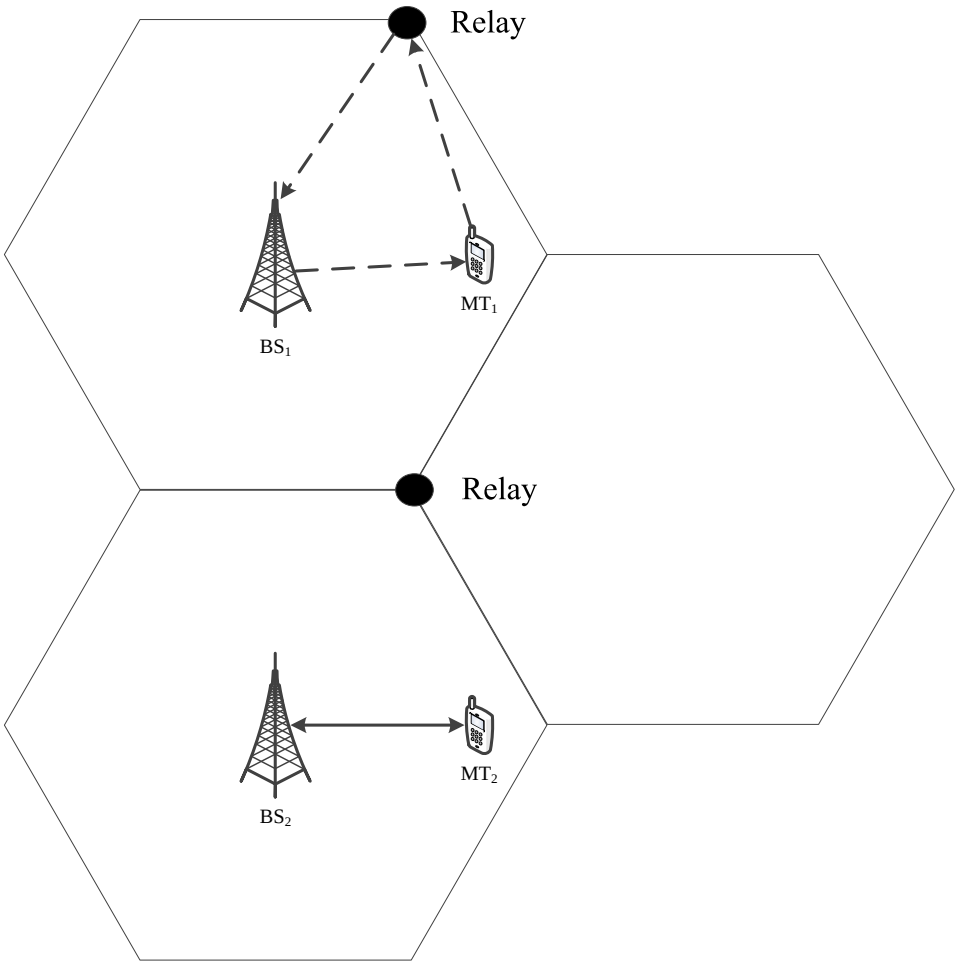

Figure 2.9: Relay cooperative communication (relay communication between MT_1 and BS_1 and direct communication between MT_2 and BS_2).

systems employing relay techniques can mitigate fading effects in point-to-(multi)point communications, the severe inter-cell interference, such as edge of cells, requires specific approaches to enhance performance, such as MIMO techniques [26].

2.5.2 Interference Coordination

Interference coordination techniques (Fig. 2.10) allow for a significant improvement of the cellular system performance with the sharing of the Channel State Information (CSI) of the direct and interfering links. Therefore, the BSs can coordinate strategies regarding the signalling procedures. Among these strategies are beamforming, power distribution allocation and scheduling. The exchange of the CSI allows the transmission strategies in different cells to adjust to the channel condition [27]. Furthermore, in overlapping

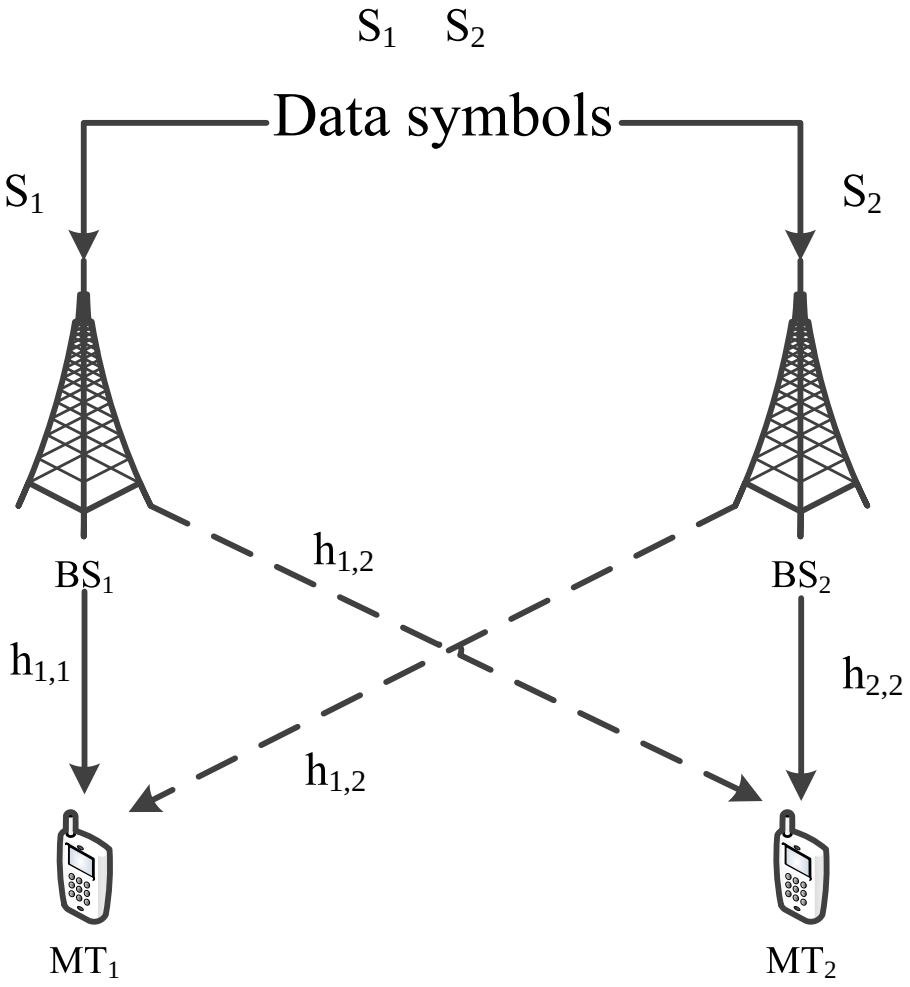

Figure 2.10: Interference coordination technique (example for the downlink).

cells networks the overall system performance can be improved by combining the different methodologies, such as coordinated power control and scheduling on the different BSs. Regarding beamforming, this technique can further improve the network performance if one considers that the BSs have multiple antennas, adding spatial resources that allow the employment of coordinated beamforming approaches [28, 29].

2.5.3 Cooperative MIMO Techniques

Fig. 2.11 illustrates an example of the multi-cell MIMO cooperation approach. As with cooperative strategies based on interference coordination and/or beamforming, the sharing of the network information, such as the CSI, can improve the overall system performance. However, when the base stations are connected via high-capacity delay-free links (for example the backhaul links), it is possible to improve even more the network performance, since not only the CSI but also the complete information of their respective MTs can be shared. Hence, if the amount of information being shared rises, then a more powerful type of cooperation can be achieved. Considering this case, the conventional approach

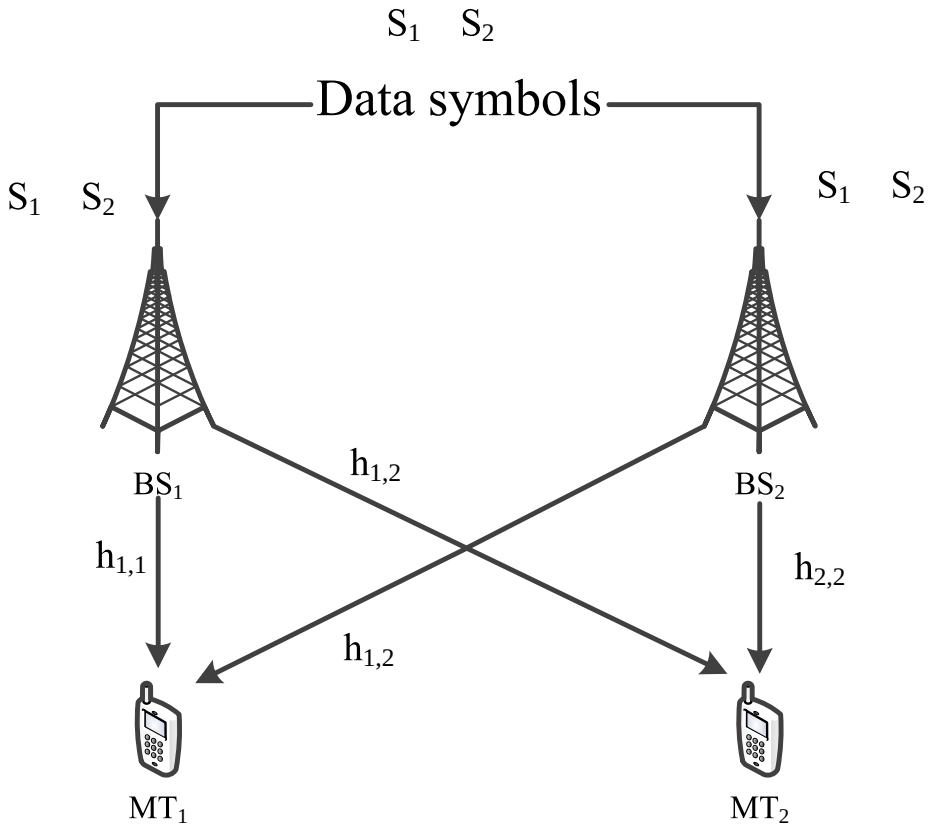

Figure 2.11: Multi-cell MIMO cooperation (example for the downlink). The BSs share both the CSI and the user data.

of one BS dedicated to connect to a single MT shifts to a scenario where all BSs can be effectively linked to each user. Cooperative MIMO systems have this particularity, in which the combined signals that each BS receives can be framed into a multiple user data stream. BS cooperation systems, as a cooperative MIMO architecture, take into account all transmission links, where interfering and "useful"links are exploited carry useful data. However, for cooperative MIMO techniques to be successful, the combined signals must be subject to an appropriate precoding/decoding process. On the contrary, when interference coordination techniques are applied, the interference is only mitigated but not exploited. The concept of multiple antennas can be considered with beamforming approaches, but only if the BSs are equipped properly. If so, there must be a compromise between eliminating the inter-cell interference and maximizing the received signal from and/or to a given MT within the cell.

CHAPTER 3

Block Transmission Techniques

This chapter describes the fundamental principles of block transmission techniques, such as Single Carrier (SC) and Multi-Carrier (MC) modulations, which includes several aspects of transmission and reception processes of each modulation. Furthermore, an analytical overview of both systems is described, as well as a comparison between them. This thesis is centered in SC modulations and chapter 3 relates the non-equalization aspects with such modulations. Furthermore, this chapter provides the derivation of the parameters that are part of the equalization and information detection processes, including proper explanations and several performance results.

Chapter 3 is organized as follows: SC and MC modulations are analyzed in sections 3.1 and 3.2, respectively. Section 3.3 describes the Orthogonal Frequency-Division Multiplexing (OFDM), with an overview of the transmission chain diagram and an analogous analysis is performed in section 3.4 for Single-Carrier with Frequency-Domain Equalization (SC-FDE) schemes. Section 3.6 introduces and analyzes the Iterative-Block Decision Feedback Equalization (IB-DFE) concept and its relation with SC-FDE and finally section 3.7 explains the derivation of the correlation coefficient, which corresponds to an important component in the detection process.

3.1 Single Carrier Modulations

In SC modulations the data is modulated and transmitted into a single carrier, where the energy associated to each symbol occupies the total transmission band. An N-symbol burst (for the sake of simplicity an even N value is assumed), in the time-domain, of a SC signal has the complex envelope given by

$$s(t) = \sum_{n=0}^{N-1} s_n r(t - nT_s), \tag{3.1}$$

in which s_n is a complex coefficient that corresponds to the n^{th} symbol, selected from a given constellation (e, g., a Quaternary Phase Shift Keying (QPSK) constellation), $r(t)$ denotes the transmission support pulse and T_s corresponds to the symbol duration. In the frequency-domain, 3.1 is obtained by applying the Fourier Transform:

$$S(f) = \mathcal{F}\{s(t)\} = \sum_{k=0}^{N-1} s_n R(f) e^{-j2\pi f n T_s}. \tag{3.2}$$

The resulting expression is characterized by the transmission band associated to each symbol s_n being the band occupied by $R(f)$, the FT of $r(t)$.

3.2 Multi-carrier Modulations

As opposed to single carrier modulated signals, where the transmitted information is sent in the time-domain, in multi-carrier modulations data symbols are transmitted in the frequency-domain. Therefore, the N symbols are distributed throughout several different sub-carriers in the same time interval T,according to

$$S(f) = \sum_{k=0}^{N-1} S_k R(f - kF). \tag{3.3}$$

In this case, N stands for the number of sub-carriers used in the modulation, S_k denotes the k^{th} frequency-domain symbol and F refers to the spacing between sub-carriers, $F = \frac{1}{T_s}$. The representation of the complex envelope of a multi-carrier modulated signal is obtained by applying of the inverse Fourier transform in 3.3, leading to

$$s(t) = \mathcal{F}^{-1}\{S(f)\} = \sum_{k=0}^{N-1} S_k r(t) e^{j2\pi k F t}. \tag{3.4}$$

Clearly, it can be interpreted that multi-carrier and single carrier modulations are dual of each other.

The simplest multi-carrier modulation is the conventional Frequency Division Multiplexing (FDM) scheme, where the spectrum related to the different sub-carriers does not overlap. When the bandwidth of $R(f)$ is smaller then F[1], the bandwidth associated to each symbol S_k will be a fraction $\frac{1}{N}$ of the total transmission band, as shown in Fig. 3.1. In order to avoid transmission without ISI, the $r(t)$ pulses must verify the following orthogonality condition

$$\int_{-\infty}^{+\infty} r(t - nT_s) r^*(t - n'T_s) dt = 0, \quad n \neq n'. \tag{3.5}$$

Due to the dual property mentioned above, in the frequency domain, the orthogonality condition between sub-carriers is given by

$$\int_{-\infty}^{+\infty} R(f - kF) R^*(f - k'F) df = 0, \quad k \neq k'. \tag{3.6}$$

[1]Clearly, F is the bilateral bandwidth and $F/2$ is the unilateral bandwidth.

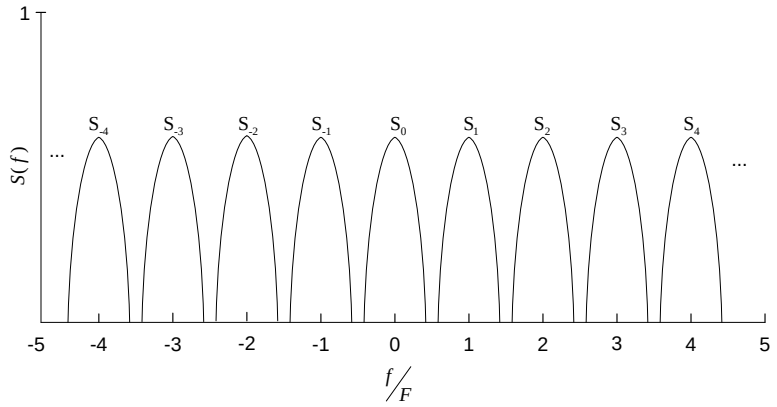

Figure 3.1: Conventional FDM

Using the Parseval's Theorem, (3.6) can be written as

$$\int_{-\infty}^{+\infty} |r(t)|^2 e^{-j2\pi(k-k')Ft} dt = 0, \quad k \neq k'. \tag{3.7}$$

For the particular case of linear SC modulations, the different pulses given by $r(t - nT_s)$ with $n = ..., -1, 0, 1, ...$, are still orthogonal even when overlaping between them exists. For example, the pulse

$$r(t) = sinc\left(\frac{t}{T_s}\right), \tag{3.8}$$

with $sinc(x) \triangleq \frac{sen(\pi x)}{\pi x}$, verifies the (3.5) condition. Similarly, for MC modulations the orthogonality is still preserved between the different sub-carriers, even when the different $R(f - kF)$ overlap. For example, the orthogonality between sub-carriers (conditions (3.6) and (3.7)) is verified when

$$R(f) = sinc\left(\frac{f}{F}\right), \tag{3.9}$$

which is equivalent to have a rectangular pulse $r(t)$ in time-domain, of $T = \frac{1}{F}$. In this case, the orthogonality condition (3.7) becomes

$$\int_{0}^{t_0+T} e^{-j2\pi(k-k')Ft} dt = 0, \quad k \neq k'. \tag{3.10}$$

3.3 OFDM Modulations

Concerning an example of a multi-carrier transmission scheme, in OFDM) [30] modulations the information data is transmitted simultaneously by N narrowband parallel sub-carriers, preserving orthogonality. Each sub-carrier takes part of only a small section of the total available bandwidth given by $N \times F$, with a sub-carrier spacing of $F \geq \frac{1}{T_B}$, where T_B denotes the period of an OFDM block. Since in OFDM schemes sub-carriers can overlap due to orthogonality between them, a better spectral efficiency can be achieved when compared to conventional FDM schemes. Fig. 3.2 depicts the Power Spectrum Density (PSD) of an OFDM signal, as well as the individual sub-carrier spectral shapes. The k^{th}

sub-carrier PSD ($f_k = \frac{k}{T_B}$) has a maximum where the adjacent sub-carriers have zero-crossings, that exists null interference between carriers and improves the overall spectral efficiency.

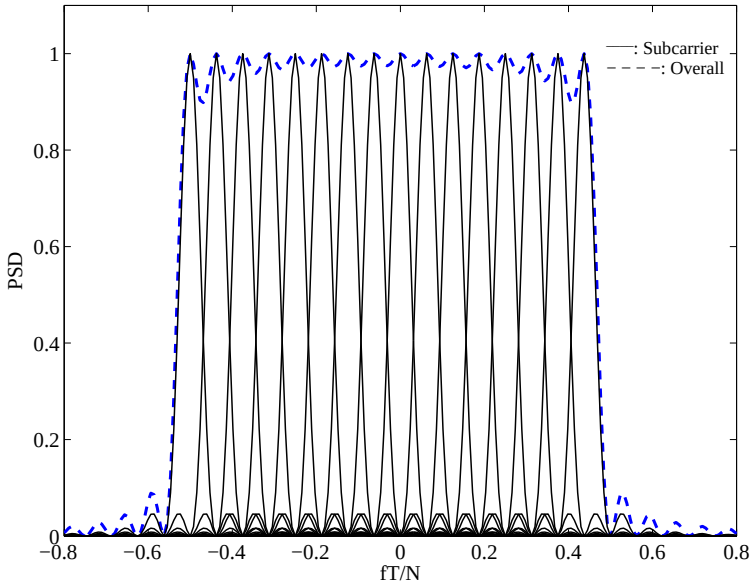

Figure 3.2: Power density spectrum of the complex envelope for an OFDM signal, with $N = 16$ orthogonal overlapping sub-carriers spectrum.

3.3.1 Transmission Chain

This subsection focus on the transmission chain of an OFDM signal (for the sake of simplicity a noiseless transmission case is considered), illustrated in Fig. 3.3. The incoming high data rate is split onto N rate sub-carriers and transmitted through frequency-domain blocks of size N, being $\{S_k; k = 0, 1, ..., N-1\}$ a block of N complex data symbols chosen from a selected constellation (for example, a QPSK constellation). At the output of the

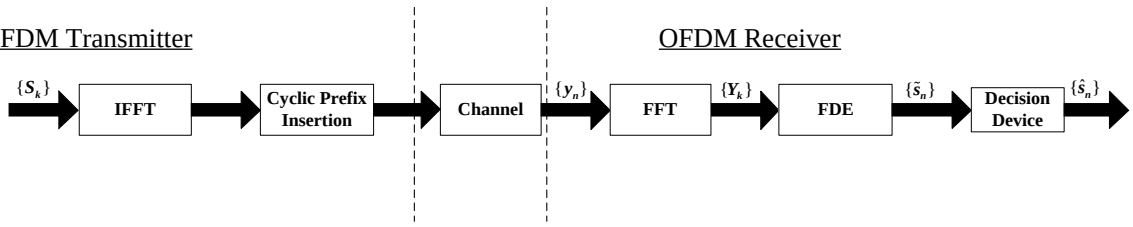

Figure 3.3: OFDM transmission chain block diagram.

Inverse Fast Fourier Transform (IFFT), a CP of N_G samples, is inserted at the beginning of each block of N IFFT coefficients. It consists of a time-domain cycle extension of the OFDM block, with size larger than the channel impulse response (i.e, the N_G samples assure that the CP length is equal to or greater than the channel length N_H). The cycle prefix is appended between each block, in order to transform the multipath linear

convolution into a circular one. Thus, the transmitted block is $\{s_n; n = -N_G, ..., N-1\}$, and the time duration of an OFDM symbol is $N_G + N$ times larger than the symbol of a SC modulation. Clearly, the CP is an overhead that costs power and bandwidth since it consists of additional redundant information data. As can be seen in Fig. 3.3 , after the channel effects, the CP removal and a FFT block, the frequency-domain remaining samples $\{Y_k; k = 0, 1, ..., N-1\}$ are subject to an FDE block, where the result estimated samples $\tilde{s}_n$ pass through a decision device. The final estimated output samples are denoted by $\hat{s}_n$. The OFDM transmission chain is very similar to the SC-FDE one, which is explained in the next subsection, with all the variables expressed.

3.4 SC-FDE Modulations

The high PMEPR and the strong envelope fluctuations are the major problems concerning OFDM modulations, with the consequence of making these schemes vulnerable to transmitter nonlinearities, namely due to power amplification. Consequently, it is desirable the employment of SC schemes, particularly in the uplink transmission (i.e., the transmission link from the MT to the BS). This allows the user terminals to be cheaper and to have higher-power amplifiers without compromising linearity.

Despite all of its advantages, when SC modulations are employed in digital communication systems, requiring transmission bit rates of Mbits/s over severely time-dispersive channels, high signal distortion levels can occur. Hence, the transmission bandwidth becomes much higher than the channels's coherence bandwidth. As a consequence, high complexity receivers will be required to overcome this problem [1]. The optimum receiver structure for time-dispersive channels corresponds to the well-known Viterbi equalizer, whose complexity grows exponentially with the channel impulse response length, making it recommendable only for channels whose impulse response spans over just a few symbols. Typically, time-domain equalizers comprehending one or more transversal filters are used to mitigate the hard ISI problem, leading to receivers much simpler than Viterbi equalizers at the expense of some performance degradation. When nonlinear structures such as DFEs are employed to compensate the distortion caused by channel frequency selectivity, their BER performance is usually much better than that of a linear equalizer and can come close to that of an optimum sequence detector implemented by the Viterbi algorithm. However, signal processing complexity of time-domain equalizers (measured in terms of the number of arithmetic operations per data symbol) increases at least linearly with the number of data symbols spanned by the CIR. This means very high receiver complexity (and the inherent power consumption) with exorbitant signal processing requirements, and, consequently, time-domain equalizers not suitable for severely time-dispersive channels.

3.4.1 Transmission Chain

Fig. 3.5 shows the basic transmission chain block diagram for a Single-Carrier with Frequency-Domain Equalization (SC-FDE) scheme, where the data is transmitted in blocks of N useful modulation time-domain symbols $\{s_n; n = 0, ..., N-1\}$, and constellation symbol s_n are selected from data according to a given mapping rule, such as a QPSK constellation with Gray mapping rule, shown in Fig. 3.4. Posteriorly, a cyclic prefix with

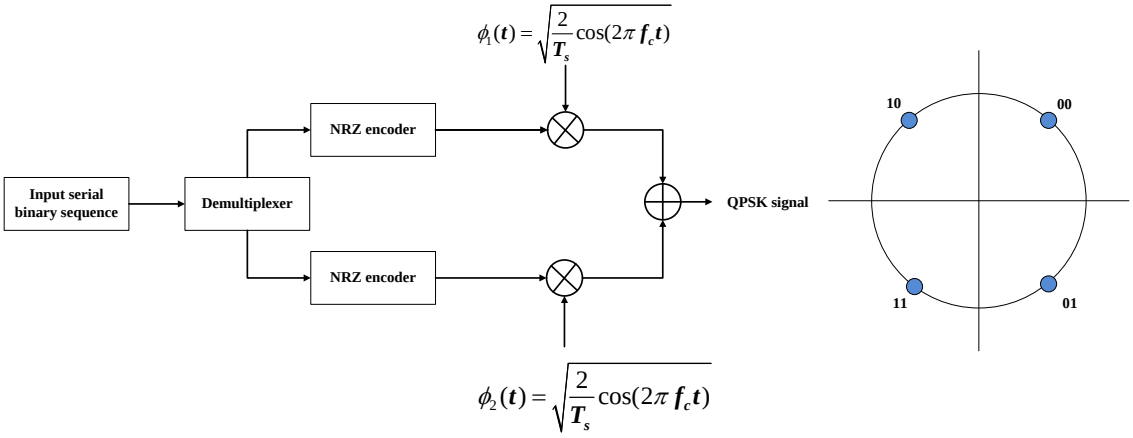

Figure 3.4: QPSK signal generator and constellation with Gray mapping rule.

length longer that the channel impulse response is inserted, in which the transmitted signal is represented as $\{s_n; n = -N_G, ..., N-1\}$. At the receiver, and after the inherent effects of

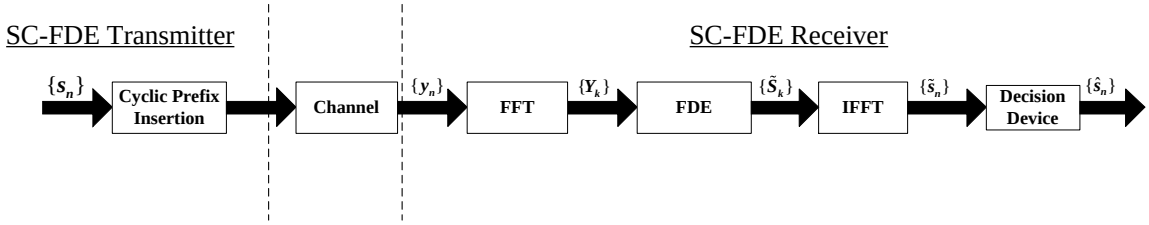

Figure 3.5: SC-FDE transmission chain block diagram.

the transmission channel, the received data is characterized by the time-domain samples $\{y_n; n = 0, ..., N-1\}$, with the CP already being removed. After the FFT operation, the y_n samples are defined by the frequency-domain samples $\{Y_k; k = 0, ..., N-1\}$, where Y_k is characterized by

$$Y_k = H_k S_k + N_k, \tag{3.11}$$

where H_k denotes the overall channel frequency response for the k^{th} block frequency, and N_k represents channel noise term in the frequency-domain. Fig. 3.6 illustrates the structure of the FDE block. The output samples of the linear FDE block are defined by the $\tilde{S}_k$ samples, given by

$$\tilde{S}_k = F_k Y_k, \tag{3.12}$$

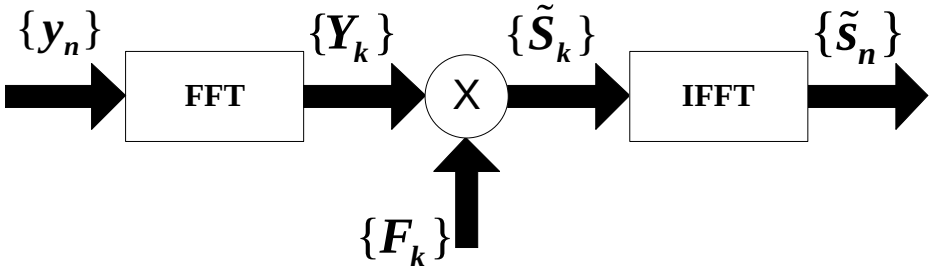

Figure 3.6: Linear FDE structure.

with F_k denoting the feedforward coefficient in the equalization process. The equalization can be performed with the F_k coefficient defined under different criterions, such as the Zero-Forcing (ZF) or the Minimum Mean Square Error (MMSE). For a ZF equalizer, the coefficient F_k is given by

$$F_k = \frac{1}{H_k}, \tag{3.13}$$

meaning that the channel is, in fact, completely inverted. Nevertheless, noise enhancement problems may arise, in the presence of a typical frequency-selective channel, caused by eventual deep notches in the channel frequency response. A possible consequence can be a diminution of the Signal-to-Noise Ratio (SNR). The MMSE criterion does not attempt to completely fully invert the channel effects in the presence of deep fades, however, the F_k coefficient allow the minimization of the combined effects of ISI and channel noise, enhancing performance. In the time-domain the Mean-Square Error (MSE) can be described by

$$\theta(k) = \frac{1}{N^2} \sum_{k=0}^{N-1} \theta_k, \tag{3.14}$$

where

$$\theta_k = \mathbb{E}\left[\left|\tilde{S}_k - S_k\right|^2\right] = \mathbb{E}\left[|Y_k F_k - S_k|^2\right]. \tag{3.15}$$

The minimization of θ_k in order to F_k requires the MSE minimization for each k, which corresponds to impose the condition

$$min_{F_k}\left(\mathbb{E}\left[|Y_k F_k - S_k|^2\right]\right), k = 0, 1, ..., N-1, \tag{3.16}$$

resulting in the set of optimized FDE coefficients F_k (see Appendix A)

$$F_k = \frac{H_k^*}{NSR + |H_k|^2}. \tag{3.17}$$

In 3.17 expression, Noise-to-Signal Ratio (NSR) can be written as

$$NSR = \frac{1}{SNR}, \tag{3.18}$$

with

$$SNR = \frac{\sigma_S^2}{\sigma_N^2}, \tag{3.19}$$

where

$$\sigma_N^2 = \frac{\mathbb{E}\left[|N_k|^2\right]}{2}\{N_k; k = 0, 1, ..., N-1\} \tag{3.20}$$

and

$$\sigma_S^2 = \frac{\mathbb{E}\left[|S_k|^2\right]}{2}\{S_k; k = 0, 1, ..., N-1\} \tag{3.21}$$

represent the variance of the real and imaginary parts of the channel noise and data sample components, respectively. In the derivation of F_k, NSR can be considered as a noise-dependent factor that avoids the noise increasing effects when low values of the channel frequency response are taken into account. In SC modulations, the data symbols in a given block are transmitted in the time-domain. Then, the equalized samples $\{\tilde{S}_k; k = 0, 1, ..., N-1\}$ are subject to a conversion back to the time-domain by an IDFT operation. The resulting samples $\{\tilde{s}_n; n = 0, 1, ..., N-1\}$ are then used to make decisions on the transmitted symbols.

For SC-FDE modulations, it is possible to extend the receiver for space diversity scenarios. Fig. 3.7 depicts a SC-FDE receiver scheme with an R-branch space diversity. Consequently, the estimated received samples at the FDE output are expressed by

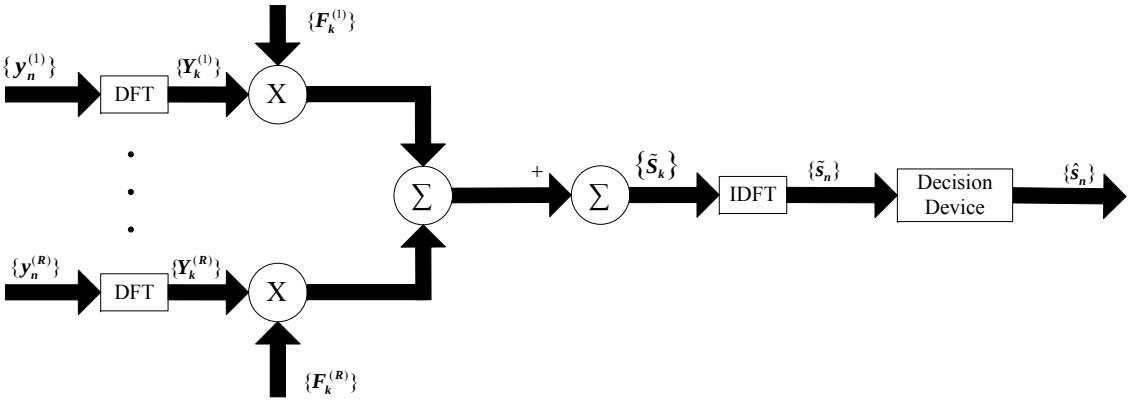

Figure 3.7: Linear FDE structure with an R-branch space diversity.

$$\tilde{S}_k = \sum_{r=1}^{R} F_k^{(r)} Y_k^{(r)}, \tag{3.22}$$

where $\{F_k^{(r)}; k = 0, 1, ..., N-1\}$ corresponds to the FDE feedforward coefficients regarding the r^{th} diversity order. In Appendix A the derivation of the optimum F_k for a linear FDE SISO system is shown. The same reasoning can be applied to the R-branch space diversity order, where F_k is given by

$$F_k^{(r)} = \frac{H_k^{(r)*}}{NSR + \sum\limits_{r'=1}^{R} \left|H_k^{(r')}\right|^2}. \tag{3.23}$$

3.5 OFDM and SC-FDE Comparison

This section deals with the comparison between OFDM and SC-FDE. The transmission chains of both modulations and an analysis of the BER performance for OFDM and SC-FDE regarding the ZF and MMSE criterions are presented. Fig. 3.8 illustrates the transmission chains of OFDM and SC-FDE. The transmission schemes can be considered

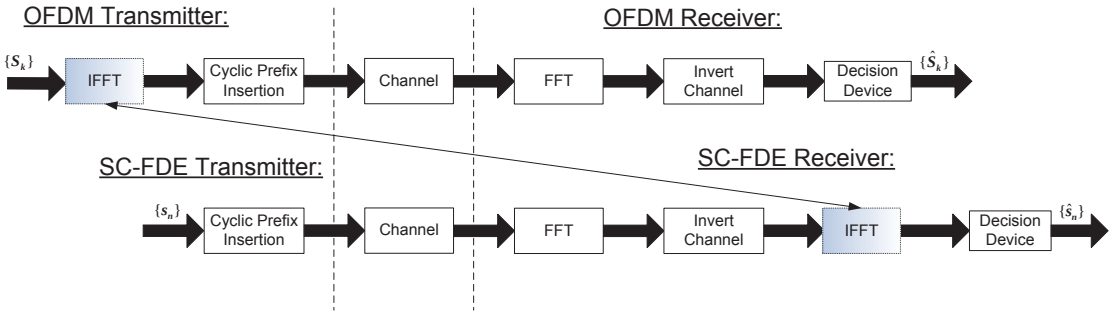

Figure 3.8: Transmission chain comparison between OFDM and SC-FDE.

as basically having the same structure, with the exception of the location of the IFFT operation block. In OFDM modulations the IFFT is placed at the transmitter side to divide the data in different parallel subcarriers and in SC-FDE the IFFT it is placed at the receiver to convert the symbols at the FDE output into the time-domain. SC-FDE requires a more complex receiver since it does not need the IDFT block at the transmitter and, consequently, it allows a lower complexity at the transmitter. The number of DFT/IDFT operation blocks indicate the overall processing complexity and both modulation schemes can be seen as equivalent [31].

Fig. 3.9 illustrates the BER performance of uncoded OFDM and SC-FDE modulations considering ZF and MMSE equalization. The transmitted blocks have size $N = 256$ QPSK data symbols ($\pm 1 \pm j$) with a cyclic prefix of 32 symbols. Severely time-dispersive channels with 32 equal power taps are considered, with uncorrelated Rayleigh fading on each tap. Moreover, Fig. 3.9 also presents the BER performance for the Matched Filter Bound (MFB). The MFB indicates the optimum error performance for a given receiver. It is obtained assuming that a single symbol is being transmitted, with no interference from neighboring symbols. Therefore, there is no lSI, only additive noise. For a given system and SNR there is an optimal value for the MFB and it is expressed by

$$BER_{MFB} = \mathbb{E}\left[Q\left(\sqrt{2\frac{E_b}{N_0}\frac{1}{N}\sum_{k=0}^{N-1}|H_k|^2}\right)\right], \tag{3.24}$$

and for an R-branch space diversity scenario

$$BER_{MFB} = \mathbb{E}\left[Q\left(\sqrt{2\frac{E_b}{N_0}\frac{1}{N}\sum_{k=0}^{N-1}\sum_{r=1}^{R}\left|H_k^{(r)}\right|^2}\right)\right], \tag{3.25}$$

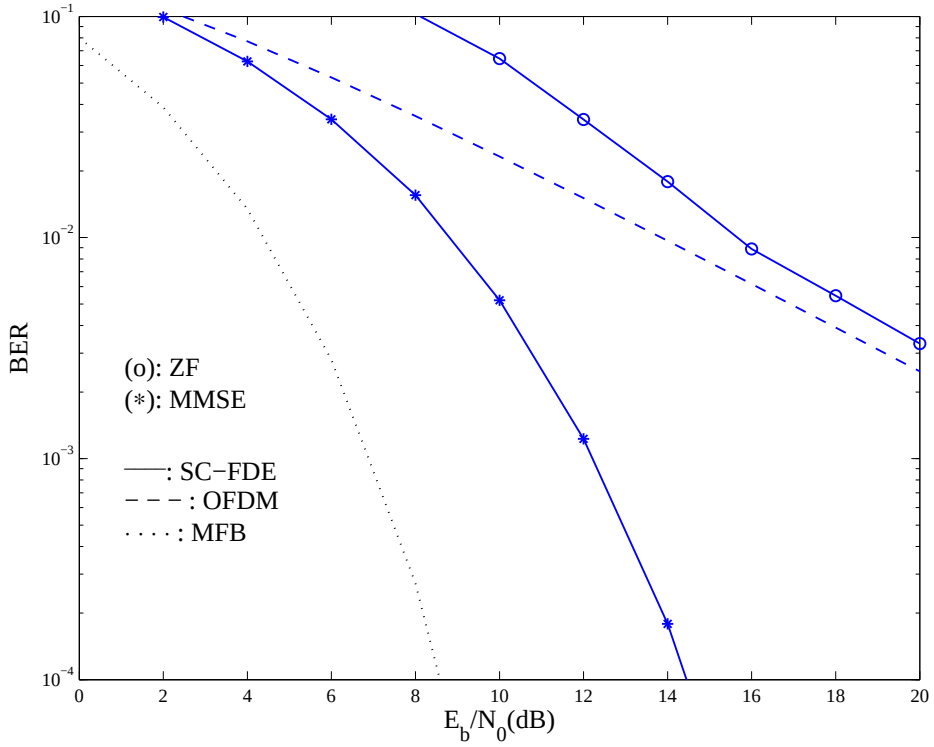

Figure 3.9: BER performance for uncoded OFDM and SC-FDE with ZF and MMSE criterium.

where the expectation is over the set of channel realizations, assuming $\mathbb{E}\left[\left|H_k^{(r)}\right|^2\right] = 1$. Moreover, $\frac{E_b}{N_0}$ denotes a normalized SNR, which provides an useful measure to compare different transmission techniques. Taking into account that there is no channel coding, the SC-FDE with ZF is very close to OFDM, and SC-FDE with MMSE has better uncoded performance under the same conditions of average power and complexity demands [6]. Moreover, OFDM is severely affected by deep-faded subcarriers. However, when combined with error correction codes, OFDM has a higher gain code when compared to SC-FDE [6]. OFDM is strongly affected in its fluctuations and requires the use of linear amplification at the transmitter. On the other hand, the lower envelope fluctuation of SC signals enables a more efficient amplification. Since it is desirable to have lower costs and complexities in power amplifiers, in the uplink transmission SC-FDE is more suitable than OFDM. Fig. 3.10 depicts the channel frequency response (top figure) and the FDE coefficient F_k under the ZF and MMSE criteria (bottom figure). It is clear from Fig. 3.10 that with ZF criterion the channel is completely inverted, which results in a perfect equalized channel after the FDE, while the MMSE criterion provides an non-perfect channel equalization. However, the noise enhancement effect can be problematic, as shown in Fig. 3.11 and 3.12. The equalized samples s_n at the FDE output are shown considering the F_k coefficient under the ZF or MMSE criteria, with and without the presence of the channel noise, respectively. In Fig. 3.11 it can be observed that by perfectly inverting the channel with F_k under the

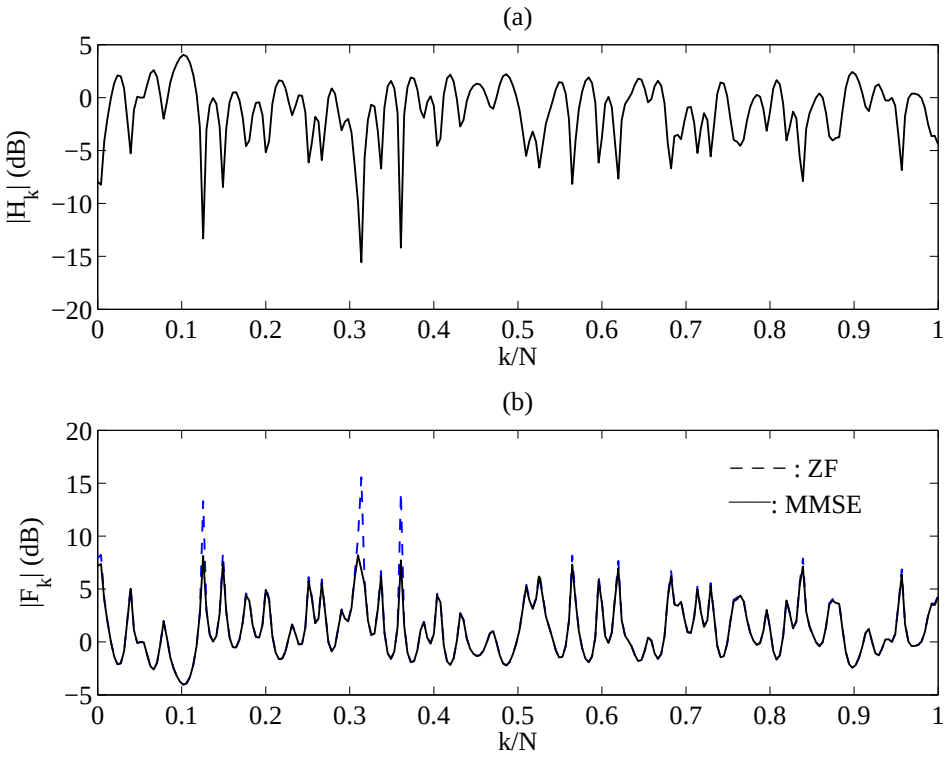

Figure 3.10: Channel frequency response (top figure (a)) and the FDE coefficient F_k under the ZF and MMSE criteria (bottom figure (b)).

ZF criterion the system leads to precise values of the data samples when no channel noise is present. On the other hand, as illustrated in Fig. 3.12, in the presence of channel noise, the noise enhancement with the ZF criteria can lead to higher spread of the equalized samples around the data sample exact values. With F_k under the MMSE criteria the samples remain closer to their true values.

Taking into account the better results when considering F_k with MMSE, Fig. 3.13 illustrates the BER performance for a SC-FDE modulation scheme considering an R-branch space diversity scenario. The power associated to the different links correspond to

$$\xi_r = 0 \text{ dB}, \tag{3.26}$$

where r indicate the r^{th} BS in the R-branch diversity scenario. Clearly, there is a significant performance improvement when the received signals associated to different BSs are combined, even when the average received power at one BS is substantially lower than the average received power at the other BS. Moreover, the macro-diversity also reduces the shadowing effects and improves overall coverage. Fig. 3.14 considers an ideal macro-diversity scenario, with the power associated to the different links characterized by

$$[\xi_{1,1}, \xi_{1,2}] = [0, \beta] \text{ (dB)}, \tag{3.27}$$

i.e, there is a main link between the MT and its BS and a secondary link to another BS

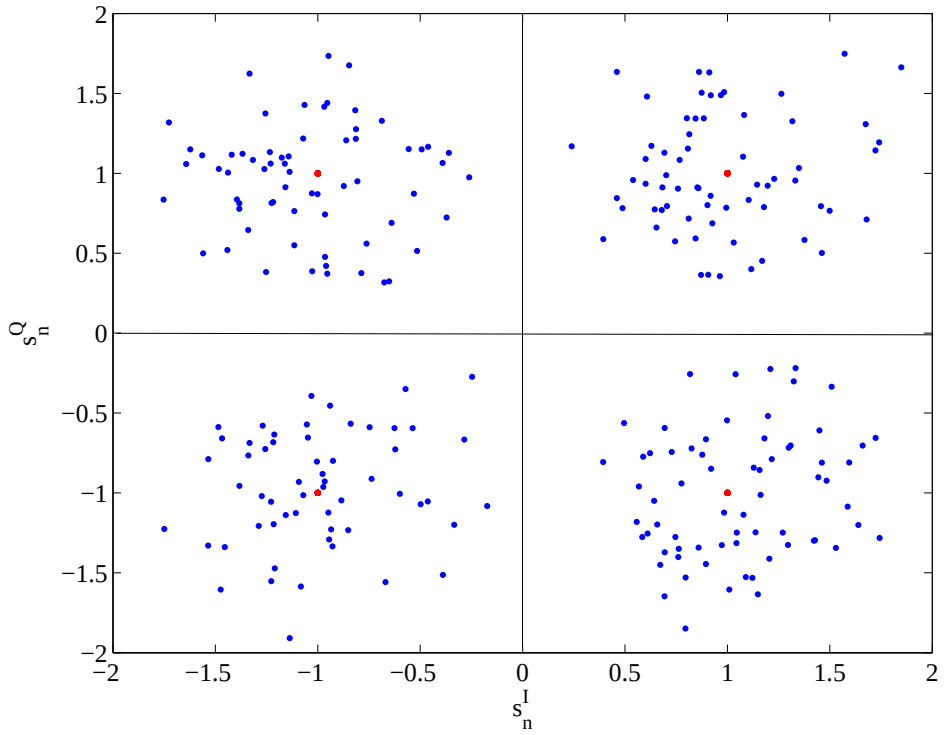

Figure 3.11: Equalized samples $\tilde{s}_n$ with an FDE coefficient F_k under the ZF criteria, with and without noise.

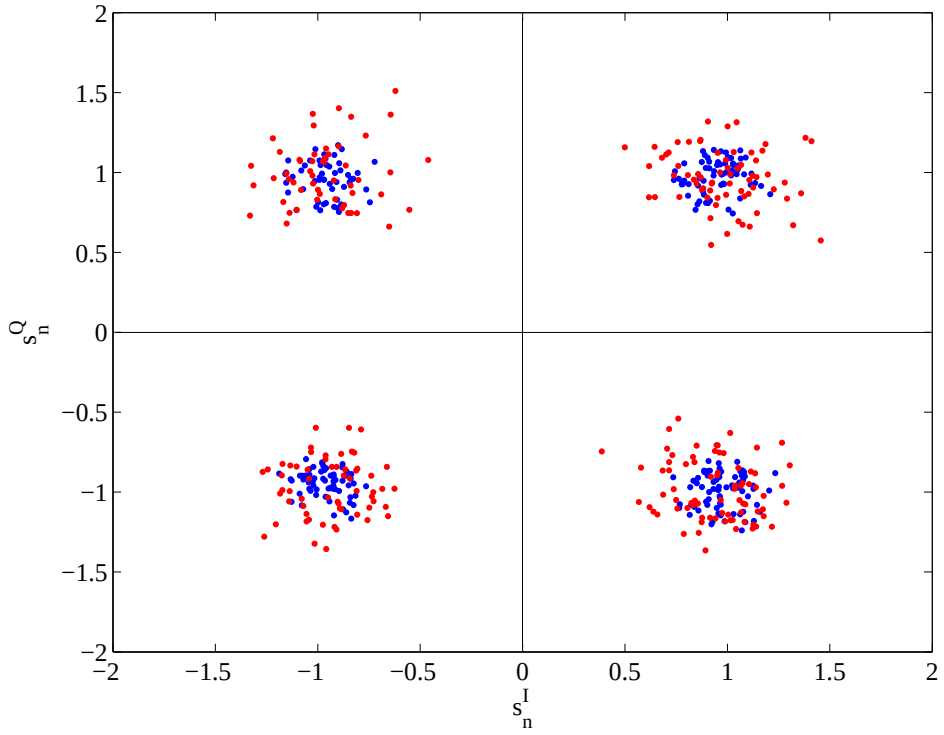

Figure 3.12: Equalized samples $\tilde{s}_n$ with an FDE coefficient F_k under the MMSE criteria, with and without noise.

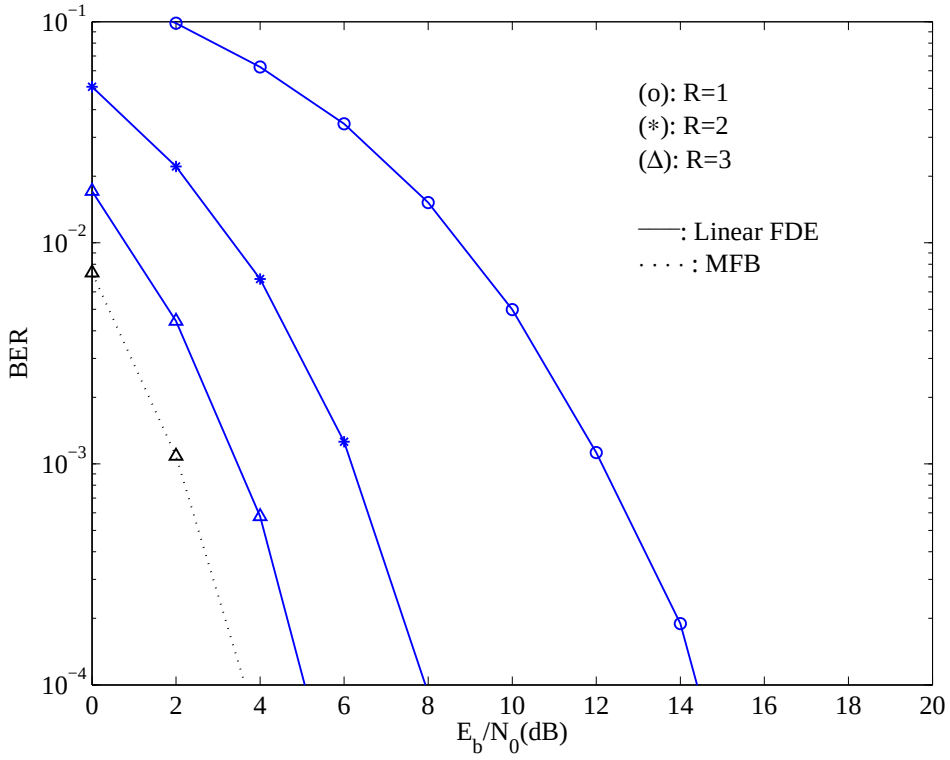

Figure 3.13: BER performance for a SC-FDE scheme with an R-branch space diversity.

whose average power is β dB below the average power associated to the main link. Clearly, $\beta = -\infty$ corresponds to the case where no cooperation in employed. Naturally, $\beta = 0$ dB corresponds to the best macro-diversity scenario, with both BSs receiving a reference value of 0 dB, and having the best BER performance.

Figs 3.15, 3.16 and 3.17 illustrate the equalized samples s_n at the output when several receiving antennas are considered, for the same R-branch space diversity scenario discussed in Fig. 3.13. As expected, the greater the R-branch value for the diversity the more precise and less spread the equalized samples are.

An important scenario to analyze is the one where there is only one MT per physical channel but only a single BS, corresponding to a conventional, non-cooperative scenario with interference (i.e., $P = 2$ and $R = 1$). The power associated to the different links are then characterized by

$$[\xi_{1,1}, \xi_{2,1}] = [0, \beta] \text{ (dB)} \tag{3.28}$$

and this can be regarded as a scenario where the average power of the interfering MT (associated to the BS of an adjacent cell), is β dB below the average power of the relevant MT. Fig. 3.18 illustrates the described scenario, where it is shown that the BER performance for different values of β (having $\beta = -\infty$ dB corresponds to the case where the interference phenomenon does not exists). From this figure, it is clear that the average received power associated to the interfering MT should be substantially lower than the

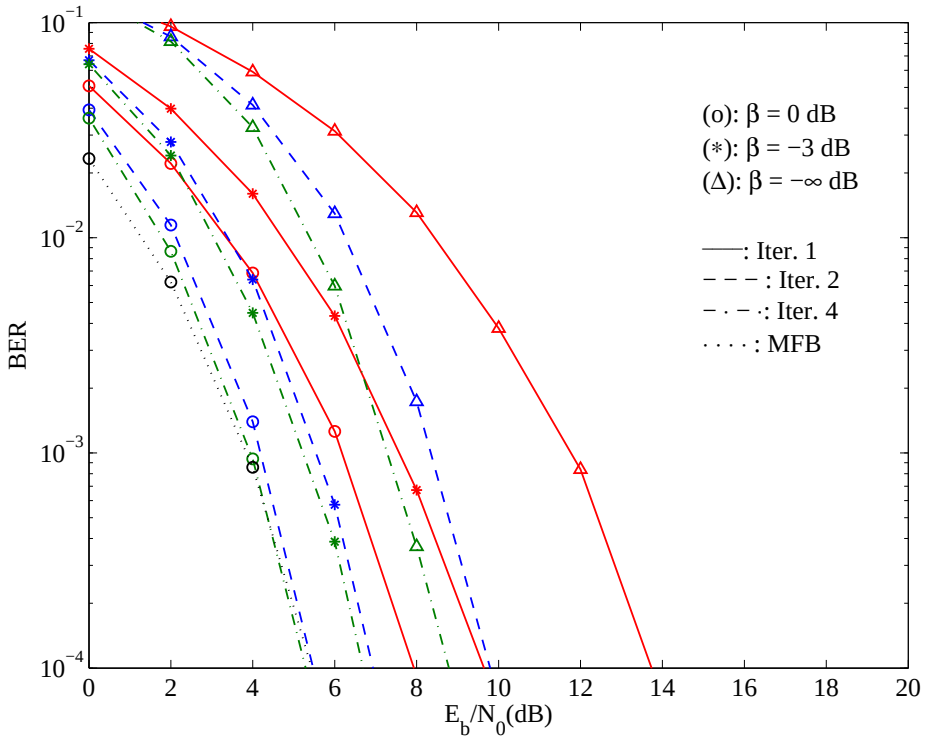

Figure 3.14: BER performance for a macro-diversity scenario with $R = 2$ cooperating BSs.

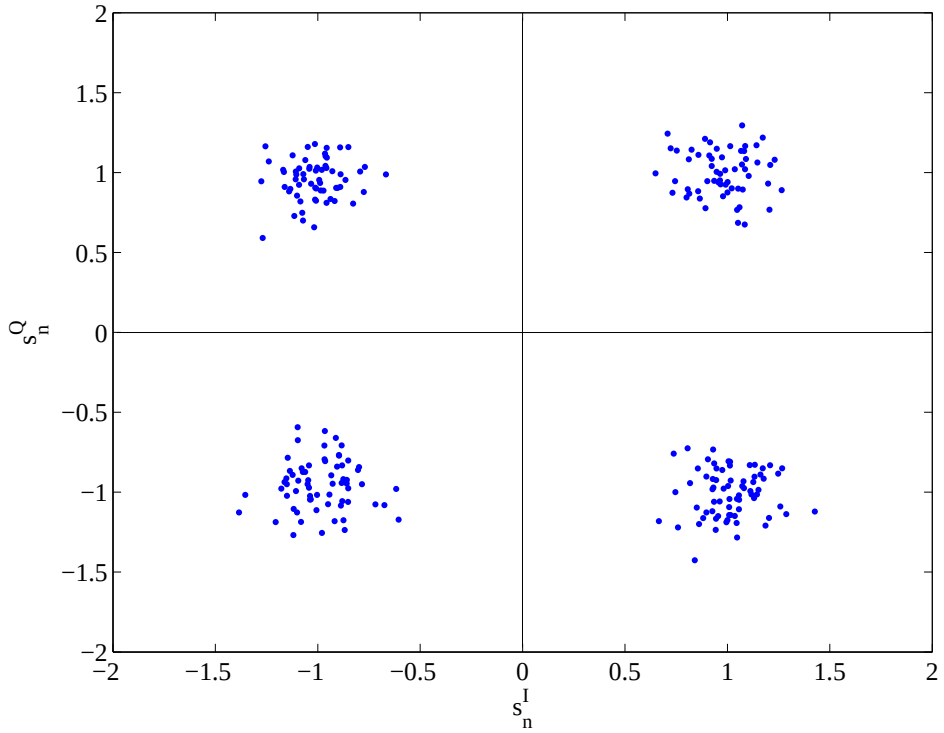

Figure 3.15: Equalized samples $\tilde{s}_n$ at the FDE output when $R = 1$.

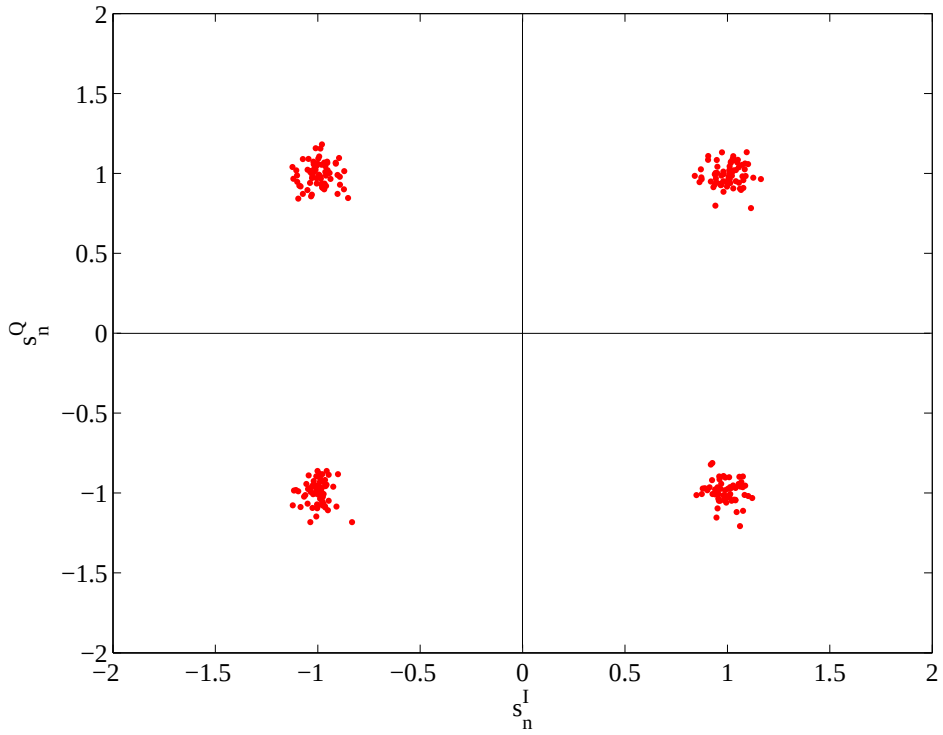

Figure 3.16: Equalized samples $\tilde{s}_n$ at the FDE output when $R = 2$.

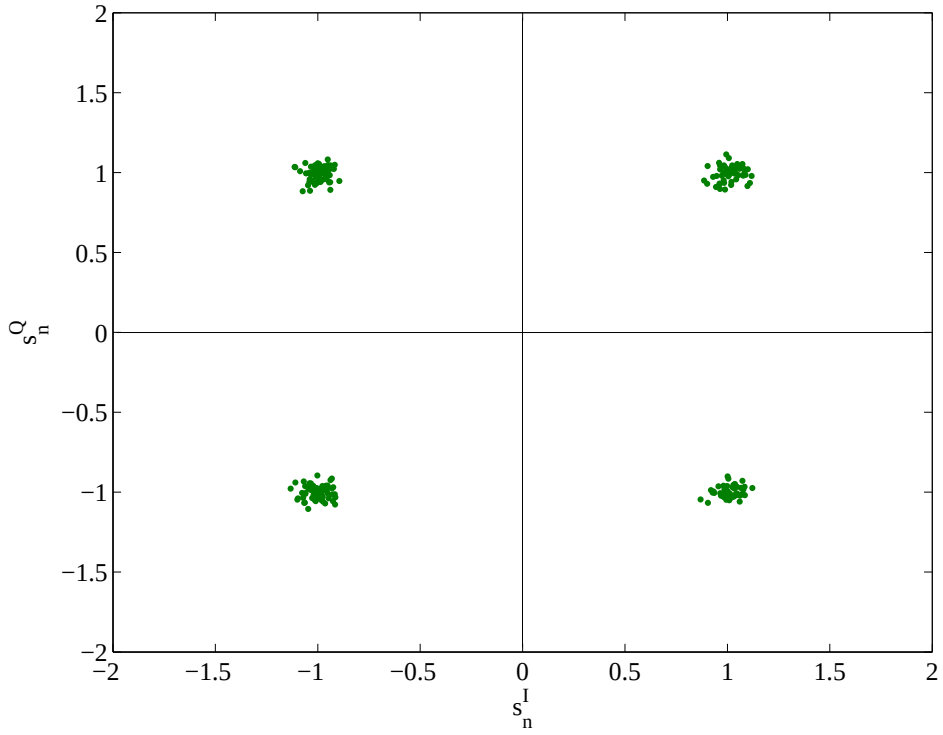

Figure 3.17: Equalized samples $\tilde{s}_n$ at the FDE output when $R = 3$.

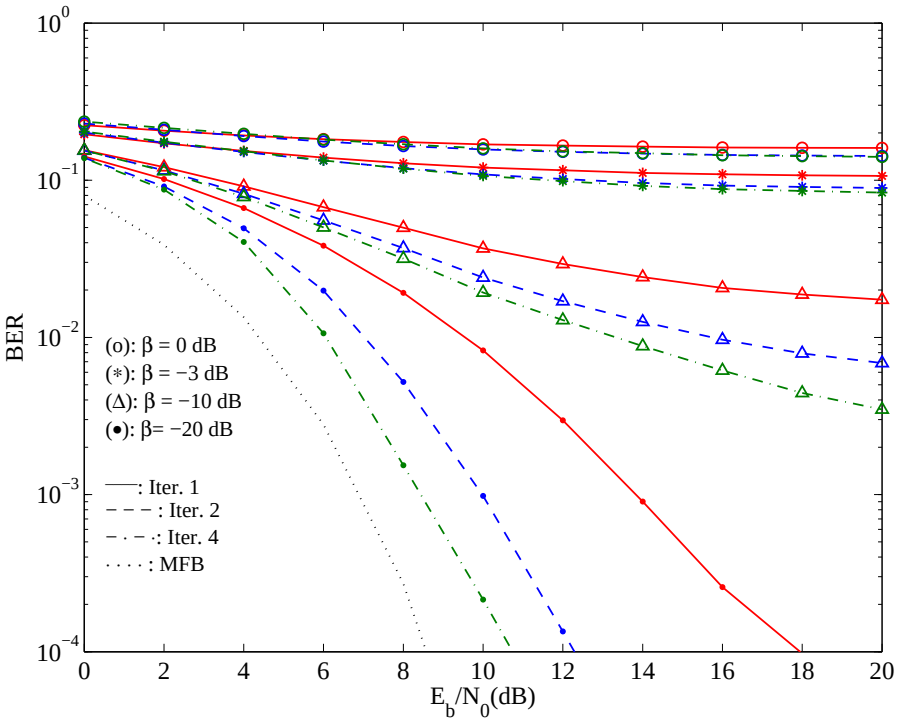

Figure 3.18: BER performance with $P = 2$ MTs and $R = 1$ BS (1st MT).

average received power of the reference MT (around 20 dB below).

3.6 DFE Iterative Receivers

Despite the reasonable complexity/performance commitment obtained with linear equalizers schemes, they still have to deal with several problems inherent to its own nature, namely noise enhancement and residual ISI. It is well-known that nonlinear equalization outperforms the linear approach [1, 7, 8]. Among nonlinear equalizers, the DFE [1] is a popular choice since it provides a good tradeoff between complexity and performance. Its basic structure is depicted in Fig. 3.19. The nonlinear equalizer, with a DFE component

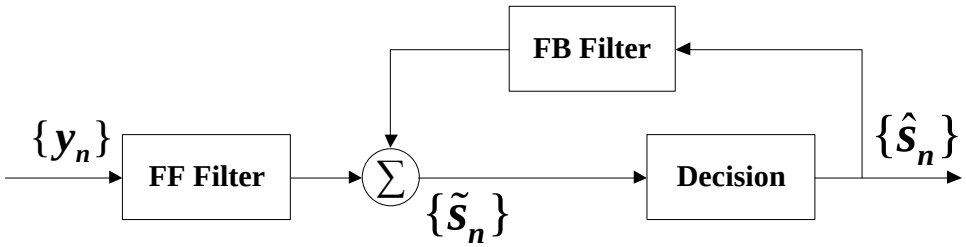

Figure 3.19: Basic DFE structure.

is nothing more than the implementation of a feedback filter (FB Filter) at the output of the feedforward block samples (wich are derived from the FF Filter), and associating this process to an iterative scheme, makes the DFE an efficient way of equalizing the received

signals. Hence, the linear FDE is replaced by an IB-DFE [8], which corresponds to an iterative DFE for SC-FDE where the feedforward and feedback operations are implemented in the frequency domain, as depicted in Fig. 3.20. For the IB-DFE implementation case,

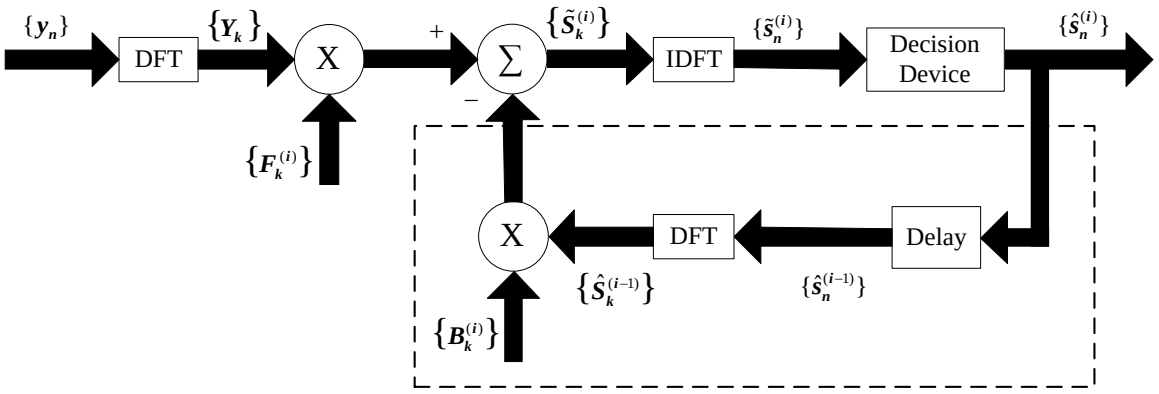

Figure 3.20: Basic IB-DFE block diagram structure.

regarding the i^{th} iteration, the frequency-domain block at the output of the equalizer is given by $\{\tilde{S}_k^{(i)}; k = 0, 1, ..., N-1\}$, with

$$\tilde{S}_k^{(i)} = F_k^{(i)} Y_k - B_k^{(i)} \hat{S}_k^{(i-1)}, \tag{3.29}$$

where $\{F_k^{(i)}; k = 0, 1, ..., N-1\}$ is the feedforward coefficient and $\{B_k^{(i)}; k = 0, 1, ..., N-1\}$ is the feedback coefficient from the DFE block. $\{\hat{S}_k^{(i-1)}; k = 0, 1, ..., N-1\}$ denotes the DFT of the "hard-decision"block $\{\hat{s}_n^{(i-1)}; n = 0, 1, ..., N-1\}$ from the previous iteration, related with the transmitted time-domain block $\{s_n; n = 0, 1, ..., N-1\}$. With hard-decisions, the symbols at the FDE output are subject to a decision device represented in Fig. 3.21.

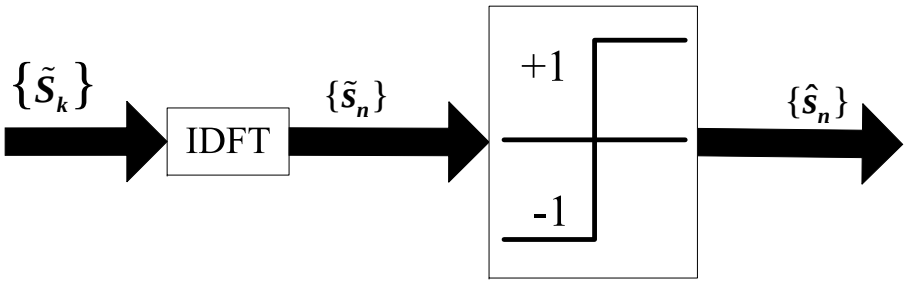

Figure 3.21: Data samples estimation with hard-decisions.

To calculate the receiver parameters in IB-DFE receivers it is assumed that the global channel frequency response is

$$F_k^{(i)} H_k. \tag{3.30}$$

The residual ISI component, in the frequency-domain, is related to the difference between the global channel frequency response, given by 3.30, and

$$\gamma^{(i)} = \frac{1}{N} \sum_{k=0}^{N-1} F_k^{(i)} H_k, \tag{3.31}$$

where $\gamma^{(i)}$ can be regarded as the average overall channel frequency response at the i^{th} iteration. Nevertheless, if the estimates of the transmitted block are reliable, the feedback filter can be employed to eliminate the residual ISI. The equalized samples related to each iteration, in the frequency-domain, are then given by

$$\tilde{S}_k^{(i)} = \gamma^{(i)} S_k + \varepsilon_k^{(i)}, \tag{3.32}$$

where $\varepsilon_k^{(i)}$ represents the global error consisting of the residual ISI plus the channel noise. The feedforward and feedback IB-DFE coefficients are chosen in order to maximize the SINR, as

$$SINR = \frac{\left|\gamma^{(i)}\right|^2 \mathbb{E}\left[\left|S_k\right|^2\right]}{\mathbb{E}\left[\left|\varepsilon_k^{(i)}\right|^2\right]}. \tag{3.33}$$

The DFE estimated frequency-domain data samples $\hat{S}_k^{(i)}$ can be expressed as

$$\hat{S}_k^{(i)} = \rho^{(i)} S_k + \Delta_k^{(i)}, \tag{3.34}$$

where ρ corresponds to a correlation coefficient and is defined as

$$\rho^{(i-1)} = \frac{\mathbb{E}\left[\hat{S}_k^{(i-1)} S_k^*\right]}{\mathbb{E}\left[\left|S_k\right|^2\right]} = \frac{\mathbb{E}\left[\hat{s}_n^{(i-1)} s_n^*\right]}{\mathbb{E}\left[\left|s_n\right|^2\right]}. \tag{3.35}$$

The correlation coefficient represents a crucial parameter to ensure a good receiver performance, since it supplies a block-wise reliability measure of the estimates employed in the feedback loop. This is done in the feedback loop by taking into account the hard decisions for each block plus the overall block reliability, which reduces error propagation problems. Furthermore, in (3.34), $\Delta_k^{(i)}$ denotes a zero-mean error term for the k^{th} frequency-domain hard decision estimate. Assuming

$$\mathbb{E}\left[\Delta_k^{(i)}\right] = 0 \tag{3.36}$$

and

$$\mathbb{E}\left[\Delta_k^{(i)} S_{k'}^{(i)*}\right] \approx 0 \tag{3.37}$$

for $k' \neq k$, then

$$\mathbb{E}\left[\left|\Delta_k^{(i)}\right|^2\right] \approx \left(1 - \left(\rho^{(i)}\right)^2 \mathbb{E}\left[\left|S_k\right|^2\right]\right). \tag{3.38}$$

Combining 3.11, 3.29 and 3.34, it can be written that

$$\tilde{S}_k^{(i)} = \gamma^{(i)} S_k + \left(F_k^{(i)} H_k - \gamma^{(i)} - \rho^{(i-1)} B_k^{(i)}\right) S_k - B_k^{(i)} \Delta_k^{(i-1)} + F_k^{(i)} N_k. \tag{3.39}$$

So, it can be concluded that $\tilde{S}_k^{(i)}$ has the following components

- The first term, $\gamma^{(i)} S_k$, denotes the useful signal component.
- The second term, $\left(F_k^{(i)} H_k - \gamma^{(i)} - \rho^{(i-1)} B_k^{(i)}\right) S_k$, refers to the residual ISI factor.

- The third term, $B_k^{(i)}\Delta_k^{(i-1)}$, denotes the noise originated by feedback errors (i.e., errors in the decision estimates $\hat{s}_n^{(i-1)}$ that are reintroduced in the system).

- The fourth term, $F_k^{(i)}N_k$, denotes the channel noise.

Finally, $\tilde{S}_k^{(i)}$, can be written as

$$\tilde{S}_k^{(i)} = \gamma^{(i)} S_k + E_k, \tag{3.40}$$

with E_k denoting the overall error for the k^{th} frequency-domain symbol, and is given by

$$E_k = \left(F_k^{(i)} H_k - \gamma^{(i)} - \rho^{(i-1)} B_k^{(i)}\right) S_k - B_k^{(i)}\Delta_k^{(i-1)} + F_k^{(i)} N_k. \tag{3.41}$$

In Appendix B it is shown how the maximization of the SINR results in the optimum values of the feedforward and feedback coefficients given by

$$F_k^{(i)} = \frac{\kappa^{(i)} H_k^*}{NSR + (1 - (\rho^{(i-1)})^2)\,|H_k|^2}, \tag{3.42}$$

and

$$B_k^{(i)} = \rho^{(i-1)}(F_k^{(i)} H_k - \gamma^{(i)}), \tag{3.43}$$

respectively, where $\kappa^{(i)}$ is selected to ensure that $\gamma^{(i)} = 1$. The correlation coefficient $\rho^{(i-1)}$ is given by (3.35 and reproduced in the following by convenience

$$\rho^{(i-1)} = \frac{\mathbb{E}\left[\hat{S}_k^{(i-1)} S_k^*\right]}{\mathbb{E}\left[|S_k|^2\right]} = \frac{\mathbb{E}\left[\hat{s}_n^{(i-1)} s_n^*\right]}{\mathbb{E}\left[|s_n|^2\right]}. \tag{3.44}$$

For the first iteration (i.e., $i = 1$), no information exists about s_n, meaning that $\rho = 0$, $B_k^{(1)} = 0$ and $F_k^{(1)}$ corresponding to the expression given by 3.17. In this situation the IB-DFE receiver is reduced to a linear FDE. After the first iteration the feedback coefficients can be applied to reduce a major part of the residual interference, and after several iterations and for a moderate-to-high SNR, the correlation coefficient tends to be $\rho \approx 1$ and the residual ISI will be almost totally canceled. Fig. 3.22 shows the BER performance evolution for a transmission system with SC-FDE modulation that uses an IB-DFE receiver with a total of 4 iterations. For the sake of comparison the performance of the MFB is also presented. From these results, it can be seen that the $\frac{E_b}{N_0}$ required for BER=10^{-4}, for the first iteration, that corresponds to the linear SC-FDE, is approximately 15.5 dB, decreasing to 11 dB after only three iterations. It is clear that the use of the iterative receiver allows a significant performance improvement. Also, the asymptotic BER performance becomes closer to the MFB after a few iterations, since the computation of the correlation coefficient becomes more reliable, due to the information from the previous iteration(s). Hence, the estimated samples become closer to the transmitted ones.

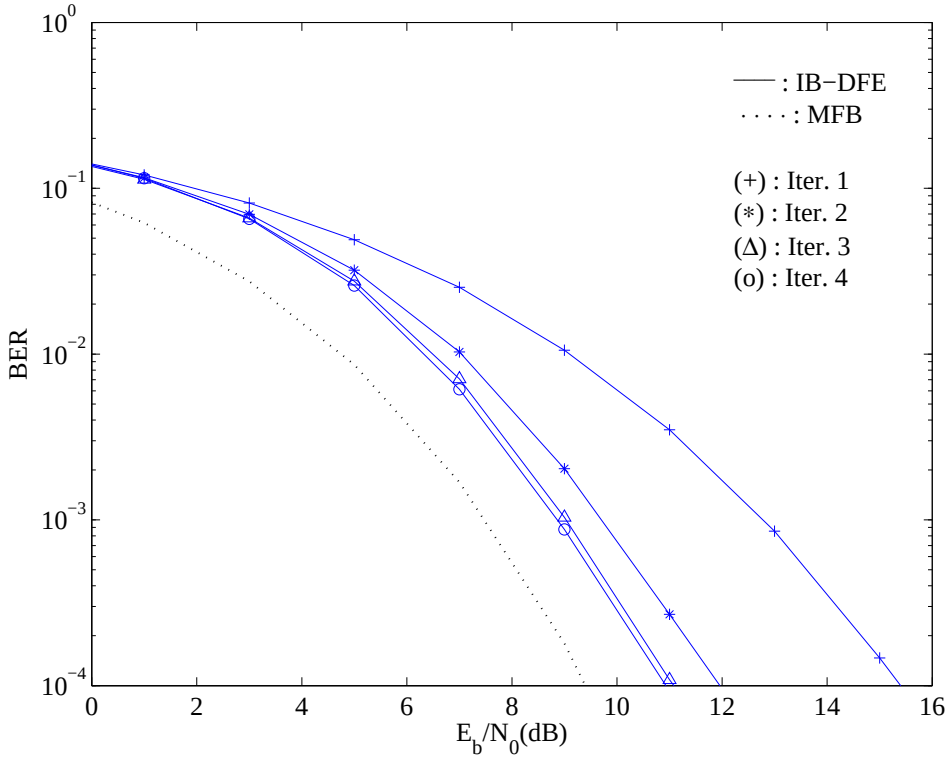

Figure 3.22: BER perfomance for an IB-DFE receiver with four iterations.

3.6.1 IB-DFE with Soft Decisions

It is possible to improve the performance of the IB-DFE receiver, by considering "soft decisions"instead of "hard decisions", which means that the "blockwise average"is substituted by "symbol averages". Hence, the $\hat{s}_n^{(i)}$ samples are substituted by soft decision samples $\bar{s}_n^{(i)}$. Under these assumptions equation 3.29 can take the form

$$\tilde{S}_k^{(i)} = F_k^{(i)} Y_k - B_k^{(i)} \bar{S}_k^{(i-1)}, \tag{3.45}$$

where

$$\bar{S}_k^{(i-1)} = \rho^{(i-1)} \hat{S}_k^{(i-1)}. \tag{3.46}$$

Since $\rho^{(i-1)}$ is a measure of the blockwise reliability of the estimates expressed by $\hat{S}_k^{(i-1)}$, then $\bar{S}_k^{(i-1)}$ represents the overall block average of $S_k^{(i-1)}$ at the output of the FDE processing. Considering a transmission system with respect to the use of a QPSK constellation, the symbols correspond to

$$s_n = \pm 1 \pm j = s_n^I + s_n^Q, \tag{3.47}$$

where

$$s_n^I = \mathrm{Re}\{s_n\} \tag{3.48}$$

and

$$s_n^Q = \mathrm{Im}\{s_n\}, \tag{3.49}$$

where the same applies to $\tilde{s}_n$, $\hat{s}_n$ and $\bar{s}_n$. Thus, the LogLikelihood Ratio (LLR) of the in-phase and quadrature bits, associated to s_n^I and s_n^Q,are given by

$$L_n^{I(i)} = \frac{2}{\sigma_i^2}\tilde{s}_n^{I(i)} \tag{3.50}$$

and

$$L_n^{Q(i)} = \frac{2}{\sigma_i^2}\tilde{s}_n^{Q(i)}, \tag{3.51}$$

respectively, with the total variance of channel and interference noise, σ_i^2, given by

$$\sigma_i^2 = \frac{1}{2}\mathbb{E}\left[\left|s_n - \tilde{s}_n^{(i)}\right|^2\right]. \tag{3.52}$$

Therefore, the conditional expectations associated with the data symbols are

$$\bar{s}_n^{(i)} = \tanh\left(\frac{L_n^{I(i)}}{2}\right) + j\tanh\left(\frac{L_n^{Q(i)}}{2}\right) = \rho_n^I\hat{s}_n^I + j\rho_n^Q\hat{s}_n^Q, \tag{3.53}$$

with the signs of L_n^I and L_n^Q defining the hard decisions $\hat{s}_n^I = \pm 1$ and $\hat{s}_n^Q = \pm 1$, respectively. In 3.53, ρ_n^I and ρ_n^Q denote the reliabilities related to the in-phase and quadrature bits of the n^{th} symbol, given by

$$\rho_n^{I(i)} = \left|\tanh\left(\frac{L_n^{I(i)}}{2}\right)\right| \tag{3.54}$$

and

$$\rho_n^{Q(i)} = \left|\tanh\left(\frac{L_n^{Q(i)}}{2}\right)\right|. \tag{3.55}$$

Intuitively, for the first iteration $\rho_n^{I(0)} = \rho_n^{Q(0)} = 0$, and consequently $\bar{s}_n = 0$. Lastly, the correlation coefficient employed in the feedforward is expressed by

$$\rho^{(i)} = \frac{1}{2N}\sum_{n=0}^{N-1}\left(\rho_n^{I(i)} + \rho_n^{Q(i)}\right). \tag{3.56}$$

The receiver structure for the IB-DFE with soft decisions, is illustrated in Fig. 3.23. It can be noted that the receiver that employs blockwise reliabilities is referred as IB-DFE with hard decisions, while the receiver that employs symbol reliabilities is referred as IB-DFE with soft decisions. The feedforward coefficients used in both types of IB-DFE receivers are given by 3.42, however the feedback loop of the IB-DFE with hard decisions uses the estimated data block, weighted by a reliability coefficient common to the entire block, while for IB-DFE with soft decisions the feedback loop uses a different reliability coefficient for each symbol. Fig. 3.24 shows the BER performance for an IB-DFE receiver when soft decisions are considered. Clearly, by taking into account symbols estimates instead of block estimates the performance is improved.

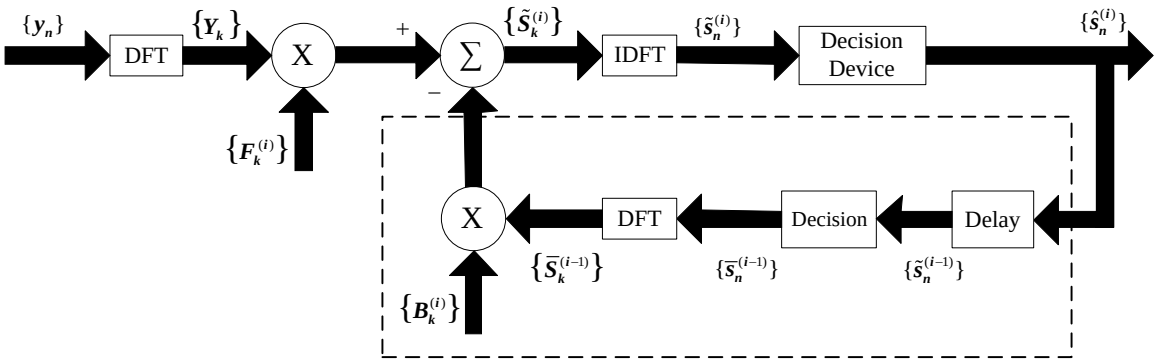

Figure 3.23: IB-DFE receiver block diagram with soft decisions from the FDE output in the feedback loop.

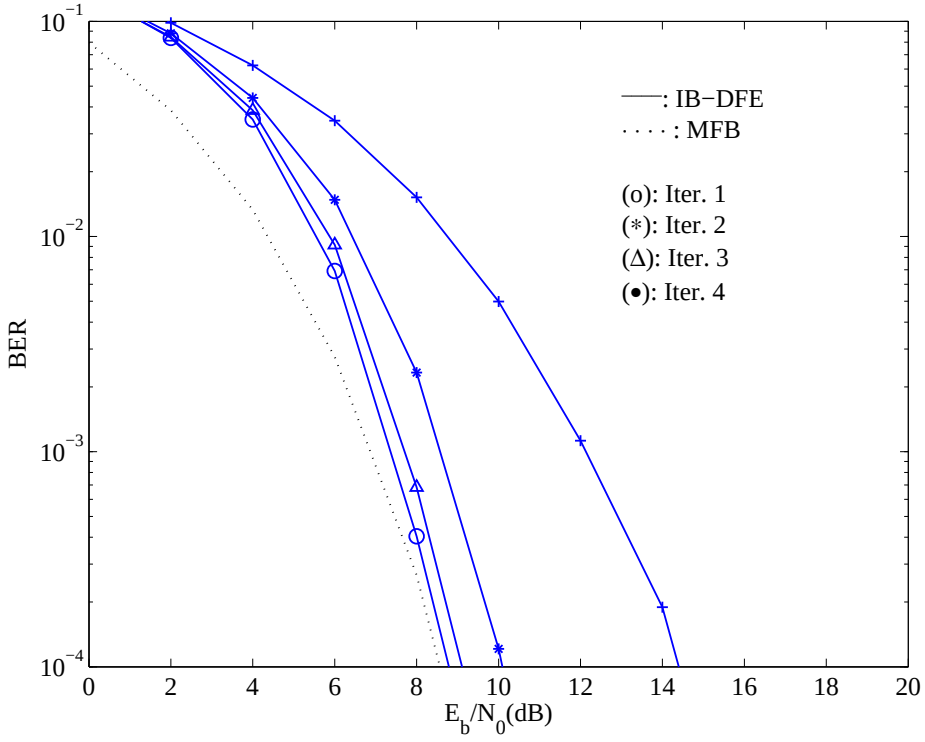

Figure 3.24: BER perfomance for an IB-DFE receiver with four iterations using soft decisions.

3.7 Correlation Coefficient Estimation

As previously mentioned in section 3.6, the ρ factor indicates an important parameter that is included in feedback loop, that corresponds to a blockwise reliability measure of the symbol's estimates. It indicates how good the estimation is and it influences the estimation of the new estimates in order to improve them. This is done by reducing the propagation of the errors that are inherent to the estimation process.

3.7.1 Correlation Coefficient Definition

The correlation coefficient was first defined in (3.35). For convenience and simplicity purposes, the expression of the ρ factor is reproduced in (3.57) as

$$\rho = \frac{\mathbb{E}\left[\hat{S}_k S_k^*\right]}{\mathbb{E}\left[|S_k|^2\right]} = \frac{\mathbb{E}\left[\hat{s}_n s_n^*\right]}{\mathbb{E}\left[|s_n|^2\right]}. \tag{3.57}$$

Being the transmitted symbols s_n selected from a QPSK constellation scheme under a Gray mapping rule, with $\{s_n; n = 0, ..., N-1\}$, s_n can be expressed as

$$s_n = s_n^I + s_n^Q = \pm d \pm jd. \tag{3.58}$$

Furthermore,

$$s_n^I = \mathrm{Re}\{s_n\} \tag{3.59}$$

and

$$s_n^Q = \mathrm{Im}\{s_n\} \tag{3.60}$$

are the in-phase and quadrature of s_n, respectively. In (3.58), d is given by

$$d = \frac{D}{2}, \tag{3.61}$$

where D indicates the minimum Euclidean distance between two constellation symbols of s_n. Hence,

$$\mathbb{E}\left[|s_n|^2\right] = \frac{D^2}{4}. \tag{3.62}$$

Considering the FDE's output samples, in the time-domain,

$$\tilde{s}_n = \tilde{s}_n^I + \tilde{s}_n^Q = s_n + \phi_n, \tag{3.63}$$

where ϕ_n is the overall error term, which is zero-mean Gaussian-distributed. The symbol estimates can be written as

$$\hat{s}_n = s_n + \vartheta_n^I + j\vartheta_n^Q, \tag{3.64}$$

where ϑ_n^I and ϑ_n^Q denote the error coefficient in $\hat{s}_n^I$ and $\hat{s}_n^Q$, respectively. In the absence of errors of $\hat{s}_n^I$ and $\hat{s}_n^Q$, then ϑ_n^I and ϑ_n^Q are null and otherwise they correspond to $\pm D$. As a consequence, ϑ_n^I and ϑ_n^Q can be considered as random variables, valued as 0 and $\pm D$ with

probabilities $1-2P_b$ and P_b, respectively. Additionally, P_b indicates a BER measure and it can be shown that

$$\rho = 1 - 2P_b. \tag{3.65}$$

Since, in practice it is not possible to know the transmitted symbols $s_n\{n = 0, ..., N-1\}$, the ρ correlation coefficient must be estimated.

3.7.2 Correlation Coefficient Estimation

In subsection 3.6.1 the ρ derivation concerning the LLRs method was already described. However, it is necessary to consider an approximated expression for the channel and interference noise variance, instead of its optimum value. Since the value of s_n is unknown, then an expression for the channel plus interference noise variance must be estimated. Therefore, σ_i^2, firstly expressed in (3.52) as

$$\sigma_i^2 = \frac{1}{2}\mathbb{E}\left[|s_n - \tilde{s}_n|^2\right] \tag{3.66}$$

can be written as

$$\hat{\sigma}_i^2 = \frac{1}{2N}\sum_{n=0}^{N-1}|\hat{s}_n - \tilde{s}_n|^2. \tag{3.67}$$

Then, the computation of the LLRs of the in-phase and quadrature bit, associated to s_n^I and s_n^Q, respectively, are given by

$$\hat{L}_n^I = \frac{2}{\hat{\sigma}_i^2}\tilde{s}_n^I \tag{3.68}$$

and

$$\hat{L}_n^Q = \frac{2}{\hat{\sigma}_i^2}\tilde{s}_n^Q. \tag{3.69}$$

For the n^{th} symbol, the estimated reliability related to the in-phase and quadrature bits are written as

$$\hat{\rho}_n^I = \left|\tanh\left(\frac{\hat{L}_n^I}{2}\right)\right| \tag{3.70}$$

and

$$\hat{\rho}_n^Q = \left|\tanh\left(\frac{\hat{L}_n^Q}{2}\right)\right|. \tag{3.71}$$

Then, the estimated value of the correlation coefficient $\hat{\rho}$ is expressed by

$$\hat{\rho} = \frac{1}{2N}\sum_{n=0}^{N-1}\left(\hat{\rho}_n^I + \hat{\rho}_n^Q\right). \tag{3.72}$$

Fig. 3.25 shows the comparison for the value of σ_i^2 considering the real approach, i.e., when computed as in (3.66) and an estimated value following the expression in (3.67). Clearly, $\hat{\sigma}_i^2$ provides a more optimistic value for the channel and interference noise variance for lower values of $Eb/N0$. On the other hand, for higher values of $Eb/N0$ both approaches have practically the same value.

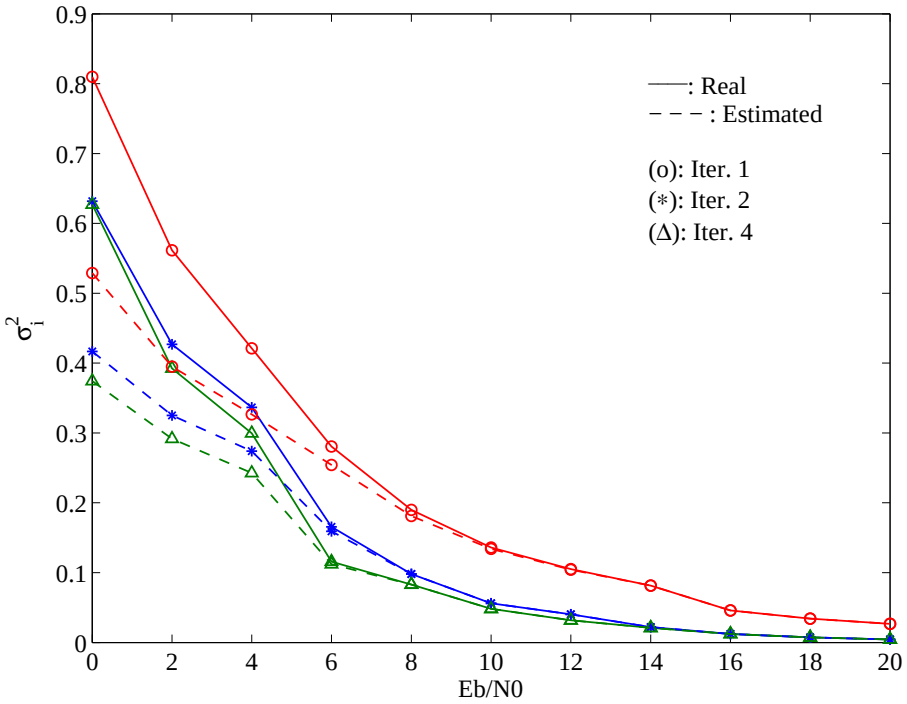

Figure 3.25: Comparison between σ_i^2 (with s_n) and $\hat{\sigma}_i^2$ (with $\hat{s}_n$).

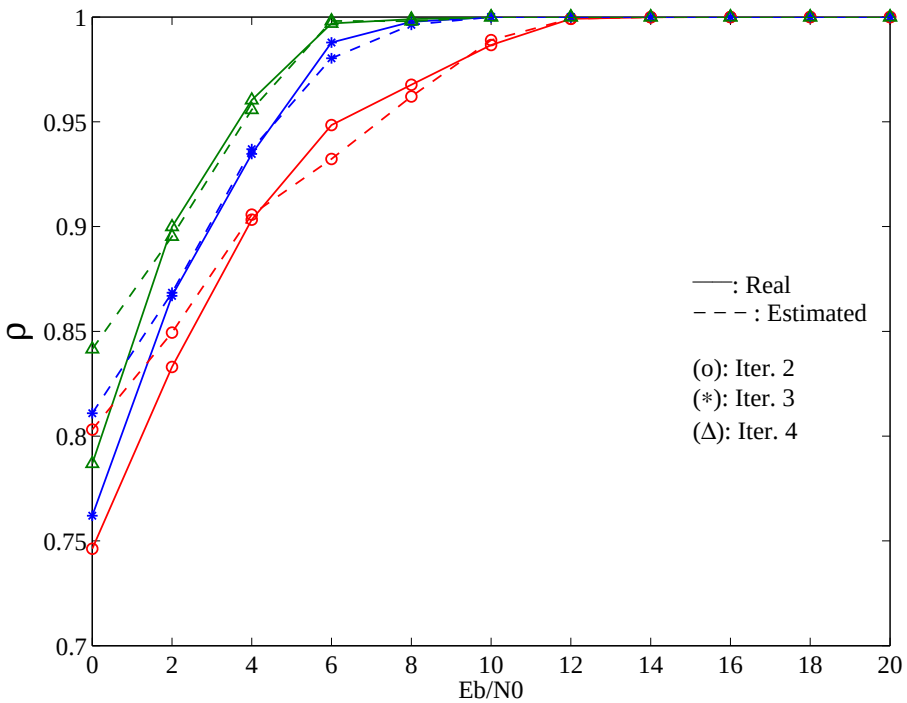

Figure 3.26: Comparison between ρ (with s_n) and $\hat{\rho}$ (with $\hat{s}_n$).

In Fig. 3.26 the comparison between the value of ρ considering the real value and an estimated version is shown. Similarly to the case presented in Fig. 3.25 with σ_i^2, with the ρ the estimation is more optimistic. Nevertheless, for medium and/or higher values of $Eb/N0$, the estimation is very accurate.

CHAPTER 4

Base Station Cooperation Systems

Chapter 3 presented an overview on multi-carrier and single carrier modulations schemes, as well as the signals related to each scheme, with OFDM modulations as an example for multi-carrier signals and SC-FDE for single carrier. Also, in chapter 3, it was shown that block transmission techniques, with appropriate cyclic prefixes and employing FDE techniques, are suitable for high data rate transmission over severely time dispersive channels. Normally, the receiver for SC-FDE schemes is a linear FDE. However, it is known that nonlinear equalizers outperform linear ones, like those based on the IB-DFE. The IB-DFE receiver can be considered as an iterative FDE receiver in which the feedforward and the feedback operations are implemented in the frequency-domain, where the iteration nature of the receiver offers better performance. Finally, chapter 3 demonstrated the difference in considering an IB-DFE receiver with soft decisions as opposed to using hard decisions when estimating the transmitted symbols and/or blocks of symbols.

This chapter presents a cellular architecture approach where IB-DFE receivers are considered where these receivers are implemented at the base station level. One of the main objectives present in chaper 4 is to extend the SC-FDE with the IB-DFE concept to a MIMO environment. Also, chapter 4 presents the deduction of the main parameters that are part of the multi-user detection process and provides an analytical method for obtaining the BER performance in BS cooperation systems.

Chapter 4 is organized as follows: Section 4.1 presents a system overview and section 4.2 characterizes the BS cooperation architecture in a block diagram with all the main elements explained. In section 4.3 the multi-user separation and/or detection process is detailed. Sections 4.4 and 4.5 provide a conventional and improved methods for obtaining the BER performance, respectively.

4.1 Base Station Cooperation Cellular Systems Overview

BS cooperation systems allow the increase of spectral-efficiency through the cooperation of the network elements, namely BS and MT. Then, efficient interference management and/or interference cancelation algorithms are desirable, especially for users at the cell edge, where the interference phenomenon is more active. In order to achieve better spectral efficiency, and because spectral resources are scarce and expensive, the frequency reuse must be well managed, and ultimately, a universal frequency reuse is desired.

In conventional cellular architectures different cells are regarded as separate entities and each MT is assigned to a given cell (and, consequently, a given BS). The MT transmits its signals to the corresponding BS and when this signal is received by another BS it is regarded as interference. Fig. 4.1 illustrates a BS cooperation architecture, where the signals between different MTs and BSs are collected and processed by a CPU so as to perform the user separation and/or interference mitigation. In the uplink transmission (i.e., the link from the MTs to the BSs) the overall signals received by different BSs (with contributions from all MTs) are sent to the CPU that performs the signal separation to extract the data blocks transmitted by each MT before sending them to the corresponding BS. In the downlink transmission (i.e., the link from the BSs to the MTs) of BS cooperation schemes this is usually achieved by appropriate pre-processing schemes [32, 33]. BS cooperation

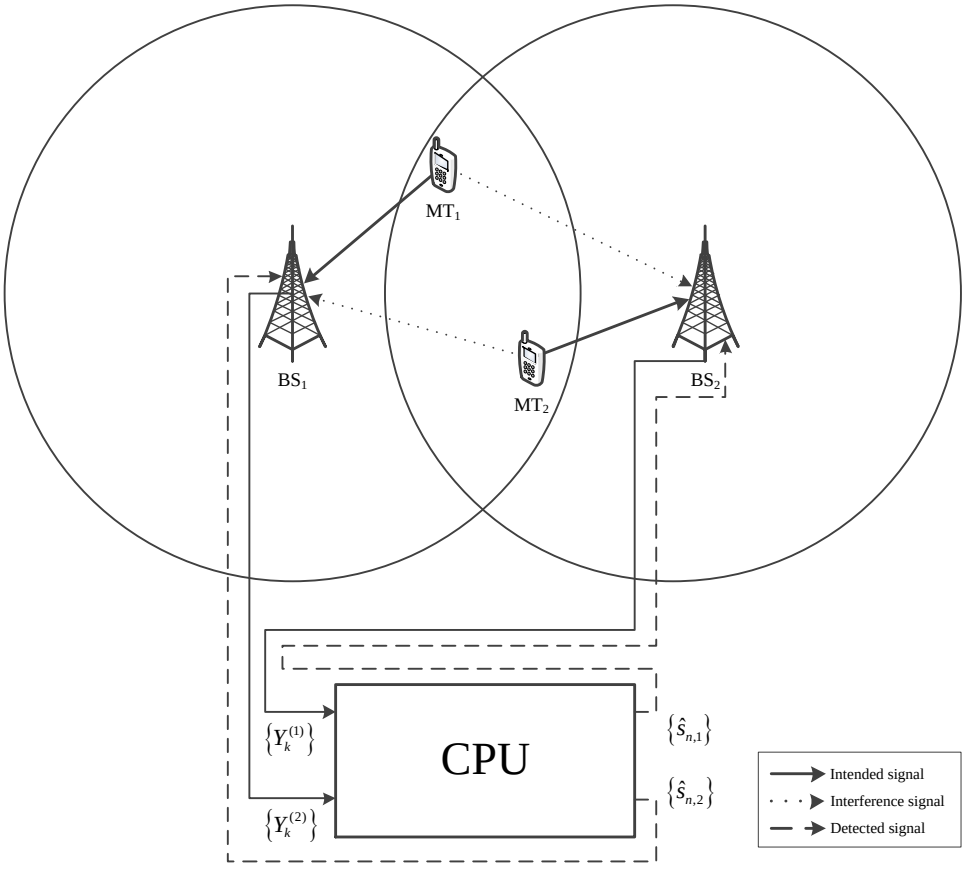

Figure 4.1: Conventional Base Station cellular scenario

schemes involve interference mitigation, allowing the use of the same physical channel by MTs in adjacent cell, which means that the overall system capacity can be significantly improved. Moreover, BS cooperation schemes also have an inherent macro-diversity nature due to the use of widely spaced antennas, allowing improved overall coverage with reduced transmit power requirements. In the next section, the BS cooperation macro-diversity effects are related to the IB-DFE receiver's concept and the BS cooperation system is characterized in what signal's processing is concerned.

4.2 System Characterization

Firstly, it is important to relate the BS cooperation system with the IB-DFE receivers nature, especially in terms of several transmitting MTs and several receiving BSs. Then, as illustrated in Fig. 4.2, this is the IB-DFE receiver presented in Fig. 3.20, now extended to a macro-diversity scenario. The system is characterized by having partially overlapping

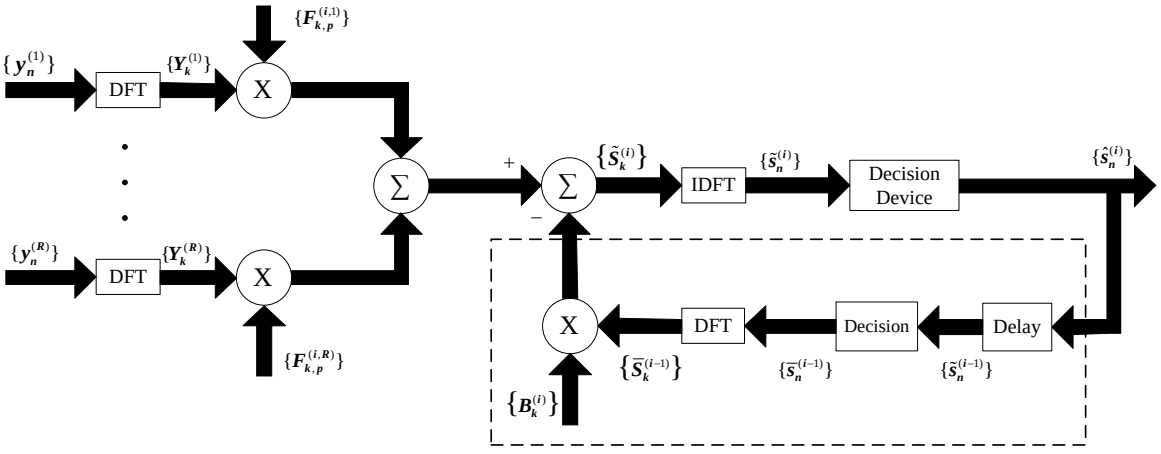

Figure 4.2: IB-DFE block diagram structure with macro-diversity.

cells, each one associated to a given BS, where P MTs share the same physical channel (i.e., they transmit simultaneously at the same frequency band) with R BSs receiving their signals which can cooperate to improve the overall system performance. Each MT employs a SC-FDE modulation scheme with an appropriate CP being appended to each data block. Assuming that initially we have free inter-cluster interference, if the CP (Cyclic Prefix) has the correct length, at a given BS r the received signal is defined by

$$Y_k^{(r)} = \sum_{p=1}^{P} S_{k,p} H_{k,p}^{eq(r)} + N_k^{(r)}, \tag{4.1}$$

where $N_k^{(r)}$ denotes the channel noise at the r^{th} $(r = 1, 2, ..., R)$ antenna and the k^{th} $(k = 0, 1, ..., N-1)$ frequency and

$$H_{k,p}^{eq(r)} = \xi_{p,r} H_{k,p}^{(r)}, \tag{4.2}$$

where $H_{k,p}^{(r)}$ denotes the channel frequency response between the p^{th} ($p = 1, 2, ..., P$) MT and the rth for the k^{th} frequency. Clearly, expression 4.1 is an extension of 3.11, described in the previous chapter, when the receiver regarding the basic transmission chain of SC-FDE schemes was explained. The coefficient $\xi_{p,r}$ is a weighting factor that accounts for the combined effects of power control and propagation losses, i.e., the average received power associated to the p^{th} MT at the r^{th} BS is $\left|\xi_p^{(r)}\right|^2$ (without loss of generality, we assume a normalized channel frequency response, i.e., $\mathbb{E}\left[\left|H_{k,p}^{(r)}\right|^2\right] = 1$).

The transmission and reception schemes can be seen as a MIMO environment (see Fig. 4.3), with $P \geq R$. So, when several BSs and MTs are considered, the IB-DFE detection

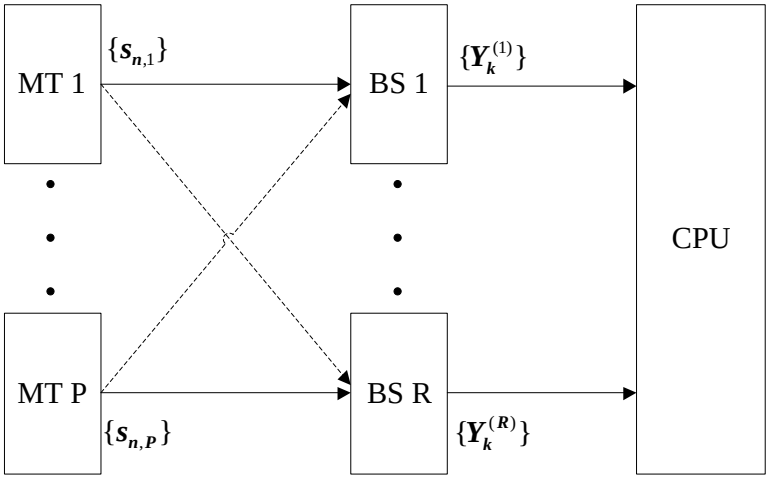

Figure 4.3: BS cooperation MIMO based scheme.

scheme for the p^{th} MT is presented in Fig. 4.4, and 4.1 can be extended to a matrix format, equivalent to

$$\mathbf{Y}_k = \mathbf{H}_k^T \mathbf{S}_k + \mathbf{N}_k, \tag{4.3}$$

with

$$\mathbf{Y}_k = \begin{bmatrix} Y_k^{(1)} \\ \vdots \\ Y_k^{(R)} \end{bmatrix}, \tag{4.4}$$

$$\mathbf{S}_k = \begin{bmatrix} S_{k,1} \\ \vdots \\ S_{k,P} \end{bmatrix}, \tag{4.5}$$

$$\mathbf{N}_k = \begin{bmatrix} N_k^{(1)} \\ \vdots \\ N_k^{(R)} \end{bmatrix}, \tag{4.6}$$

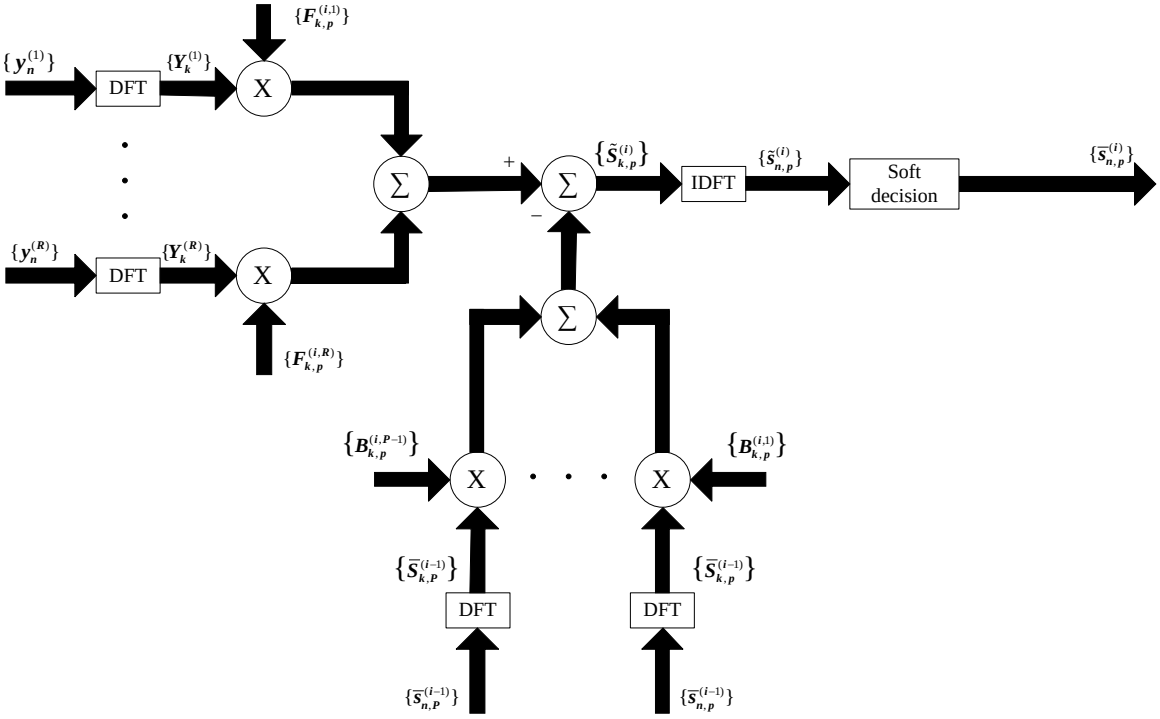

Figure 4.4: IB-DFE block diagram for the detection of the p^{th} MT.

and

$$\mathbf{H}_k^T = \begin{bmatrix} H_{k,1}^{eq^{(1)}} & \cdots & H_{k,P}^{eq^{(1)}} \\ \vdots & \ddots & \vdots \\ H_{k,1}^{eq^{(R)}} & \cdots & H_{k,P}^{eq^{(R)}} \end{bmatrix}, \tag{4.7}$$

where each variable possesses the total contributions from all MTs and/or BSs.

4.3 Iterative Frequency-Domain Multi-User Separation

This section presents, in detail, the component aspects of the receiver design concerning BS cooperation and considering an iterative frequency-domain receiver based on IB-DFE processing, where the several MTs are detected and their signals separated. Different users should be ordered according to the signal-to-noise plus overall interference (including residual ISI and residual inter-user interference) at the FDE output, but usually there is strong correlation with the overall power associated to that MT, so MTs are sorted according to their overall power, given by

$$\sum_{k=1}^{N-1} \sum_{r=1}^{R} \left| \xi_{p,r} H_{k,p}^{(r)} \right|^2. \tag{4.8}$$

The considered iterative receiver is highly robust to the detection order, provided that the number of iterations is high enough. In fact, the main advantage of a proper detection order is that, typically it is possible to slightly reduce the number of required iterations for best performance. For each iteration the MTs are detected in a successive way, using the

most updated estimates of the transmitted data symbols associated to each MT to cancel the corresponding residual interference. Therefore, this IB-DFE receiver can be regarded as an iterative Successive Interference Cancelation (SIC) scheme, as demonstrated in Fig. 4.5. However, as with conventional IB-DFE receivers, the reliability of data estimates

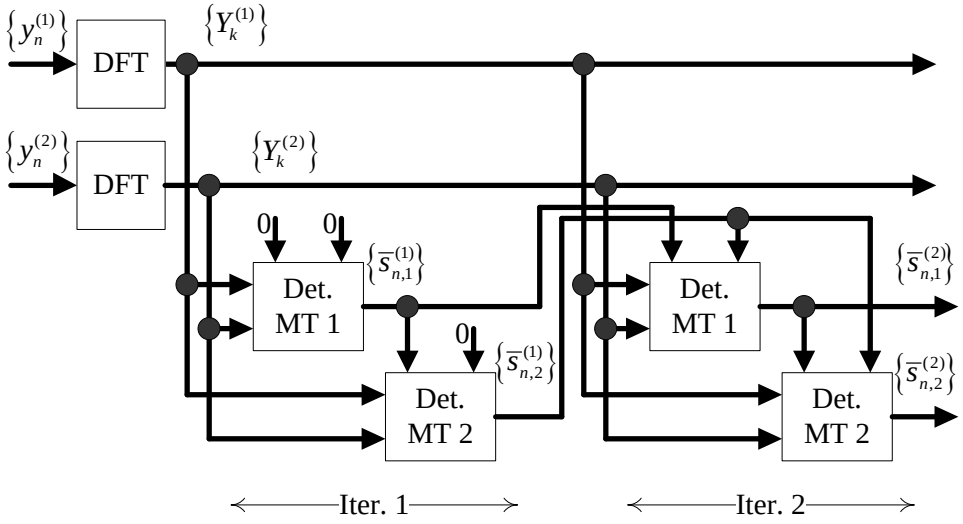

Figure 4.5: Iterative receiver structure for P = 2 MTs and R = 2 cooperating BSs.

associated to MTs for each detection (and interference cancelation) procedure is taken into account.

When detecting the p^{th} MT, at the i^{th} iteration, the estimated symbols $\{\hat{s}_{n,p}^{(i)}; n = 0,1,...,N-1\}$ are the hard decisions of the time-domain detector output $\{\tilde{s}_{n,p}^{(i)}; n = 0,1,...,N-1\}$ = IDFT $\{\tilde{S}_{k,p}^{(i)}; k = 0,1,...,N-1\}$, where $\tilde{S}_{k,p}^{(i)}$ is given by

$$\tilde{S}_{k,p}^{(i)} = \mathbf{F}_{k,p}^{(i)^T}\mathbf{Y}_k - \mathbf{B}_{k,p}^{(i)^T}\bar{\mathbf{S}}_{k,p}^{(i-1)}, \tag{4.9}$$

with

$$\mathbf{F}_{k,p}^{(i)^T} = \left[F_{k,p}^{(i,1)},...,F_{k,p}^{(i,R)}\right] \tag{4.10}$$

and

$$\mathbf{B}_{k,p}^{(i)^T} = \left[B_{k,p}^{(i,1)},...,B_{k,p}^{(i,P)}\right] \tag{4.11}$$

denoting the feedfoward and feedback coefficients, respectively. The $\bar{\mathbf{S}}_{k,p}^{(i-1)}$ vector is expressed by

$$\bar{\mathbf{S}}_{k,p}^{(i-1)} = \left[\bar{S}_{k,1}^{(i)}, \bar{S}_{k,p-1}^{(i)}, \bar{S}_{k,p}^{(i-1)},..., \bar{S}_{k,P}^{(i-1)}\right]^T \tag{4.12}$$

where the block $\{\bar{S}_{k,p}^{(i)}; k = 0,1,...,N-1\}$ is the DFT of the block with the time-domain average values conditioned by the detector output $\{\bar{s}_{n,p}^{(i)}; n = 0,1,...,N-1\}$ for user p and iteration i. The elements of $\bar{\mathbf{S}}_{k,p}^{(i-1)}$ are associated to the soft decisions of the current iteration for MTs already estimated in this iteration and the previous iteration for the MT currently being detected, as well as the MTs that were not yet detected in the current

iteration. This is a natural consequence of the SIC nature of the iterative receiver. As in expression 3.46, it can be shown that

$$\bar{\mathbf{S}}_k^{(i-1)} \simeq \mathbf{P}^{(i-1)} \hat{\mathbf{S}}_k^{(i-1)}, \tag{4.13}$$

where

$$\mathbf{P}^{(i-1)} = \mathrm{diag}(\rho_1^{(i-1)}, ..., \rho_P^{(i-1)}) \tag{4.14}$$

with the correlation coefficient $\rho_p^{(i-1)}$ defined previously in 3.35. Moreover, $\hat{\mathbf{S}}_k^{(i-1)}$ corresponds to

$$\hat{\mathbf{S}}_k^{(i-1)} \approx \mathbf{P}^{(i-1)} \mathbf{S}_k + \mathbf{\Delta}_k, \tag{4.15}$$

where

$$\mathbf{\Delta}_k = \left[\Delta_{k,1}, ..., \Delta_{k,P}\right]^T \tag{4.16}$$

is a zero mean and uncorrelated with $\mathbf{P}^{(i-1)}$. For the first iteration, i.e. $i = 1$, $\bar{\mathbf{S}}_k^{(0)}$ is a null vector and $\mathbf{P}^{(0)}$ is a null matrix.

Coefficients $\mathbf{F}_{k,p}$ and $\mathbf{B}_{k,p}$ are chosen in order to maximize the SINR for each user p, at a given iteration, defined by

$$\mathrm{SINR}_p = \frac{|\gamma_p|^2 \, \mathbb{E}\left[\left|S_{k,p}\right|^2\right]}{\mathbb{E}\left[\left|\Theta_{k,p}\right|^2\right]}, \tag{4.17}$$

where $\Theta_{k,p}$ designates the MSE of the frequency-domain samples $\tilde{S}_{k,p}$ expressed by

$$\Theta_{k,p} = \mathbb{E}\left[\left|\tilde{S}_{k,p} - S_{k,p}\right|^2\right] = \mathbb{E}\left[\left|\mathbf{F}_k^T \mathbf{Y}_k - \mathbf{B}_k^T \bar{\mathbf{S}}_k - \mathbf{S}_k\right|^2\right]. \tag{4.18}$$

Maximizing the SINR is equivalent to minimizing $\mathbb{E}\left[\left|\Theta_{k,p}\right|^2\right]$. Knowing that the definition of the expected value can be written as

$$\mathbb{E}\left[\left|\tilde{S}_{k,p}\right|^2\right] = \mathbb{E}\left[\left|\tilde{S}_{k,p}^* \tilde{S}_{k,p}\right|^2\right] \tag{4.19}$$

and that the following matrix manipulations are possible

$$a^T b = b^T a, \tag{4.20}$$

$$a^H b = b^T a^* \tag{4.21}$$

and

$$a^H = (a^*)^T, \tag{4.22}$$

then the MSE can be expressed as

$$MSE_{k,p} = \mathbb{E}\left[\left(\mathbf{F}^H \mathbf{Y}^* - \mathbf{B}^H \bar{\mathbf{S}}^* - S_p^*\right)\left(\mathbf{Y}^T \mathbf{F} - \bar{\mathbf{S}}^T \mathbf{B} - S_p\right)\right]. \tag{4.23}$$

Furthermore, 4.23 can be written as

$$\begin{aligned} MSE_{k,p} = &\mathbb{E}\left[\mathbf{F}^H\mathbf{Y}^*\mathbf{Y}^T\mathbf{F}\right] + \mathbb{E}\left[\mathbf{B}^H\bar{\mathbf{S}}^*\bar{\mathbf{S}}^T\mathbf{B}\right] + \mathbb{E}\left[S_p^*S_p\right] \\ &- \mathbb{E}\left[\mathbf{F}^H\mathbf{Y}^*\bar{\mathbf{S}}^T\mathbf{B} + \mathbf{B}^H\bar{\mathbf{S}}^*\mathbf{Y}^T\mathbf{F}\right] \\ &- \mathbb{E}\left[\mathbf{F}^H\mathbf{Y}^*S_p + S_p^*\mathbf{Y}^T\mathbf{F}\right] \\ &+ \mathbb{E}\left[\mathbf{B}^H\bar{\mathbf{S}}^*S_p + S_p^*\bar{\mathbf{S}}^T\mathbf{B}\right]. \end{aligned} \tag{4.24}$$

It can be shown that the expected values in 4.24 are given by

$$\mathbb{E}\left[\mathbf{F}^H\mathbf{Y}^*\mathbf{Y}^T\mathbf{F}\right] = \mathbf{F}^H\mathbf{R}_{\mathbf{Y}}\mathbf{F}, \tag{4.25}$$

$$\mathbb{E}\left[\mathbf{B}^H\bar{\mathbf{S}}^*\bar{\mathbf{S}}^T\mathbf{B}\right] = \mathbf{B}^H\mathbf{R}_{\bar{\mathbf{S}}\bar{\mathbf{S}}}\mathbf{B}, \tag{4.26}$$

$$\mathbb{E}\left[S_p^*S_p\right] = \mathbf{R}_S, \tag{4.27}$$

$$\begin{aligned} \mathbb{E}\left[\mathbf{F}^H\mathbf{Y}^*\bar{\mathbf{S}}^T\mathbf{B} + \mathbf{B}^H\bar{\mathbf{S}}^*\mathbf{Y}^T\mathbf{F}\right] &= \mathbb{E}\left[\mathbf{B}^H\bar{\mathbf{S}}^*\mathbf{Y}^T\mathbf{F} + \mathbf{Y}^H\mathbf{F}^*\mathbf{B}^T\bar{\mathbf{S}}\right] \\ &= \mathbb{E}\left[\mathbf{B}^H\bar{\mathbf{S}}^*\mathbf{Y}^T\mathbf{F} + \mathbf{B}^T\bar{\mathbf{S}}\mathbf{Y}^H\mathbf{F}^*\right] \\ &= 2\mathrm{Re}\{\mathbf{B}^H\mathbf{R}_{\bar{\mathbf{S}}\mathbf{Y}}\mathbf{F}\}. \end{aligned} \tag{4.28}$$

Moreover,

$$\mathbb{E}\left[\mathbf{B}^H\bar{\mathbf{S}}^*S_p + S_p^*\bar{\mathbf{S}}^T\mathbf{B}\right] = 2\mathrm{Re}\{\mathbf{B}^H\mathbf{R}_{\bar{\mathbf{S}}S_p}\} \tag{4.29}$$

and

$$\mathbb{E}\left[\mathbf{F}^H\mathbf{Y}^*S_p + S_p^*\mathbf{Y}^T\mathbf{F}\right] = 2\mathrm{Re}\{\mathbf{F}^H\mathbf{R}_{\mathbf{Y}S_p}\} \tag{4.30}$$

following the same logic shown in (4.28). Therefore, (4.24) is expressed as

$$\begin{aligned} MSE_{k,p} = &\mathbf{F}^H\mathbf{R}_Y\mathbf{F} + \mathbf{B}^H\mathbf{R}_{\bar{\mathbf{S}}\bar{\mathbf{S}}}\mathbf{B} + \mathbf{R}_S \\ &- 2\mathrm{Re}\{\mathbf{B}^H\mathbf{R}_{\bar{\mathbf{S}}\mathbf{Y}}\mathbf{F}\} \\ &+ 2\mathrm{Re}\{\mathbf{B}^H\mathbf{R}_{\bar{\mathbf{S}}S_p}\} \\ &- 2\mathrm{Re}\{\mathbf{F}^H\mathbf{R}_{\mathbf{Y}S_p}\}. \end{aligned} \tag{4.31}$$

The different correlation matrices are given by

$$\mathbf{R}_{\mathbf{Y}} = \mathbb{E}\left[\mathbf{Y}^*\mathbf{Y}^T\right] = \mathbf{H}^H\mathbf{R}_S\mathbf{H} + \mathbf{R}_N, \tag{4.32a}$$

$$\mathbf{R}_S = \mathbb{E}\left[\mathbf{S}^*\mathbf{S}^T\right] = 2\sigma_S^2\mathbf{I}_P, \tag{4.32b}$$

$$\mathbf{R}_N = \mathbb{E}\left[\mathbf{N}^*\mathbf{N}^T\right] = 2\sigma_N^2\mathbf{I}_R, \tag{4.32c}$$

$$\mathbf{R}_{\bar{\mathbf{S}}\bar{S}} = \mathbb{E}\left[\bar{\mathbf{S}}^*\bar{\mathbf{S}}^T\right] = \mathbf{P}^2\mathbf{R}_S, \tag{4.32d}$$

$$\mathbf{R}_{\mathbf{Y},S_p} = \mathbb{E}\left[\mathbf{Y}^*S_p\right] = \mathbf{H}^H\mathbf{R}_S\mathbf{e}_p, \tag{4.32e}$$

$$\mathbf{R}_{\bar{\mathbf{S}},S_p} = \mathbb{E}\left[\bar{\mathbf{S}}^*S_p\right] = \mathbf{P}^2\mathbf{R}_S\mathbf{e}_p, \tag{4.32f}$$

$$\mathbf{R}_{\bar{\mathbf{S}},\mathbf{Y}} = \mathbb{E}\left[\bar{\mathbf{S}}^{*}\mathbf{Y}^{T}\right] = \mathbf{P}^{2}\mathbf{R}_{S}\mathbf{H}, \tag{4.32g}$$

with σ_S^2 and σ_N^2 indicating the signal and noise variances, respectively. $\mathbf{I}_P$ is a $P \times P$ identity matrix and $\mathbf{e}_p$ is a column vector of size P with 0 in all positions except the p^{th} position that is 1. The minimization of the MSE provides the optimum $\mathbf{F}_{k,p}$ and $\mathbf{B}_{k,p}$ coefficients at each subcarrier $\Theta_{k,p}$. Defining the Lagrange function

$$J = \mathbb{E}\left[\left|\Theta_{k,p}\right|^{2}\right] + \lambda_p\left(\gamma_p - 1\right), \tag{4.33}$$

where $\{\lambda_p; p = 1, ..., P\}$ correspond to the Lagrange multipliers and assuming the condition

$$\gamma_p = \frac{1}{N}\sum_{k=0}^{N-1}\sum_{r=1}^{R} F_{k,p}^{(r)} H_{k,p}^{eq(r)} = 1, \tag{4.34}$$

the optimum coefficients $\mathbf{F}_k$ and $\mathbf{B}_k$ can be obtained by solving the system of equations

$$\begin{cases} \nabla_{\mathbf{F}} J = 0 \Longleftrightarrow \mathbf{R}_{\mathbf{Y}}\mathbf{F} - \mathbf{R}_{\mathbf{Y}S_p} - \mathbf{R}_{\bar{\mathbf{S}}\mathbf{Y}}^{H}\mathbf{B} + \lambda\mathbf{H}^{H}\mathbf{e}_p = 0 \\ \nabla_{\mathbf{B}} J = 0 \Longleftrightarrow \mathbf{R}_{\bar{\mathbf{S}}\bar{\mathbf{S}}}\mathbf{B} + \mathbf{R}_{\bar{\mathbf{S}}S_p} - \mathbf{R}_{\bar{\mathbf{S}}\mathbf{Y}}\mathbf{F} = 0 \\ \nabla_{\lambda} J = 0 \Longleftrightarrow \gamma_{\mathbf{p}} = \mathbf{1}. \end{cases} \tag{4.35}$$

Knowing the following rules for the gradient of matrix products

$$\nabla_x\left(x^{H}Rx\right) = 2Rx, \tag{4.36a}$$

$$\nabla_x\left(x^{H}p\right) = \nabla_x\left(p^{T}x^{*}\right) = 2p, \tag{4.36b}$$

$$\nabla_x\left(p^{H}x\right) = \nabla_x\left(x^{T}p^{*}\right) = 0, \tag{4.36c}$$

$$\nabla_x\left(2\mathrm{Re}\{p^{H}x\}\right) = \nabla_x\left(p^{H}x + p^{T}x^{*}\right) = \nabla_x\left(\mathrm{Re}\{x^{H}p\}\right) = 2p, \tag{4.36d}$$

the optimum coefficients are given by

$$\mathbf{F} = \kappa\mathbf{\Lambda}\mathbf{H}^{H}\mathbf{e}_p \tag{4.37}$$

and

$$\mathbf{B} = \mathbf{H}\mathbf{F} - \mathbf{e}_p, \tag{4.38}$$

with

$$\mathbf{\Lambda} = \left(\mathbf{H}^{H}\left(\mathbf{I}_P - \mathbf{P}^{2}\right)\mathbf{H} + \frac{1}{SNR}\mathbf{I}_R\right)^{-1}, \tag{4.39}$$

and κ selected to ensure that $\gamma_p = 1$, in order to have a normalized FDE with $\mathbb{E}\left[\tilde{s}_{n,p}\right] = s_{n,p}$.

Particularizing for a given iteration, if only one MT is considered ($P = 1$) the optimum values are given by

$$F_{k,p}^{(r)} = \frac{\kappa H_{k,p}^{eq(r)*}}{NSR + \sum_{r'=1}^{R}\left|H_{k,p}^{eq(r')}\right|^{2}} \tag{4.40}$$

and

$$B_{k,p} = \sum_{r'=1}^{R} F_{k,p}^{(r')} H_{k,p}^{eq(r')} - 1. \tag{4.41}$$

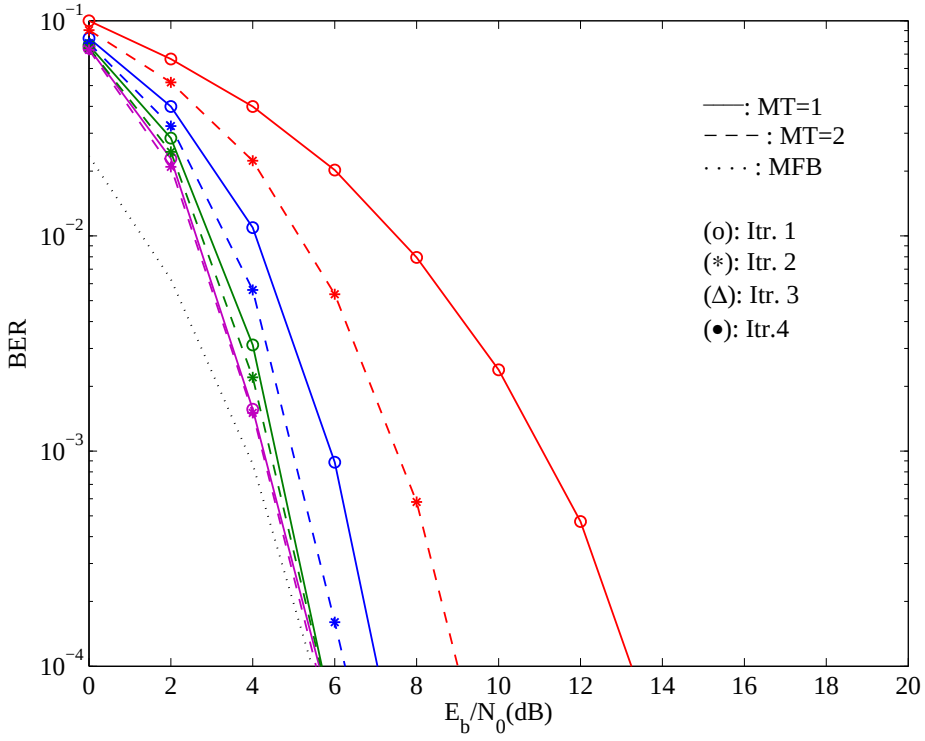

Figure 4.6: BER performance for a BS cooperation scenario with $P = 2$ MTs and $R = 2$ BSs.

Fig. 4.6 illustrates the BER performance in a BS cooperation case where $P = 2$ MTs transmitting information to the corresponding $R = 2$ BSs are considered, with the scenario presented in Fig. 4.1. For MT p and BS r, the power associated with the different links $\xi_{p,r}$ is given by

$$\mathbf{\Xi} = \begin{bmatrix} \xi_{1,1} & \xi_{1,2} \\ \xi_{2,1} & \xi_{2,2} \end{bmatrix} = \begin{bmatrix} 0 & 0 \\ 0 & 0 \end{bmatrix} \text{ (dB)}. \tag{4.42}$$

It is clear that the BER performance improves significatively as the number of iterations progresses, being closer to the MFB just after 4 iterations. This is because the signals being detected, for both MTs, for the current iteration use the information from the previous ones, except for the first iteration. Being a process of successive detection and/or separation of MTs, the second one displays better performance as a consequence of being detected previously the first MT. It can be concluded that the presented iterative receiver is able to efficiently separate the MTs while taking advantage of the signal contributions associated to a given MT at each BS. Regarding the same cellular scenario previously presented, Fig. 4.7 depicts the BER performance for a case with strong interference between MTs at both BSs, expressed by

$$\mathbf{\Xi} = \begin{bmatrix} \xi_{1,1} & \xi_{1,2} \\ \xi_{2,1} & \xi_{2,2} \end{bmatrix} = \begin{bmatrix} -3 & -3 \\ -3 & -3 \end{bmatrix} \text{ (dB)}. \tag{4.43}$$

Here, both MTs are at the cell's edge and, as expected, in comparison with Fig. 4.6, the system exhibits a worst performance due to the strong interference. However, after

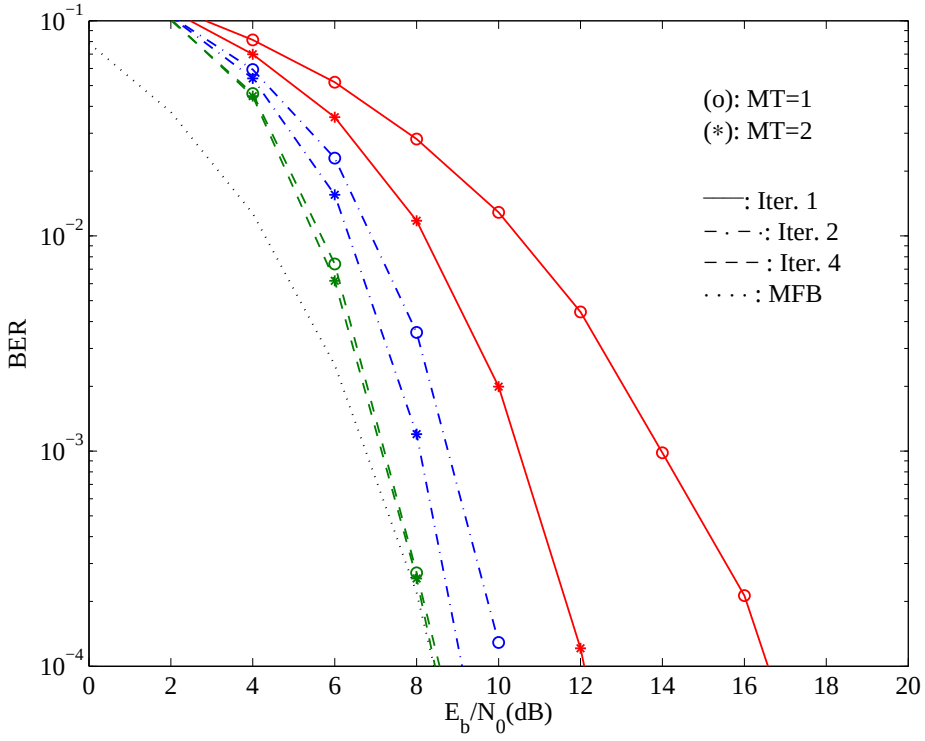

Figure 4.7: BER performance for a BS cooperation scenario with $P = 2$ MTs and $R = 2$ BSs.

4 iterations, the BER for both MTs is comparable. Furthermore, only iterations 1, 2 and 4 are presented, since from the third and fourth iterations there is not a considerable difference. Fig. 4.8 shows the BER performance for a BS cooperation scenario ($P = R = 2$), where there is one MT at the cell's edge and the other MT is closer to its BS. Considering perfect average power control, the links between each MT are given by

$$\mathbf{\Xi} = \begin{bmatrix} \xi_{1,1} & \xi_{1,2} \\ \xi_{2,1} & \xi_{2,2} \end{bmatrix} = \begin{bmatrix} -0 & -20 \\ -0 & -0 \end{bmatrix} \text{ (dB)}. \tag{4.44}$$

The performance for the second MT is better than for the first one because the power control does not take into account the fact that we are receiving two strong links, one at each BS.

4.4 Analytical BER Performance Evaluation

The previous section presented a performance result set for the BER measure concerning a BS cooperation scenario in a MIMO environment, which was obtained from a lengthly Monte Carlo simulation. Although Monte Carlo simulations are important, nevertheless a solid theoretical approach to the problem is desirable. This section presents a simple and accurate analytical model for obtaining the corresponding BER performance and the corresponding receiver optimization.

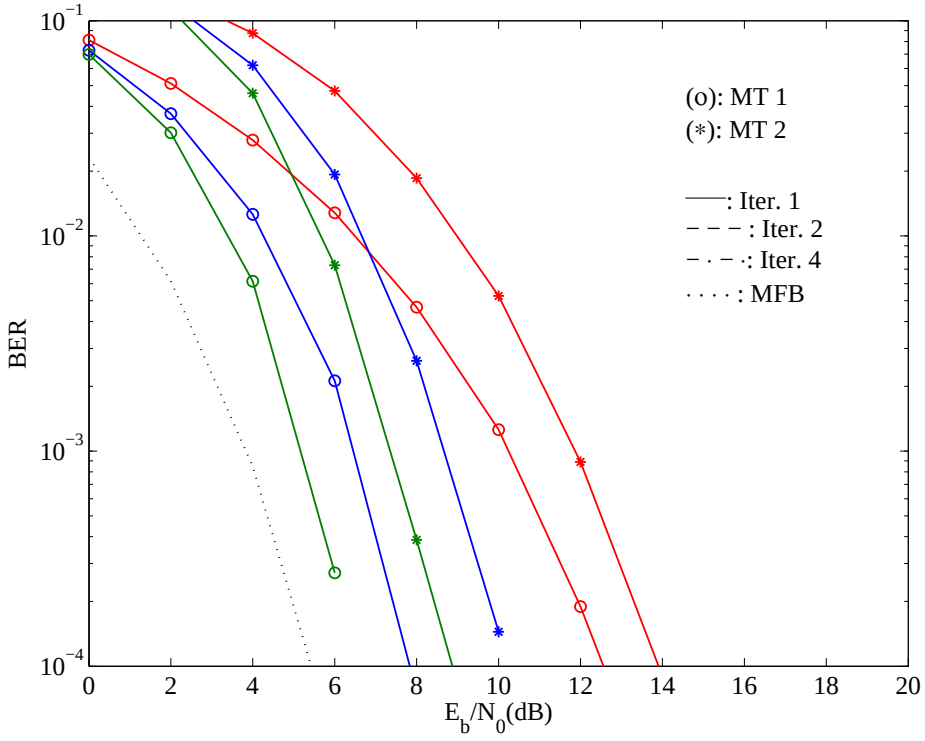

Figure 4.8: BER performance for a BS cooperation scenario with $P = 2$ MTs and $R = 2$ BSs.

A Gaussian-based approach is the starting point for the theoretical analysis for obtaining the BER performance. For a given iteration and for detecting the MT p, coefficients $\mathbf{F}_{k,p}$ and $\mathbf{B}_{k,p}$ specify the state of the iterative receiver. These coefficients are chosen to minimize MSE (Mean Squared Error) criterium also, minimizing the BER performance. These coefficients are selected to minimize the BER performance. Regarding a QPSK constellation with a Gray mapping scheme, the BER is given by

$$BER_p \simeq Q\left(\sqrt{\frac{1}{\theta_p}}\right), \tag{4.45}$$

where $Q(x)$ corresponds to the Gaussian error function and,

$$\theta_p = \frac{1}{N^2}\sum_{k=0}^{N-1}\Theta_{k,p}, \tag{4.46}$$

with

$$\Theta_{k,p} = \mathbb{E}\left[\left|\tilde{S}_{k,p} - S_{k,p}\right|^2\right] = \mathbb{E}\left[\left|\mathbf{F}_k^T\mathbf{Y}_k - \mathbf{B}_k^T\bar{\mathbf{S}}_k - \mathbf{S}_k\right|^2\right] \tag{4.47}$$

indicating the MSE on the frequency-domain samples $\tilde{S}_{k,p}$. Moreover, the optimum coefficients $\mathbf{F}_{k,p}$ and $\mathbf{B}_{k,p}$ are given by (4.37) and (4.38), respectively, and reproduced here by convenience

$$\mathbf{F} = \kappa\mathbf{\Lambda}\mathbf{H}^H\mathbf{e}_p \tag{4.48}$$

and

$$\mathbf{B} = \mathbf{HF} - \mathbf{e}_p, \tag{4.49}$$

with

$$\mathbf{\Lambda} = \left(\mathbf{H}^H \left(\mathbf{I}_P - \mathbf{P}^2\right)\mathbf{H} + \frac{1}{SNR}\mathbf{I}_R\right)^{-1}. \tag{4.50}$$

Having the theoretical BER defined, Fig. 4.9 (1st MT) and 4.10 (2nd MT) illustrate the BER performance containing the simulated and theoretical approaches. The channel

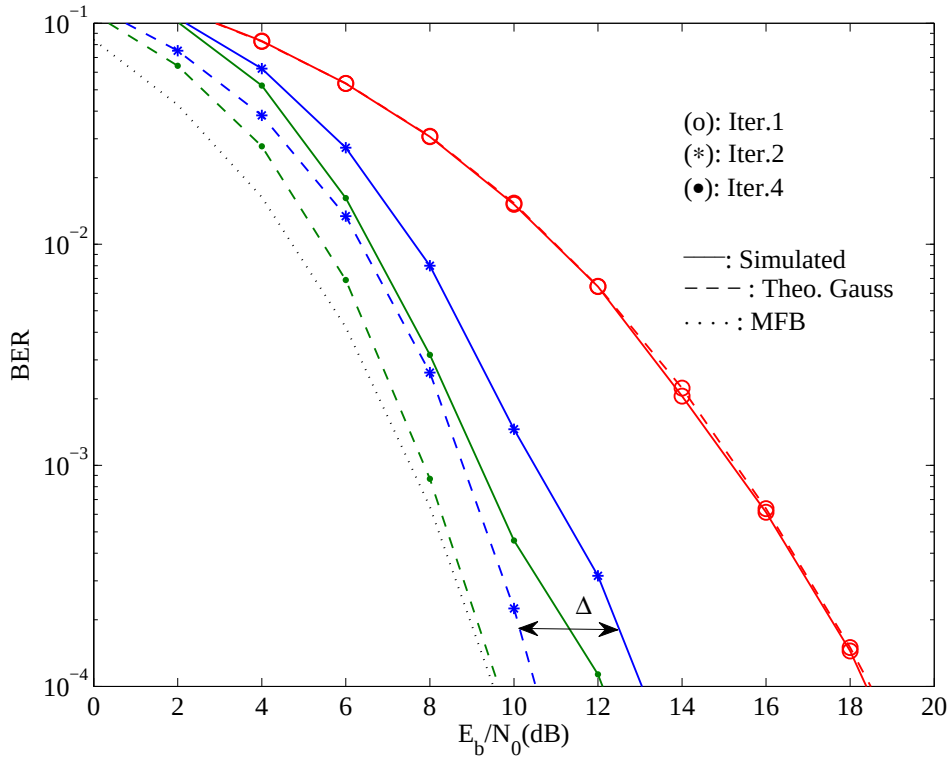

Figure 4.9: BER performance with 8 rays in the multipath environment (1st MT).

is a Rayleigh fading considering 8 rays multipath environment. Furthermore, Fig. 4.11 and 4.12, for the 1st and 2nd MTs, respectively, show the same results, this time with 32 multipath rays. Both MTs have the same power

$$\xi_{p,r} = \frac{\sqrt{2}}{2} \tag{4.51}$$

and the performance results are all compared with the Matched Filter Bound (MFB). Comparing the simulated and the analytical performances, there is a difference between them, corresponding to a value of Δ dB, except for the linear FDE case. Furthermore, the performance increases and approaches the MFB as the number of rays in the multipath increases.

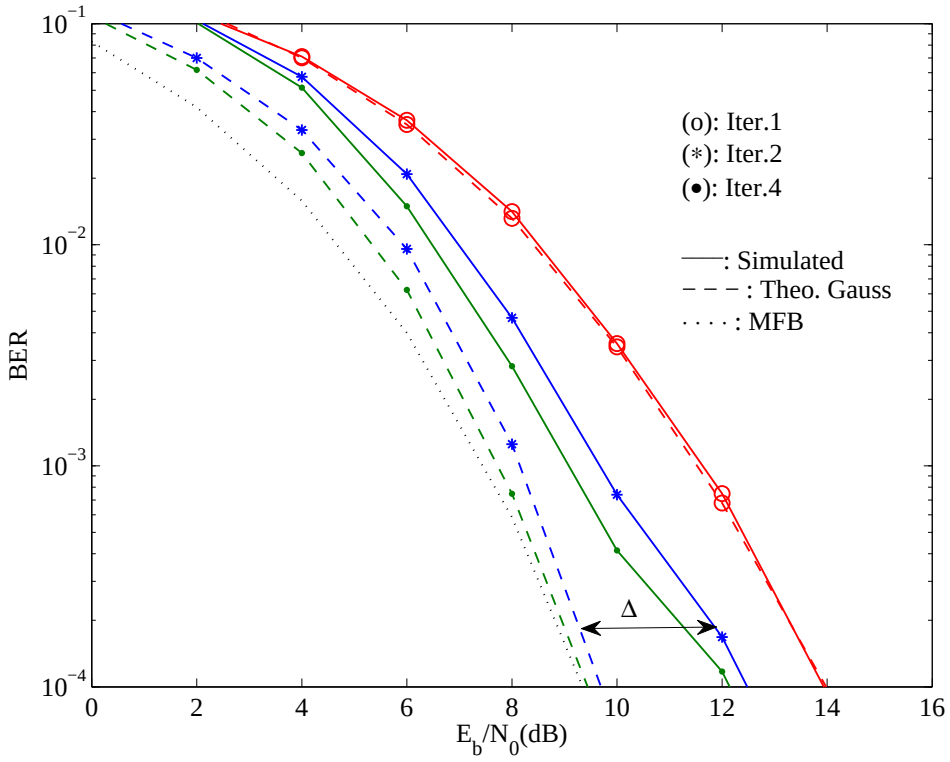

Figure 4.10: BER performance with 8 rays in the multipath environment ($2^{\mathbf{nd}}$ MT).

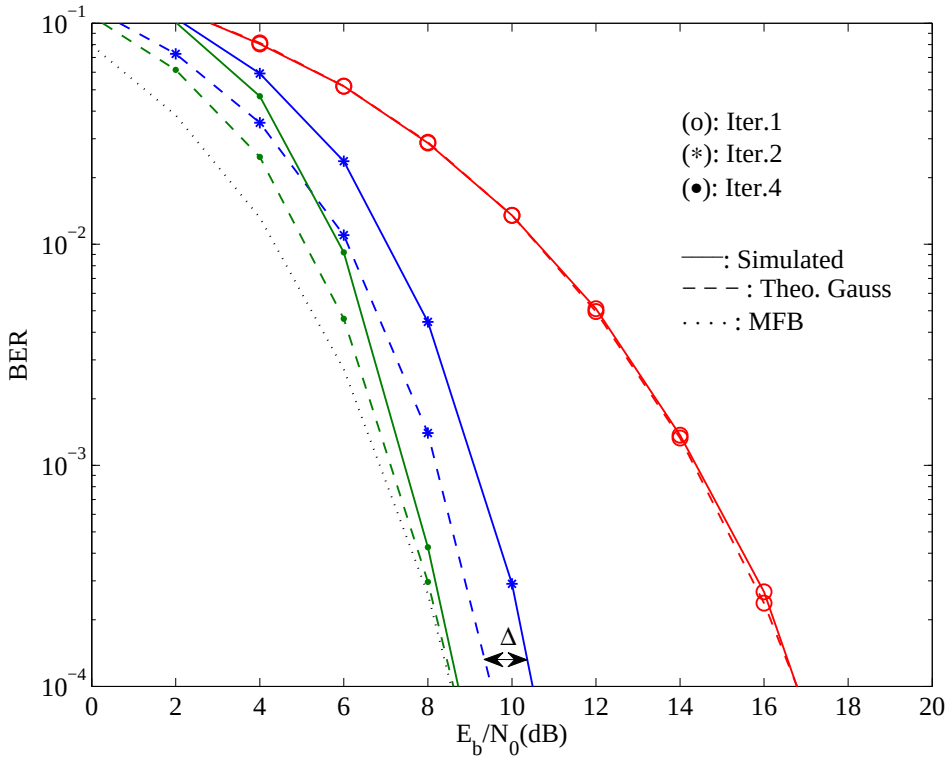

Figure 4.11: BER performance with 32 rays in the multipath environment ($1^{\mathbf{st}}$ MT).

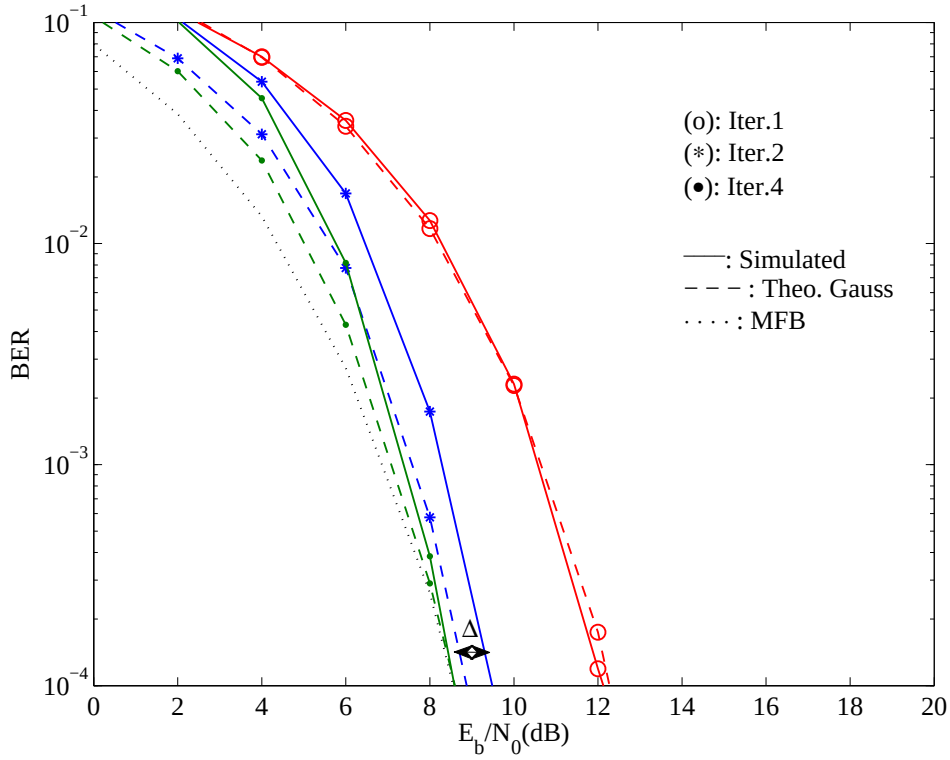

Figure 4.12: BER performance with 32 rays in the multipath environment (2nd MT).

4.5 Improved Analytical BER Performance Evaluation

Despite the results being similar, it is of best interest to try to improve the method for obtaining the theoretical BER performance by compensating the Δ difference between simulated and theoretical results. Relating Δ with equation 4.45 it can be shown that

$$P_b \simeq Q\left(\sqrt{\frac{1}{\Delta MSE}}\right) \tag{4.52}$$

and the correct compensation of the Δ factor comes from understanding its behavior as a function of the number of rays in the multipath. Fig. 4.13 shows, for both MTs, the Δ values for the 2nd iteration with 8, 16, 32, 64, 128 and 256 rays. The Δ curves that correspond to the reference values in the BER performance are considered: 10^{-2}, 10^{-3} and 10^{-4}. Analyzing Fig. 4.13, the Δ results present a decreasing exponential behavior, that can be written as

$$f(x) = ae^{-bx} + c, \tag{4.53}$$

where x indicates the number of rays considered in the multipath. Fig. 4.14 (1st MT) and 4.15 (2nd MT) illustrate the curve fitting with the approximation used by (4.53), demonstrating its accuracy. The optimum values that define the decreasing exponential for each BER reference are emphasized in Fig. 4.16. In order to compensate for the Δ factor, it is necessary to correctly perform its fitting. Therefore, parameters a, b and c,

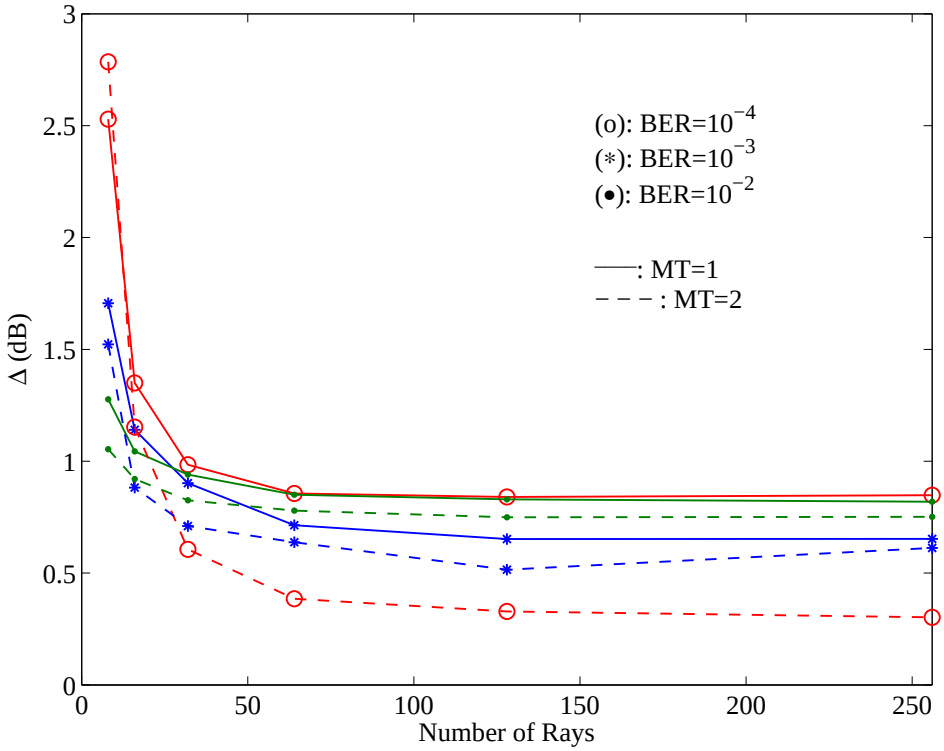

Figure 4.13: Δ behavior for the 2^{nd} iteration and BER values of 10^{-4}, 10^{-3} and 10^{-2} (1^{st} MT and 2^{nd} MT).

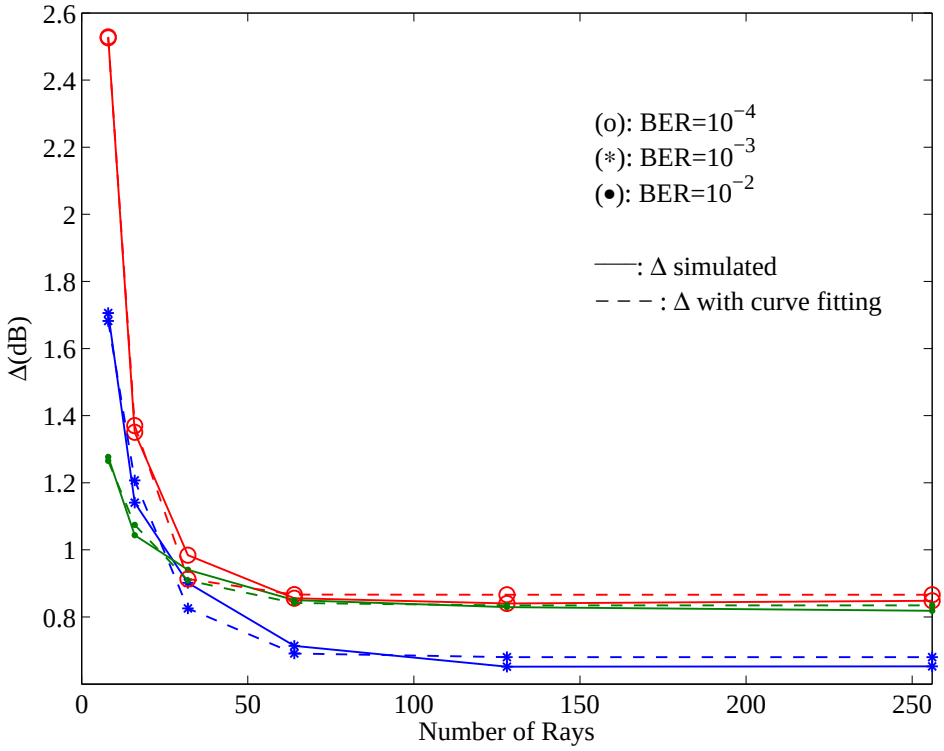

Figure 4.14: Δ behavior for the 2^{nd} iteration and BER values of 10^{-2}, 10^{-3} and 10^{-4} with curve fitting (1^{st} MT).

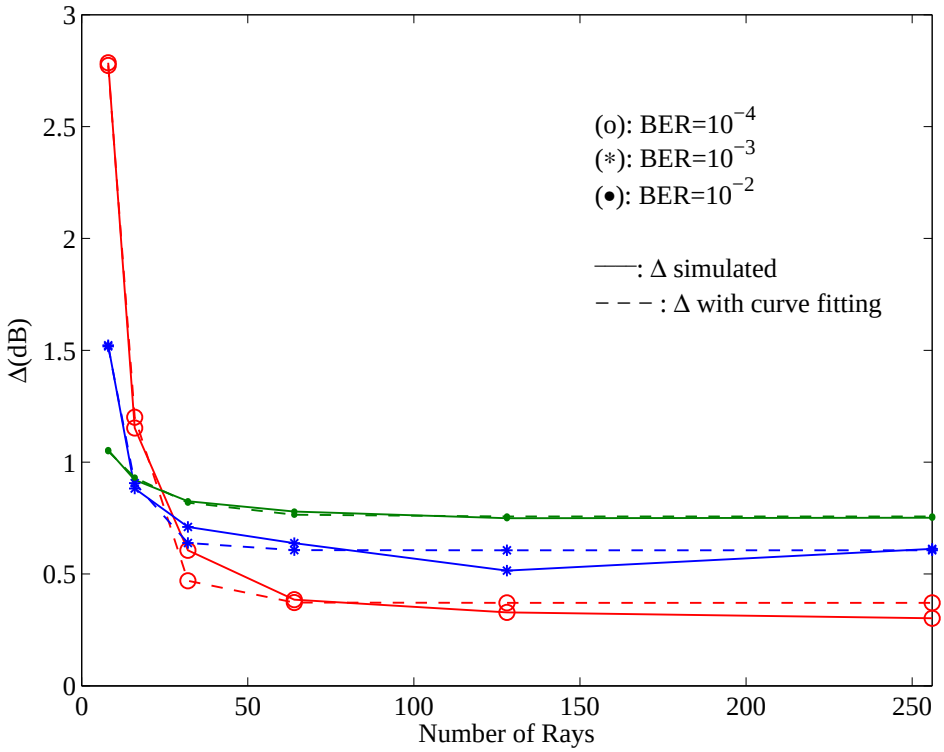

Figure 4.15: Δ behavior for the $2^{\mathbf{nd}}$ iteration and BER values of 10^{-2}, 10^{-3} and 10^{-4} with curve fitting ($2^{\mathbf{nd}}$ MT).

1^{st} MT	a	b	c
10^{-4}	5.4664	0.1490	0.8664
10^{-3}	1.9060	0.0804	0.6802
10^{-2}	0.7734	0.0731	0.8343

2^{nd} MT	a	b	c
10^{-4}	6.9560	0.1329	0.3709
10^{-3}	2.7700	0.1389	0.6059
10^{-2}	0.4893	0.0646	0.7571

Figure 4.16: Optimum values a, b and c for the $2^{\mathbf{nd}}$ iteration.

which are part of the approximation, must be computed as well. Firstly, it is important to understand that we want to relate Δ with the BER evaluation and in turn with its corresponding MSE. To do so, we can use expression 4.45, and the BER values of 10^{-4}, 10^{-3} and 10^{-2} indicating their MSE corresponds to 0.07, 0.1041 and 0.1890 respectively. Fig. 4.17 and 4.18 illustrate the approximation performed regarding the three parameters that constitute the Δ exponential likeness, for the 1$^{\text{st}}$ and 2$^{\text{nd}}$ MTs, respectively. After

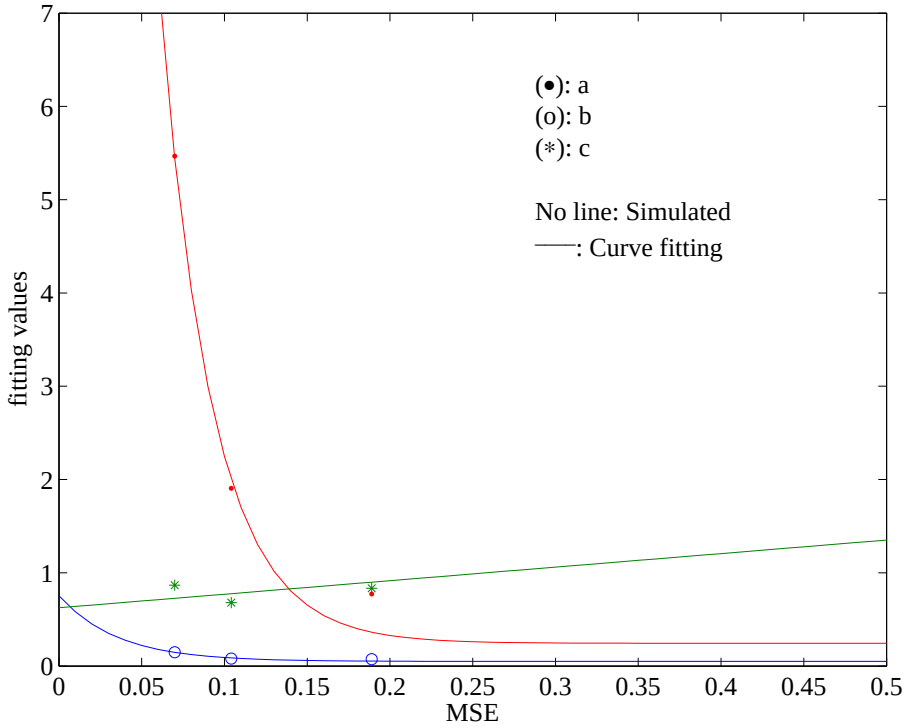

Figure 4.17: Fitting of the Δ exponential approximation parameters a, b and c, for the 2$^{\text{nd}}$ iteration (1$^{\text{st}}$ MT).

computing the fitting process for the a, b and c parameters of both MTs, the expressions that define the parameters, as a function of the MSE, are given by

$$a(MSE) = 48.12e^{-31.79MSE} + 0.2442, \tag{4.54}$$

$$b(MSE) = 0.7036e^{-28.29MSE} + 0.04994 \tag{4.55}$$

and

$$c(MSE) = 1.452MSE + 0.625, \tag{4.56}$$

for the 1$^{\text{st}}$ MT and

$$a(MSE) = 44.33e^{-26.57MSE} + 0.03952, \tag{4.57}$$

$$b(MSE) = -0.04405MSE + 0.1206 \tag{4.58}$$

and

$$c(MSE) = 2.177MSE + 0.3102, \tag{4.59}$$

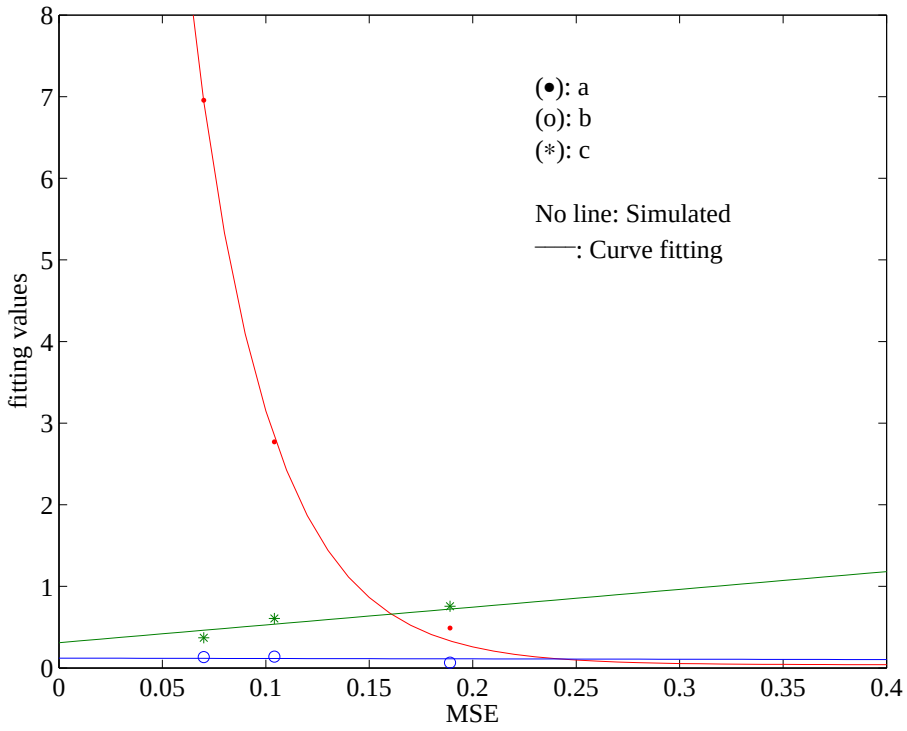

Figure 4.18: Fitting of the Δ exponential approximation parameters a, b and c, for the 2$^{\text{nd}}$ iteration (2$^{\text{nd}}$ MT).

for the 2$^{\text{nd}}$ MT.

With all the exponential approximation parameters defined, it is possible, in a similar fashion to correctly compensate the Δ differences of iterations 3 and 4, even though in these cases the value of Δ tend to be smaller when compared to the Δ in the 2$^{\text{nd}}$ iteration. The performance obtained with the Δ correction in a multipath with 8 rays is shown in Fig. 4.19 and 4.20, for the 1$^{\text{st}}$ and 2$^{\text{nd}}$ MTs, respectively. The scenario with 32 rays is illustrated in Fig. 4.21 (1$^{\text{st}}$ MT) and 4.22 (2$^{\text{nd}}$ MT).

This method for analytically obtaining the BER performance improves a Gaussian-based approach for its purpose. The method that allows the improvement of the theoretical approach is based on the compensation of the difference, designated by Δ, between the simulated and theoretical BER performance results. The results show that this method is precise and the Δ compensation is accurate.

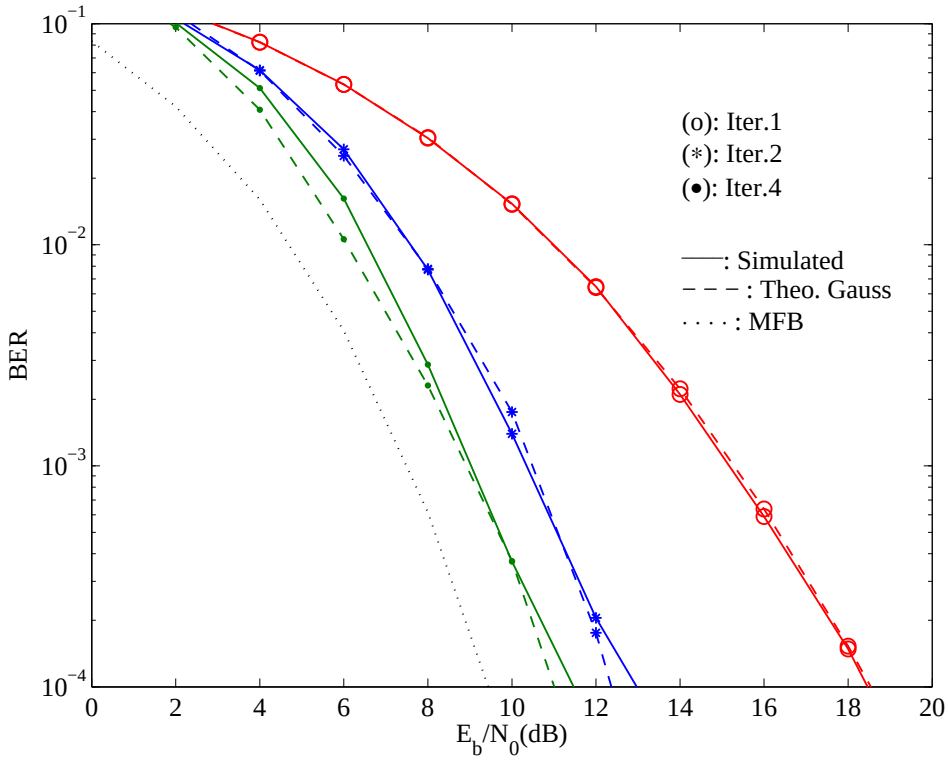

Figure 4.19: BER performance with Δ correction and 8 rays in the multipath ($1^{\mathbf{st}}$ MT).

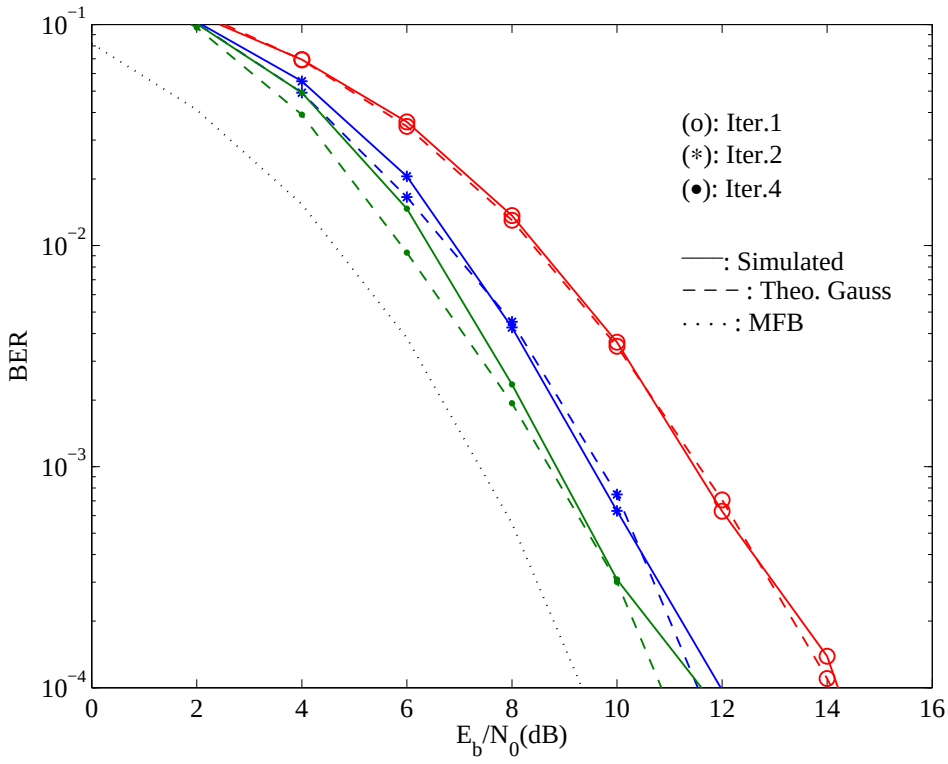

Figure 4.20: BER performance with Δ correction and 8 rays in the multipath ($2^{\mathbf{nd}}$ MT).

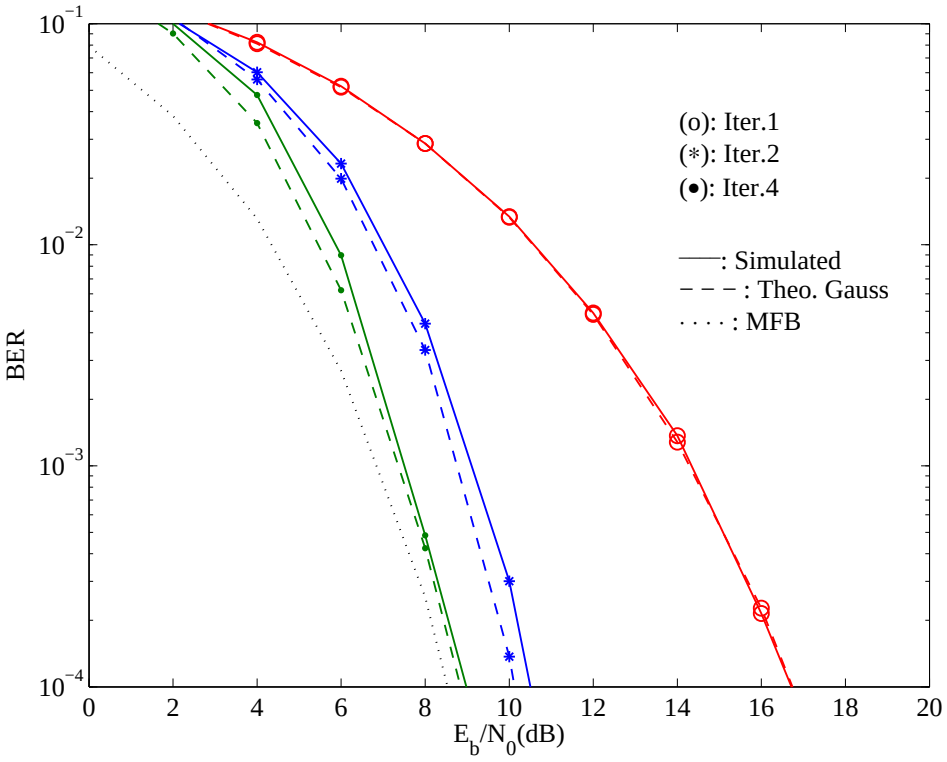

Figure 4.21: BER performance with Δ correction and 32 rays in the multipath (1st MT).

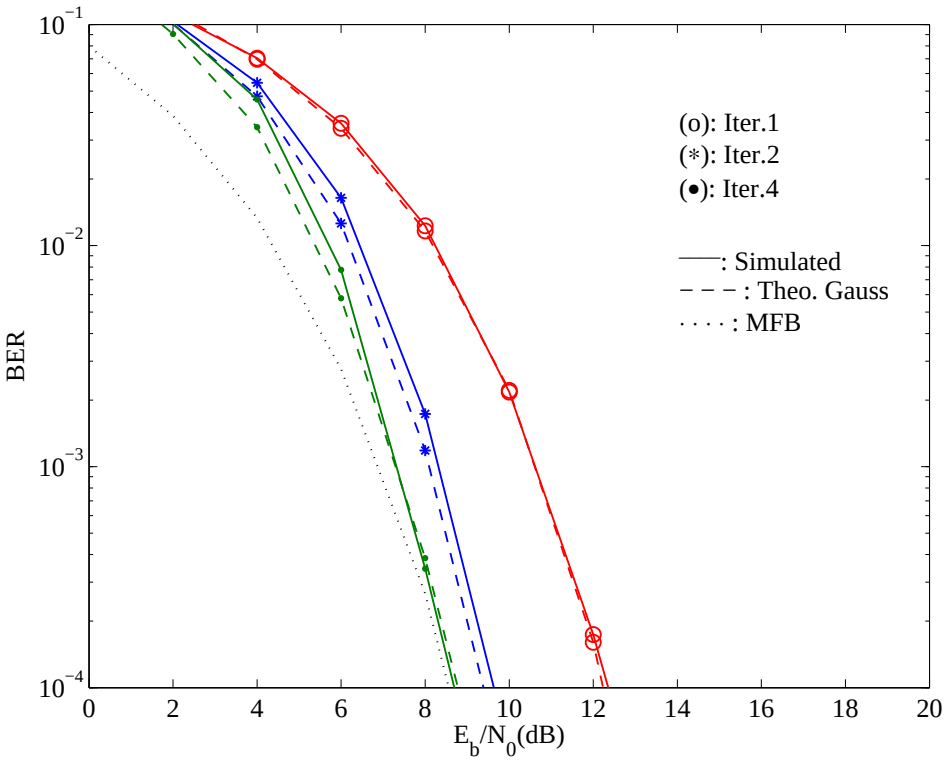

Figure 4.22: BER performance with Δ correction and 32 rays in the multipath (2nd MT).

CHAPTER 5

Quantization in BS Cooperation Systems

The previous chapter introduced and developed the Base Station (BS) cooperation concept, with all the expressions and equations being explained, either experimental or analytical. In turn, this chapter extends the BS cooperation concept including an analysis for an efficient detection and quantization requirements for the uplink of such systems. Moreover, this chapter is focus on the spectral characterization of the quantization noise and its impact on the multi-user detection processing.

Chapter 5 is organized as follows: Section 5.1 introduces the quantization basic concepts and section 5.2 characterizes the system when quantization is employed. Furthermore, section 5.2 presents several approaches for obtaining the spectral characterization of the quantization noise, which is a crucial element for designing robust receivers. Section 5.3 presents performance results taking into account the different approaches for obtaining the spectral characterization of the quantization noise, described in the previous section.

5.1 Quantization Basic Concepts

Quantization, as an analog-to-digital conversion, is an inherent process present in every digital system, with the major objective of decreasing the amount of information of a certain signal by constraining it into a discrete, i.e., finite, number of parts [34]. Usually, it is directly related with the sampling operation, where firstly, the signal is sampled and then those samples are quantized, with a decision digital value addressed to each sample. One logical example of the application of sampling and quantization is the well known Pulse Code Modulation (PCM) scheme [1, 35], illustrated in Fig 5.1. As noticed, in a PCM stream, the magnitude of the analog signal is sampled periodically at uniform intervals, with each sample being quantized to the nearest value within a range of digital steps (dotted points). There are several approaches regarding the quantization procedure, namely

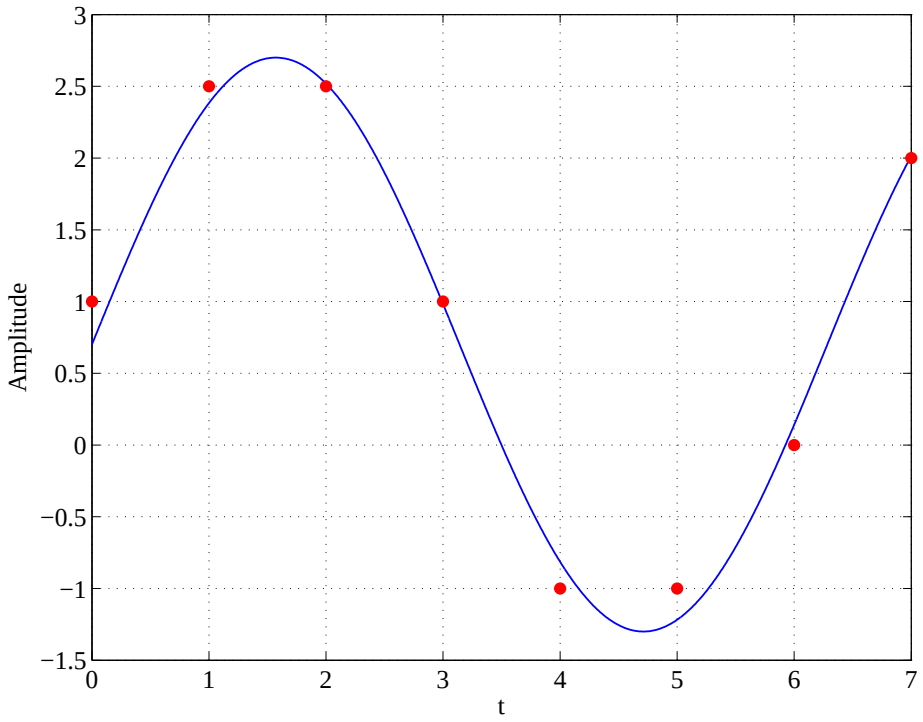

Figure 5.1: Sampling and Quantization.

uniform and nonuniform quantization [36]. Yet this thesis focus on the uniform scheme. Fig. 5.2 illustrates the characteristic of a uniform mid-riser quantizer. The uniform quantizer can either be defined as mid-riser or mid-tread, with different characteristic functions from one to another [34]. The depicted quantizer is characterized by $L = 2^m - 1$ decisions levels, where m corresponds to the number of bits used to address each quantization level. There are two saturations barriers, $A_M = -5$ and $A_M = 5$, with the difference between each decision level is denoted by $\Delta = \frac{2A_M}{2^m - 1}$, where Δ is the quantization step.

Quantization is an irreversible process, with associated losses, and posteriorly, when the recovery of the signal is necessary there is always some noise due to the analog-to digital conversion. Then, the assumptions from the sampling theory [37] must be respected, and they are naturally assumed. Hence, the quantization noise always present in this system, has the well known expression for a uniform quantizer $q_{noise} = \frac{\Delta^2}{12}$.

5.2 System Characterization Employing Quantization

In this work, the signals from the different MTs received at a given BS are collected, sampled and quantized by an ADC (Analog-to-Digital Converter), with the objective of decreasing the overall backhaul communication requirements. Posteriorly, at the CPU, the signal separation methodology is performed through frequency-domain receivers based on the IB-DFE concept. Regarding the sampled and quantized signals, the resulting quantization noise can lead to substantial performance degradation, so if the spectral characteristics of

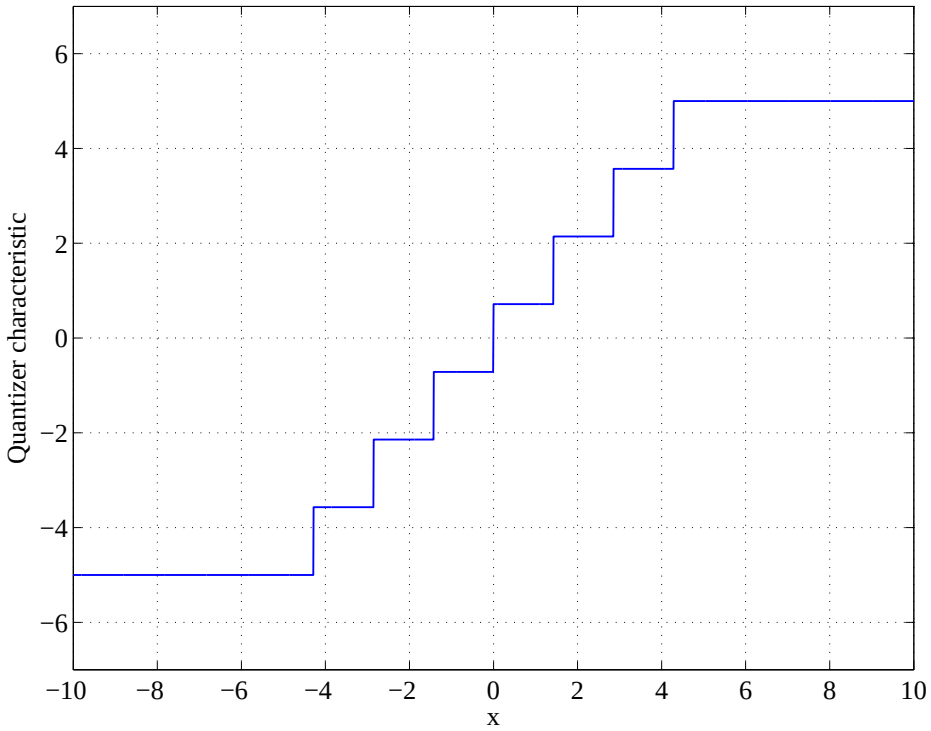

Figure 5.2: Characteristic of a mid-riser quantizer.

the quantization noise are known, it is possible to design robust receivers that can cope with the corresponding degradation. The received samples in the frequency-domain, at a given BS r are already expressed in 4.1 and reproduced by convenience here

$$Y_k^{(r)} = \sum_{p=1}^{P} S_{k,p} H_{k,p}^{eq(r)} + N_k^{(r)}, \tag{5.1}$$

which correspond to the DFT of the time-domain samples $y_n^{(r)}$ given by

$$y_n^{(r)} = \sum_{p=1}^{P} \xi_{p,r} s_{n,p} \circledast h_{n,p}^{(r)} + \nu_n^{(r)}. \tag{5.2}$$

To decrease the amount of information to be transmitted through the backhaul link, the received time-domain signals $y_n^{(r)}$ are quantized, leading to $y_n^{Q(r)}$ and are expressed by

$$y_n^{Q(r)} = f_Q\left(\frac{\mathrm{Re}\{y_n^{(r)}\}}{\sigma_y^{(r)}}\right)\sigma_y^{(r)} + j f_Q\left(\frac{\mathrm{Im}\{y_n^{(r)}\}}{\sigma_y^{(r)}}\right)\sigma_y^{(r)}, \tag{5.3}$$

where $f_Q(\cdot)$ denotes the quantization characteristics and $\sigma_y^{(r)}$ the variance of the signal component. Since we are considering severely time-dispersive channels, with rich multi-path propagation environment, which are the typical channel conditions behind SC-FDE schemes, the received time-domain samples $y_n^{(r)}$ can be accounted for as samples of a

zero-mean complex Gaussian process, i.e., $y_n^{(r)} \sim \mathcal{CN}\left(0, 2\sigma_y^{(r)^2}\right)$, with

$$2\sigma_y^{(r)^2} = \mathbb{E}\left[\left|y_n^{(r)}\right|^2\right] = \sum_{p=1}^{P} |\xi_{p,r}|^2 \, \mathbb{E}\left[|s_{n,p}|^2\right] + \mathbb{E}\left[\left|\nu_n^{(r)}\right|^2\right] = \sum_{p=1}^{P} |\xi_{p,r}|^2 \, 2\sigma_s^2 + 2\sigma_\nu^2, \tag{5.4}$$

where

$$\sigma_s^2 = \mathbb{E}\left[|\mathrm{Re}\{s_n\}|^2\right] = \mathbb{E}\left[|\mathrm{Im}\{s_n\}|^2\right] \tag{5.5}$$

and

$$\sigma_\nu^2 = \mathbb{E}\left[|\mathrm{Re}\{\nu_n\}|^2\right] = \mathbb{E}\left[|\mathrm{Im}\{\nu_n\}|^2\right]. \tag{5.6}$$

Moreover, σ_s^2 and σ_ν^2 correspond to the symbol and noise variances, respectively. According to the Bussgang's theorem [38, 39], the Gaussian nature of $y_n^{(r)}$ allows the quantized signals to be decomposed as the sum of uncorrelated useful and distortion terms, which leads to

$$y_n^{Q(r)} \approx \alpha y_n^{(r)} + d_n^{(r)}, \tag{5.7}$$

with $d_n^{(r)}$ denoting the quantization noise term. The α parameter is a constant which depends only on the nonlinear characteristic due to the quantization process, and can be computed as

$$\alpha = \int_{-\infty}^{\infty} \omega f_Q(\omega) \frac{1}{\sqrt{2\pi}} e^{-\frac{\omega^2}{2}} d\omega. \tag{5.8}$$

In the frequency-domain, the block associated with the quantized signal at the BS r corresponds to

$$Y_k^{Q(r)} \approx \alpha Y_k^{(r)} + D_k^{(r)} \approx \alpha \sum_{p=1}^{P} \xi_{p,r} S_{k,p} H_{k,p}^{(r)} + N_k^{Tot(r)}, \tag{5.9}$$

which is the DFE of the time-domain signal $y_n^{Q(r)}$. $N_k^{Tot(r)} = \alpha N_k^{(r)} + D_k^{(r)}$ accounts for the global noise from the transmitted and quantized signals, in which

$$2\sigma_D^{(r)^2} = \mathbb{E}\left[\left|D_k^{(r)}\right|^2\right] = N\mathbb{E}\left[\left|d_n^{(r)}\right|^2\right]. \tag{5.10}$$

Furthermore,

$$2\sigma_N^{Tot(r)^2} = \mathbb{E}\left[\left|N_k^{Tot(r)}\right|^2\right] = 2\sigma_D^{(r)^2} + 2\sigma_N^2 |\alpha|^2. \tag{5.11}$$

The robustness of the receiver design requires the knowledge of the quantization noise variance σ_d^2, which in the general case is a function of k, i.e., it is not flat in the frequency. To understand the quantization's impact on this system, several methods for obtaining the spectral characterization of the quantization noise can be considered. The basic approach is to consider that the quantization noise has a constant PSD, i.e., a flat spectrum, and its power is given by $\frac{\Delta^2}{12}$ [1]. This approach is only appropriated when the input signals have a rectangular form, not oversampled, and the quantizers are linear with inconsequential saturation effects, meaning that $A_M/\sigma = +\infty$.

Another approach is to consider that in the quantization process the input signals have Gaussian characteristics, with the output signals expressed as in (5.7). At the r^{th}

BS, when the signal to be quantized has a flat spectrum, the quantization noise frequency characteristics are also flat and according to [38] its variance can be expressed as

$$\sigma_d^{(r)^2} = \sigma_{y^Q}^{(r)^2} - |\alpha|^2 2\sigma_y^{(r)^2}, \tag{5.12}$$

with $\sigma_y^{(r)^2}$ designating the average power of the input signal and the output power $\sigma_{y^Q}^{(r)^2}$ given by

$$\sigma_{y^Q}^{(r)^2} = 2\int_{-\infty}^{+\infty} f^2(y)p(y)dy. \tag{5.13}$$

Despite this approach accounting for quantization noise and saturation effects, it is only suitable for input signals with a rectangular spectrum.

The method presented in [40] theoretically characterizes the quantization noise through an IMP (Inter-Modulation Product) measurement, which is suitable for signal inputs that have arbitrary spectral distributions, i.e., they are not rectangular, and/or for oversampled signals. With this approach, the idea is to obtain the spectral distributions of the distinct inter-modulation products at the quantizer output and add them to obtain the PSD of the quantized signal. The accuracy of the PSD of the quantized signal depends on the number of IMPs, since the larger the number of IMPs, the better the accuracy. As a consequence, despite this approach works well for smooth nonlinearities, it may present complexity and/or convergence problems when nonlinearities are severe. Some quantizers present low number of bits of resolution and/or low clipping levels, which fall into the cases where nonlinearities are severe, requiring an approximation by a large number of polynomial terms. According to [40], the PSD of the quantized signal is obtained through the DFT of the output autocorrelation

$$G_{y^Q,k} = \mathrm{DFT}\left(R_{y^Q,n}\right), \tag{5.14}$$

where $R_{y^Q,n}$ is expressed by

$$R_{y^Q,n} = \sum_{\gamma=0}^{+\infty} 2P_{2\gamma+1}\frac{(R_{y,n})^{2\gamma+1} + j\,(\mathrm{Im}R_{y,n})^{2\gamma+1}}{R_{y,0}^{2\gamma+1}}, \tag{5.15}$$

in which $R_{y,0} = 2\sigma_y^2$ indicates the input signal average power. $P_{2\gamma+1}$ designates the power associated with the inter-modulation product of order $2\gamma+1$ and is defined as

$$P_{2\gamma+1} = \frac{\left(\int_{-\infty}^{+\infty} f(y)p(y)H_{2\gamma+1}\left(\frac{y}{\sqrt{2}\sigma_y}\right)dy\right)^2}{2^{2\gamma+a}\,(2\gamma+1)!}, \tag{5.16}$$

where $H_{2\gamma+1(\cdot)}$ indicates the Hermite polynomial of order $2\gamma+1$ and $f(y)$ the quantizer characteristics. This approach is difficult since it requires a high number of IMPs n_γ when 5.15 is being truncated for the polynomial approximation. Fig. 5.3 illustrates the simulated and theoretical PSD of a quantized signal for $n_\gamma = 2$ and $n_\gamma = 10$. The quantizer is characterized by employing $m = 2$ resolution bits and has a normalized saturation level of $A_M/\sigma = 0.5$. For the transmission, $P = 2$ MTs are considered and the blocks have a

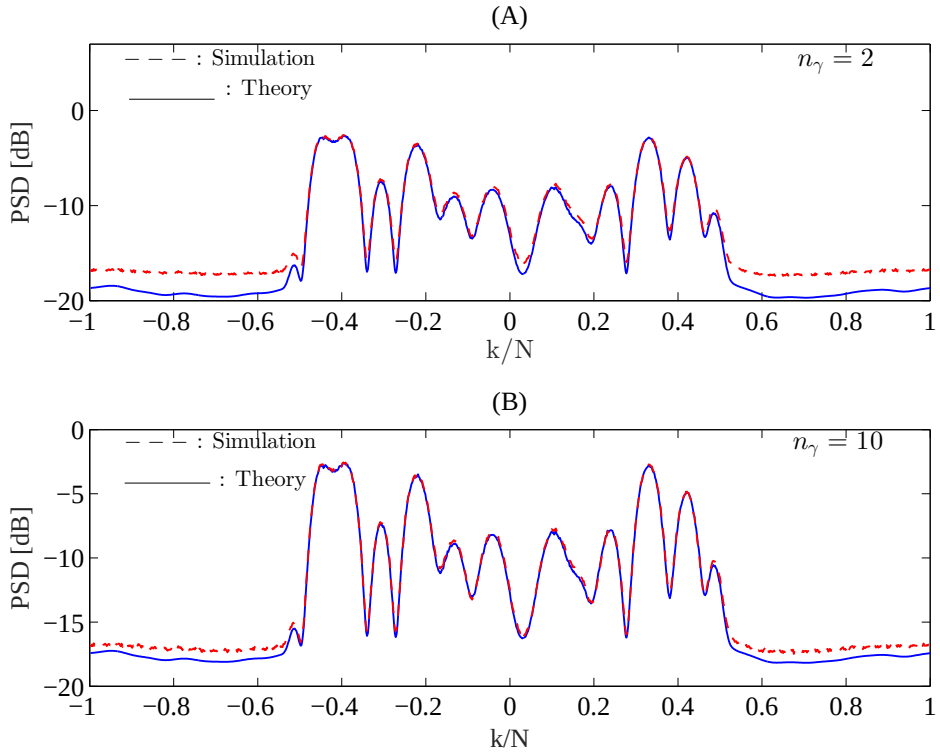

Figure 5.3: PSD of a quantized signal obtained with $n_\gamma = 2$ (A) and with $n_\gamma = 10$ (B).

size of $N = 512$ symbols. Moreover, an oversampling factor of $M = 2$ and time-dispersive channels with 32 rays in the multipath environment are taken into account. Fig. 5.3 shows that when $n_\gamma = 2$ there are considerable differences between the simulated and theoretical results in both the in-band and out-of-band regions. It can be seen that the results are only approximately matched in the in-band part of the spectrum and when $n_\gamma = 10$. The out-of-band region demonstrates the convergence and/or complexity issues in this approach, since there is a significant difference between simulated and theoretical results. Fig. 5.4 shows the spectrum of a quantized signal received at a given BS. The number of MTs transmitting is $P = 3$, the transmission block size is $N = 512$ with $M = 2$ oversampling factor and there are 32 rays in the multipath profile between each MT and the BS. This illustrates the total PSD of the quantized signal obtained with expression (5.15) and the spectral distributions of the IMP of order $2\gamma + 1$. It is possible to notice that the PSD of P_5, which is associated to the IMP of $\gamma = 2$ has very low fluctuations and it is almost constant regarding the $P_7\,(\gamma = 3)$ case. In the time-domain, the autocorrelations of these PSDs can be approximated by Dirac delta functions. This means that all autocorrelations from a given order $\gamma = \gamma_{max}$ can be approximated by the autocorrelation associated to the IMP of order $\gamma = \gamma_{max}$, that concentrates the power of the IMPs from $\gamma = \gamma_{max}$ to $\gamma = +\infty$. Following this idea, and taking into account the issues presented with the previous approach, [41] proposes a method to obtain an equivalent nonlinearity $g(y)$, in

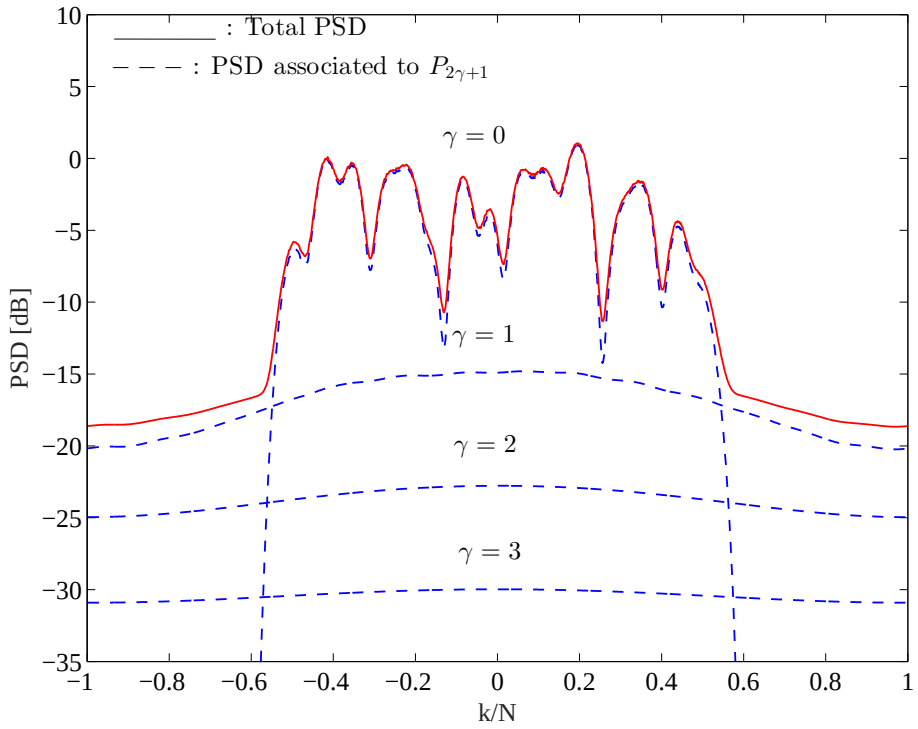

Figure 5.4: PSD of a quantized signal and the individual spectral distributions of the IMPs of order $2\gamma+1$.

which the IMPs are related to the IMPs of $f(y)$ according to

$$P^{g}_{2\gamma+1} = \begin{cases} P^{f}_{2\gamma+1}, & 0 \leq \gamma < \gamma_{\max} \\ P^{f}_{\text{out}} - \sum_{\gamma=0}^{\gamma_{\max}-1} P^{f}_{2\gamma+1}, & \gamma = \gamma_{\max} \\ 0, & \gamma \geq \gamma_{\max}, \end{cases} \tag{5.17}$$

with P^{f}_{out} given by (5.13) and the value of γ_{max} being selected to ensure that the PSD of the IMP of order $2\gamma_{max}+1$ is constant. The use of the superscript f or g differentiates between the conventional quantization characteristics and the equivalent nonlinearity, respectively.

So, the equivalent nonlinearity, designated as $g(x)$ is expressed by

$$g(y) = \sum_{\gamma'=0}^{\gamma_{max}} T_{\gamma'} y^{2\gamma'+1}, \tag{5.18}$$

in which $\{T_{\gamma'}; \gamma' = 0, 1, ..., \gamma_{max}\}$ indicate the polynomial coefficients. To obtain these coefficients it is necessary to relate the IMPs power of $g(y)$ with the corresponding expression. Since there is not a linear relation with them, as the definition of power associated to a given IMP shows (see (5.16)), the IMPs of $g(y)$ are redefined by

$$P^{g}_{2\gamma+1} = \frac{\left(\nu^{g}_{2\gamma+1}\right)^2}{2^{2\gamma+1}(2\gamma+1)!}, \tag{5.19}$$

where the coefficients $\{\nu^g_{2\gamma+1}; \gamma = 0, 1, ..., \gamma_{\max}\}$ are expressed as

$$\begin{aligned}\nu^g_{2\gamma+1} &= \int_{-\infty}^{+\infty} g(y)p(y)H_{2\gamma+1}\left(\frac{y}{\sqrt{2}\sigma_y}\right)\mathrm{d}y \\ &= \sqrt{P^g_{2\gamma+1}}\sqrt{2^{2\gamma+1}(2\gamma+1)!}. \end{aligned} \tag{5.20}$$

Clearly, in (5.20), the coefficients $\{\nu^g_{2\gamma+1}; \gamma = 0, 1, ..., \gamma_{max}\}$ have a linear relation with $g(y)$. Furthermore, the polynomial coefficients $\{T_{\gamma'}; \gamma' = 0, 1, ..., \gamma_{max}\}$ can be obtained by substituting (5.18) in the first line of (5.20), expressed as

$$\begin{aligned}\nu^g_{2\gamma+1} &= \int_{-\infty}^{+\infty}\sum_{\gamma'=0}^{\gamma_{\max}} T_{\gamma'}y^{2\gamma'+1}p(y)H_{2\gamma+1}\left(\frac{y}{\sqrt{2}\sigma_y}\right)\mathrm{d}y \\ &= \sum_{\gamma'=0}^{\gamma_{\max}} T_{\gamma'}\underbrace{\int_{-\infty}^{+\infty} y^{2\gamma'+1}p(y)H_{2\gamma+1}\left(\frac{y}{\sqrt{2}\sigma_y}\right)\mathrm{d}y}_{\beta_{\gamma\gamma'}} \\ &= \sum_{\gamma'=0}^{\gamma_{\max}} \beta_{\gamma\gamma'}T_{\gamma'}. \end{aligned} \tag{5.21}$$

In Fig. 5.5 one can notice that the equivalent nonlinearity $g(y)$ approach presents a smoother quantization characteristic when compared to the conventional one, represented by $f(y)$. The quantizer is characterized by a saturation level of $A_M/\sigma_y = 1$ and $m = 3$ bits of resolution. With this approach, the spectral characterization of the quantization noise $\sigma^2_D(k)$ can be shown in Fig. 5.6, which illustrates the theoretical and simulation results. The signal received at a given BS is a sum of all the contributions from $P = 3$ MTs with a single transmission block having size of $N = 512$. We consider 32 rays in the multipath propagation environment and the oversampling factor is $M = 2$. Furthermore, the quantizer is characterized by the employment of $m = 4$ resolution bits and a normalized clipping level of $A_M/\sigma_y = 1$. From Fig. 5.6 it can be seen that the average PSD approach is not adequate when one takes into account the oversampling effects. The PSD obtained through the equivalent nonlinearity approach is very accurate even for a reduced amount of terms (i.e., $\gamma_{max} = 5$), contrarily to the IMP analysis approach, which presents a higher complexity methodology. Hence, the IMP analysis method requires $n_\gamma = 10$ to provide the same accuracy when the equivalent nonlinearity approach is considered. Furthermore, even for a large number of IMPs, the IMP analysis approach presents considerable errors in the out-of-band region when compared to the results obtained by simulation.

Considering the spectral characteristics of the quantization noise, it is possible to analyze in Fig. 5.7 the evolution of the average value of the PSD as in function of the normalized clipping level A_M/σ_y obtained by theory and simulation. The signal received at the BS and the quantizer characteristics are the same as in Fig. 5.6, however there is no oversampling considered (i.e., $M = 1$). Clearly, the IMP analysis approach has less accuracy for high values of the normalized saturation level, even for a high number of IMPs

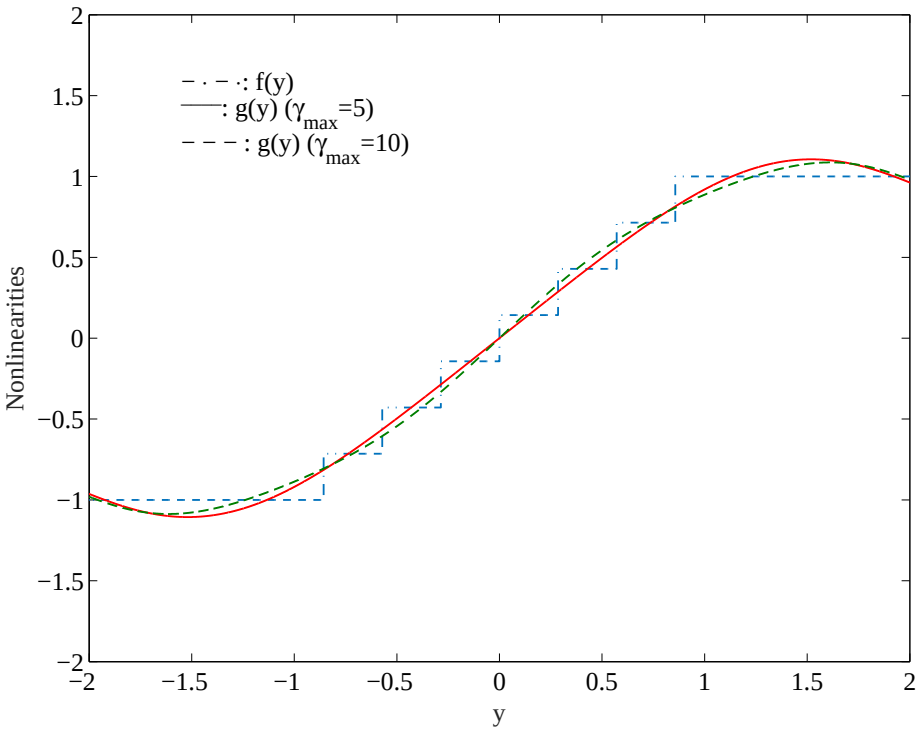

Figure 5.5: Quantizer characteristic and its equivalent nonlinearity considering $\gamma_{max} = 5$ and $\gamma_{max} = 10$.

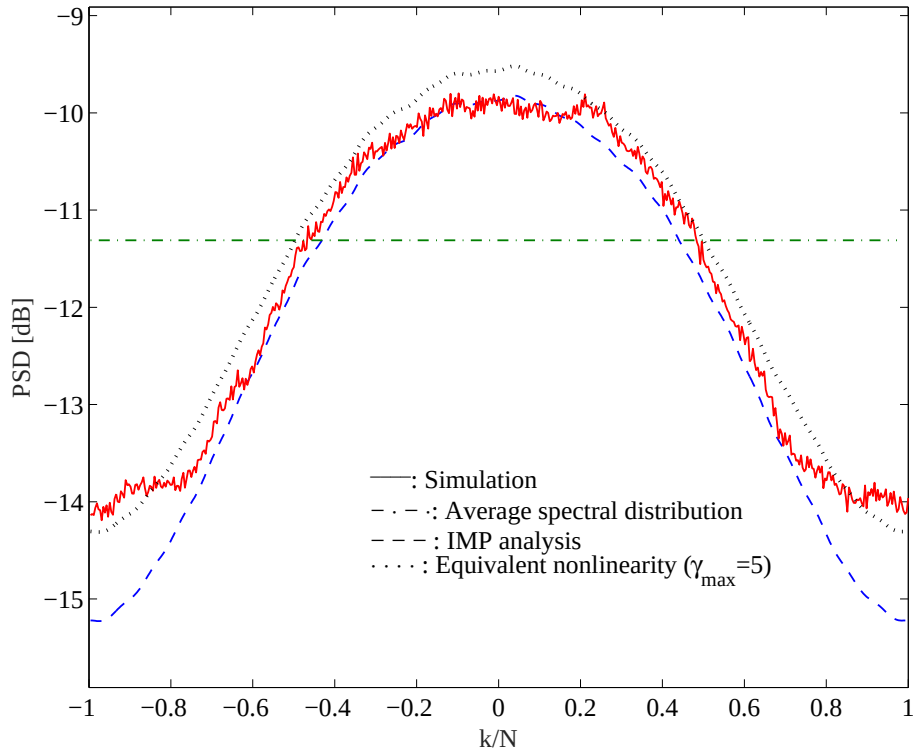

Figure 5.6: Spectral characterization of the quantization noise obtained theoretically and by simulation. Comparison of several approaches considering an oversampling factor of $M = 2$.

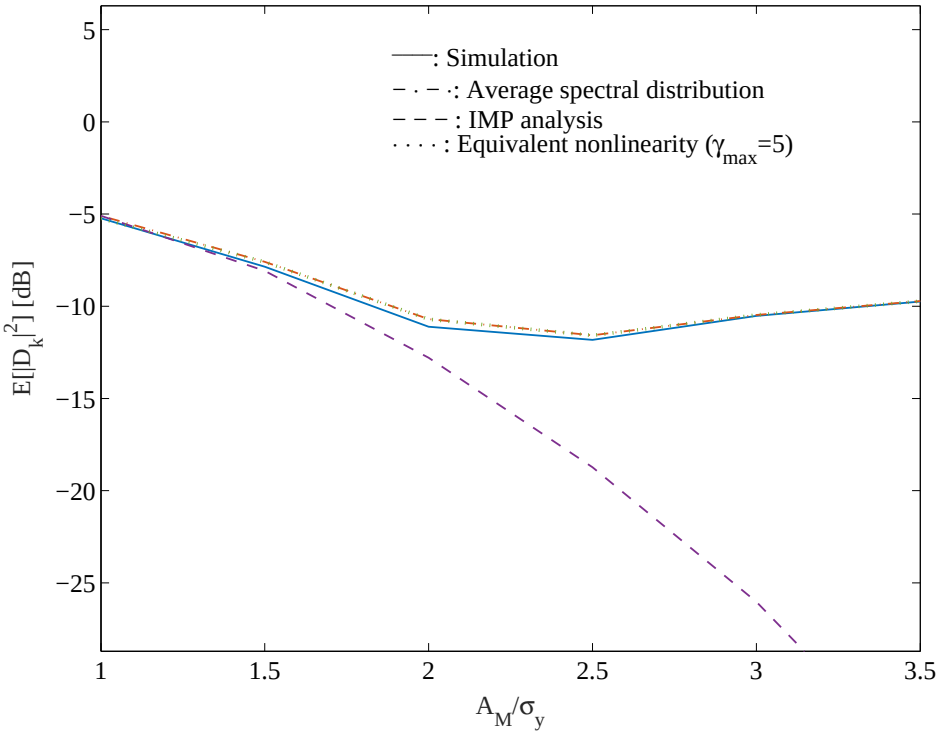

Figure 5.7: Average PSD of the quantization noise obtained theoretically and by simulation. Comparison of several approaches without oversampling ($M = 1$).

$n_\gamma = 10$. On the other hand, the equivalent nonlinearity approach with $\gamma_{max} = 5$ is very accurate, and its results are very close to the ones obtained by simulation.

Analyzing the influence of the oversampling factor, Fig. 5.8 illustrates the distortion caused by the quantization process ,i.e., spectrum of the quantization noise, when the received signal is the sum of the signals transmitted from $P = 2$ MTs. Each block has size of $N = 256$ and $I = 64$ multipath rays were considered. The quantizer is characterized by the employment of $m = 3$ resolution bits and there are three values of the oversampling factor taken into account, $M = 1$ (where there is no oversampling), $M = 2$ and $M = 4$. Clearly, there is a higher value for degradation when the oversampling factor approaches 1 due to aliasing issues. Moreover, since the spectrum from distortion is almost constant and the one from the output signal has a lot of fluctuations, the SIR (Signal-to-Interference Ratio) can be very low for frequencies in deep fade. One can notice that when M changes from 1 to 2 there is a gain of approximately 2 dB. Moreover, when the resolution bits are $2m$ instead of m it is possible to have gains of $6m$ dB, which indicates that the best option is to increase the resolution bits instead of the oversampling factor M. For this reason, the following performance results do not consider signals with oversampling (i.e., $M > 1$).

As previously performed in Chapter 4 and taking into account the effects of sampling and quantizing the input signals, one can obtain the BER performance as

$$BER_p \simeq Q\left(\sqrt{\frac{1}{\theta_p}}\right), \tag{5.22}$$

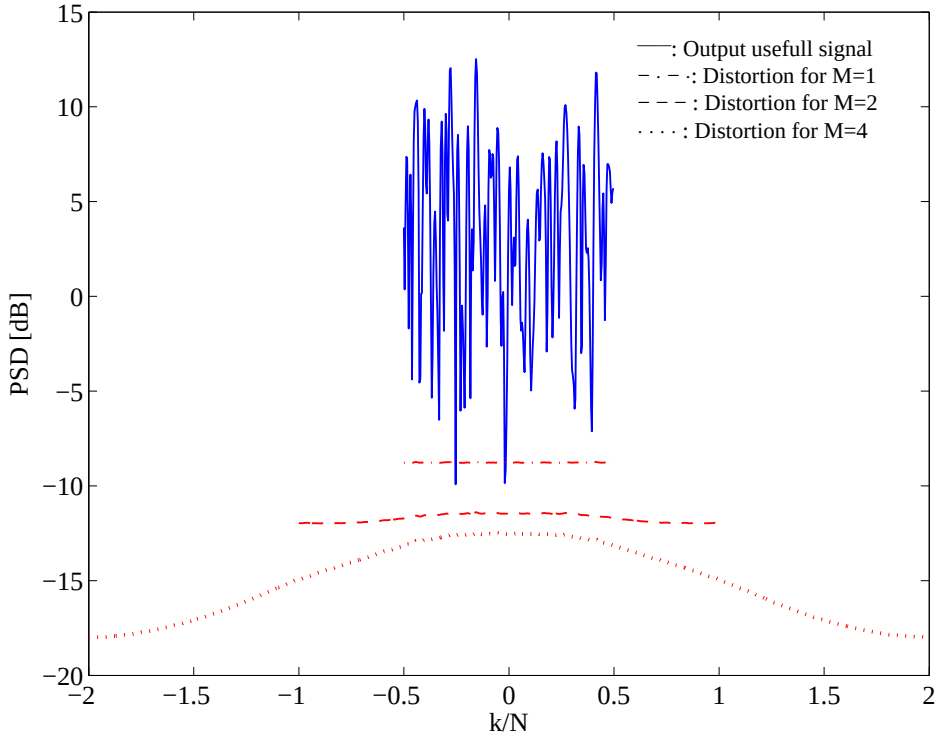

Figure 5.8: Quantization noise spectrum for different oversampling factors.

with,

$$\theta_p = \frac{1}{N^2} \sum_{k=0}^{N-1} \Theta_{k,p}, \tag{5.23}$$

and

$$\Theta_{k,p} = \mathbb{E}\left[\left|\tilde{S}_{k,p} - S_{k,p}\right|^2\right] = \mathbb{E}\left[\left|\mathbf{F}_{k,p}^T \mathbf{Y}_k^Q - \mathbf{B}_{k,p}^T \bar{\mathbf{S}}_{k,p} - S_{k,p}\right|^2\right]. \tag{5.24}$$

Consequently, the optimum coefficients $\mathbf{F}$ and $\mathbf{B}$ are expressed as

$$\mathbf{F} = \kappa \mathbf{\Lambda} \mathbf{H}^H \mathbf{e}_p \tag{5.25}$$

and

$$\mathbf{B} = \alpha \mathbf{H}\mathbf{F} - \mathbf{e}_p, \tag{5.26}$$

with

$$\mathbf{\Lambda} = \left(\mathbf{H}^H \left(\mathbf{I}_P - \mathbf{P}^2\right) \mathbf{H} + \mathbf{R}_{N^{Tot}} \mathbf{R}_S^{-1} |\alpha|^{-2}\right)^{-1}. \tag{5.27}$$

In (5.27),

$$\mathbf{R}_{N^{Tot}} = \mathbb{E}\left[\mathbf{N}^{\mathbf{Tot}^*} \mathbf{N}^{\mathbf{Tot}^T}\right] = |\alpha|^2 \mathbf{R}_N + \mathbf{R}_D \tag{5.28}$$

indicates the correlation matrix of $\mathbf{N}^{\mathbf{Tot}}$, with

$$\mathbf{R}_N = 2\sigma_N^2 \mathbf{I}_R \tag{5.29}$$

and

$$\mathbf{R}_D = 2\text{diag}(\sigma_D(k)^{(1)^2}, \sigma_D(k)^{(2)^2}, ..., \sigma_D(k)^{(R)^2}) \tag{5.30}$$

corresponds to the correlation matrices of the channel and quantization noises, respectively. It should be pointed out that when the quantization effects are ignored, then $\mathbf{R}_{N^{Tot}} = \mathbf{R}_N$ and $\alpha = 1$.

5.3 Performance Results

The previous section presented several methodologies to obtain the spectral characterization of the quantization noise. Moreover, the optimum coefficients $\mathbf{F}$ and $\mathbf{B}$ were expressed when the quantization process is taken into account. In this section several performance results are presented to evaluate such methodologies. The blocks associated with the transmission of each MT have N data symbols, selected from a QPSK constellation under a Gray mapping rule. Furthermore, an oversampling factor of M was considered. The transmission channels between the MTs and the BSs are severely time-dispersive with I symbols-spaced taps and uncorrelated Rayleigh fading on the different multipath components. It is assumed that the channels are uncorrelated and that there is a perfect synchronization and channel estimation. The quantization process is defined by a "mid-rise"quantizer employing m resolution bits and a normalized saturation level A_M/σ.

Fig. 5.9 illustrates the BER performance of a BS cooperation scenario with $P = 2$ MTs and $R = 2$ BSs. In this case we do not consider any quantization performed on the

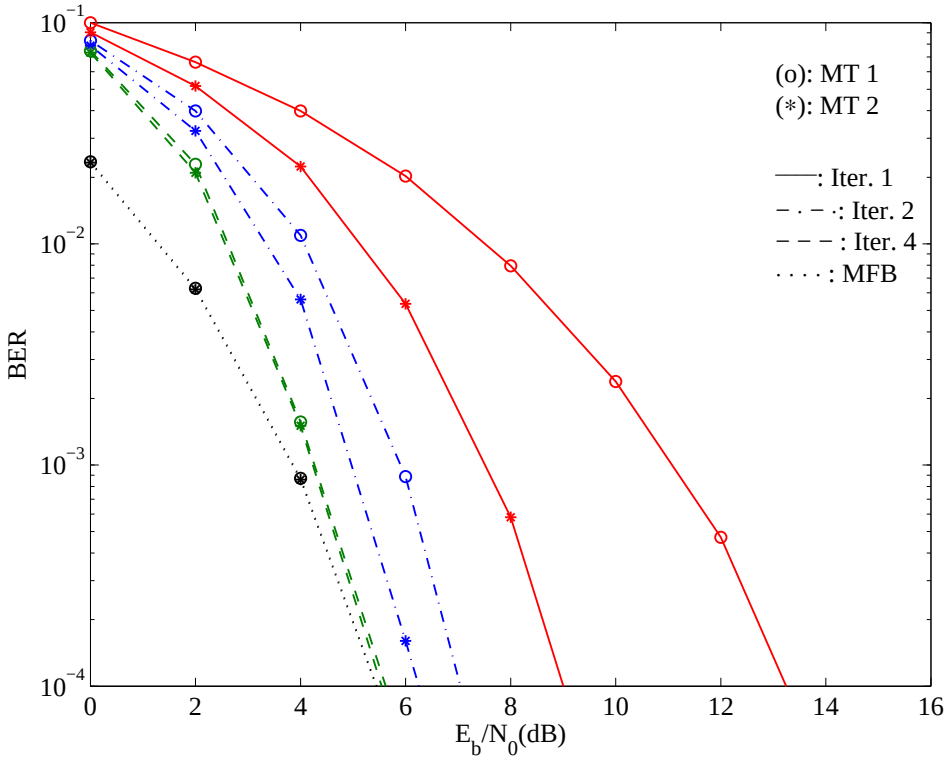

Figure 5.9: BER performance for a BS cooperation scenario with $P = 2$ MTs, $R = 2$ BSs and without quantization.

transmitted data. The power associated with the different transmission links is $\xi_{p,r} = 0$ dB, where all MTs transmit with the same average power to all BSs. This figure is illustrated for comparison purposes when the inclusion of quantization is done, in the next figures.

Regarding the scenario illustrated in Fig. 5.9, Fig. 5.10 and Fig. 5.11 show, for the 1st and 12nd MTs, respectively, the comparison of results when quantization is employed. The quantizer is characterized by the use of $m = 3$ and $m = 4$ resolution bits and a

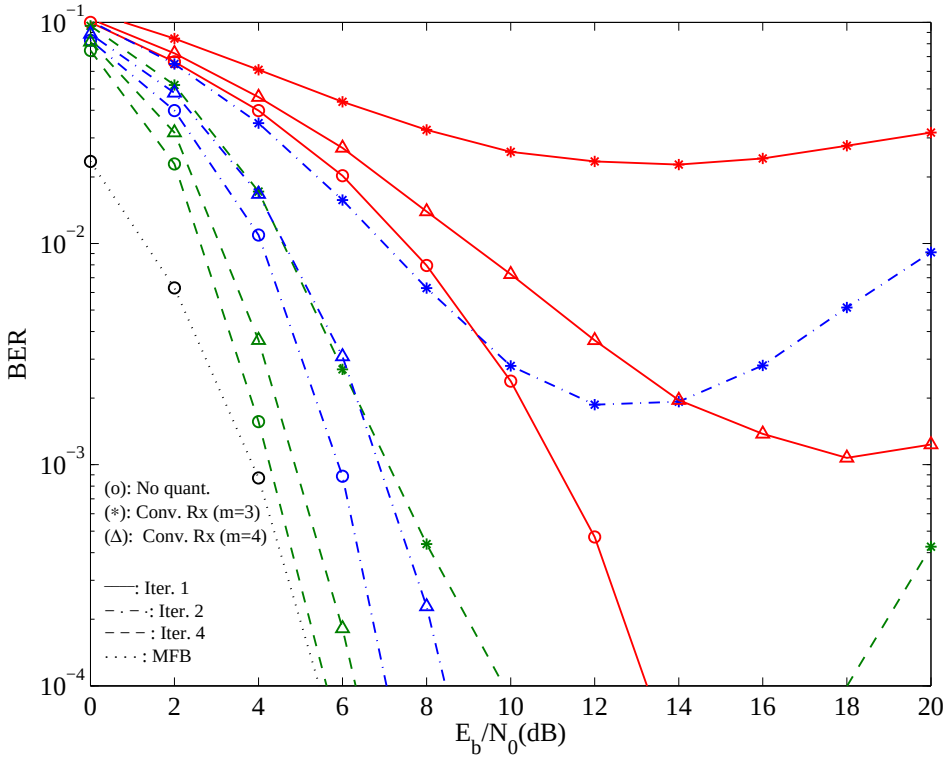

Figure 5.10: BER performance for a BS cooperation scenario with $P = 2$ MTs and $R = 2$ BSs. Comparison of results without quantization and quantization with $m = 3$ and 4 bits of resolution employing a conventional receiver (1st MT).

conventional approach is considered for the receiver, designated as "Conv. Rx", in which the quantization effects are not taken into account. This means that the distortion from the quantization noise is $\sigma_d^2 = 0$. As expected, when quantization is employed, there is a degradation on the performance, specially for lower values of m and higher values of SNR.

Fig. 5.12 and Fig. 5.13 illustrate the BER performance for a scenario with quantization when "Conv. Rx"and "Robust Rx"are considered. With the "Robust Rx", the receiver takes into account the spectral characterization of the quantization noise following the method described with the equivalent nonlinearities approach. Furthermore, for the detection with this method the γ_{max} parameter corresponds to $\gamma_{max} = 6$. Both figures demonstrate worst performance results when the "Conv. Rx"is considered, especially for high values of SNR. Moreover, one can notice that the robust receivers that account for $\sigma_D^2(k)$ can cope with the degradation provided by the employment of conventional receivers.

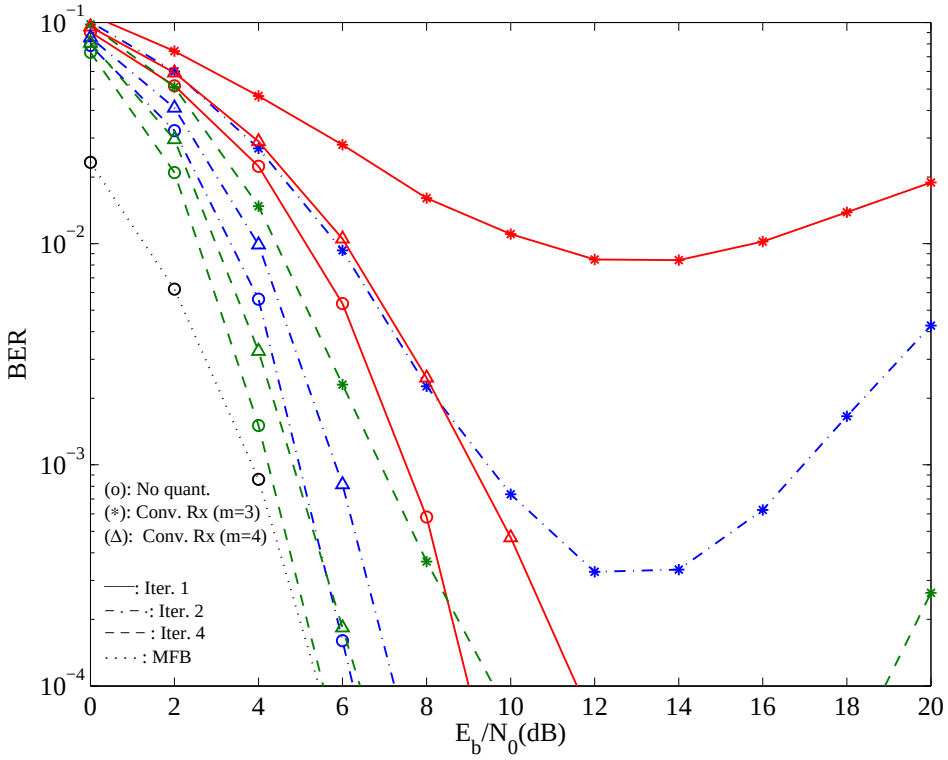

Figure 5.11: BER performance for a BS cooperation scenario with $P = 2$ MTs and $R = 2$ BSs. Comparison of results without quantization and quantization with $m = 3$ and 4 bits of resolution employing a conventional receiver (2^{nd} MT).

For the 1^{st} and 2^{nd} MTs, respectively, Fig. 5.14 and Fig. 5.15 compare the quantization effects of the "Robust Rx"results with a simplified version of the robust receiver, designated as "Simp. Robust Rx". In the "Simp. Robust Rx"receiver the quantization noise characteristics are given by equation 5.12, which can be seen as an average value of the spectral distribution for the quantization noise. From these figures it can be noticed that the results from the "Simp. Robust Rx"are similar to those provided by the full robust version, which indicates that the approach used in the "Robust Rx"does not present a clear advantage in terms of compensating of having a higher complex method for obtaining the spectral characterization of the quantization noise in the considered iterative receivers. These results show a very good agreement for the performance values which are quite acceptable when the quantization employs $m = 4$ bits of resolution.

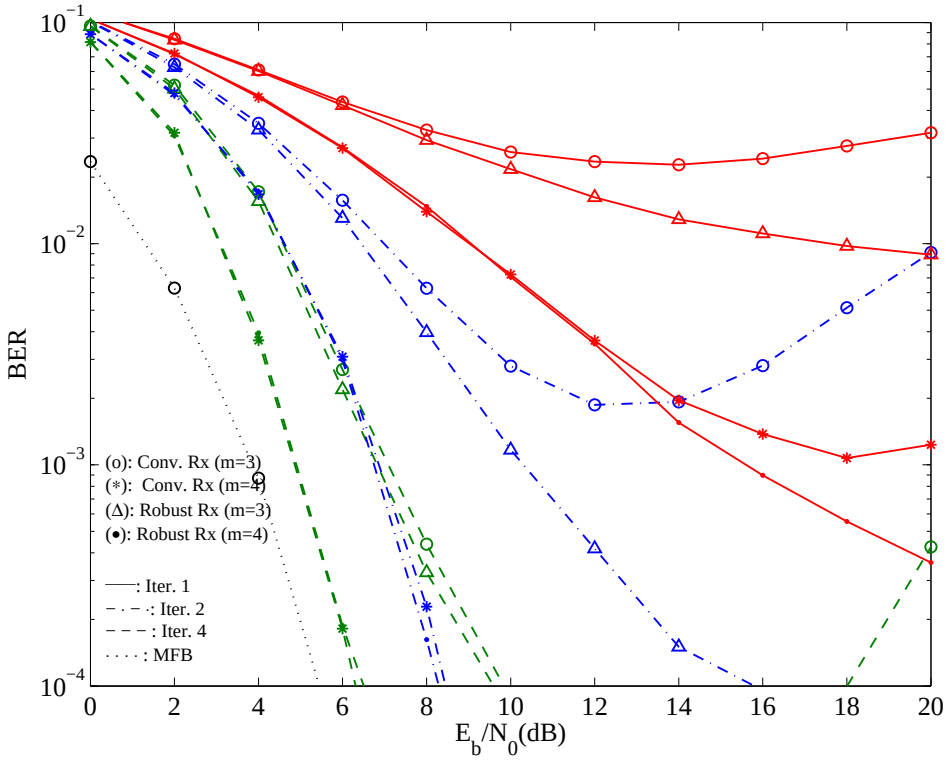

Figure 5.12: BER performance for a BS cooperation scenario with $P = 2$ MTs and $R = 2$ BSs. Comparison of results with quantization with $m = 3$ and 4 bits of resolution employing a conventional and robust receivers (1^{st} MT).

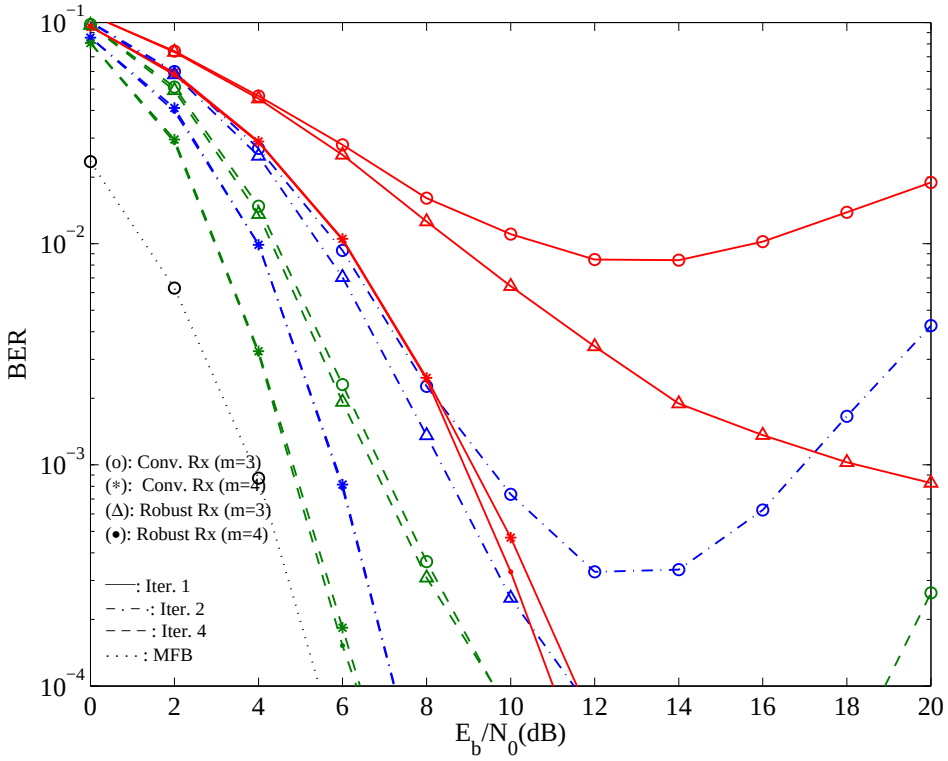

Figure 5.13: BER performance for a BS cooperation scenario with $P = 2$ MTs and $R = 2$ BSs. Comparison of results with quantization with $m = 3$ and 4 bits of resolution employing a conventional and robust receivers (2^{nd} MT).

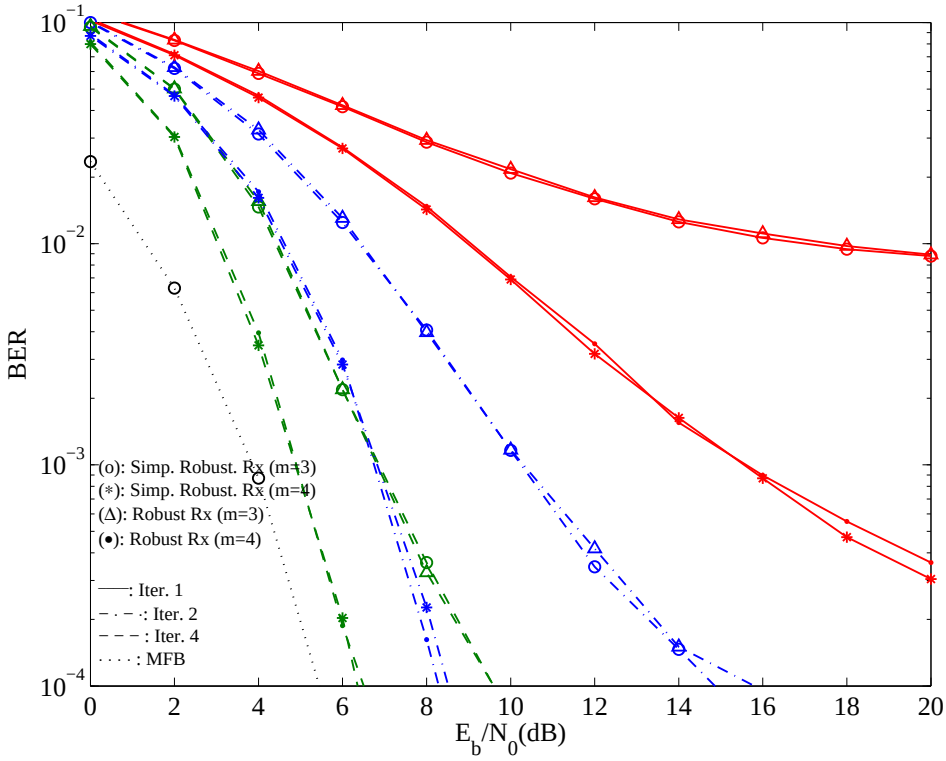

Figure 5.14: BER performance for a BS cooperation scenario with $P = 2$ MTs and $R = 2$ BSs. Comparison of results with quantization with $m = 3$ and 4 bits of resolution employing simplified robust and robust receivers (1^{st} MT).

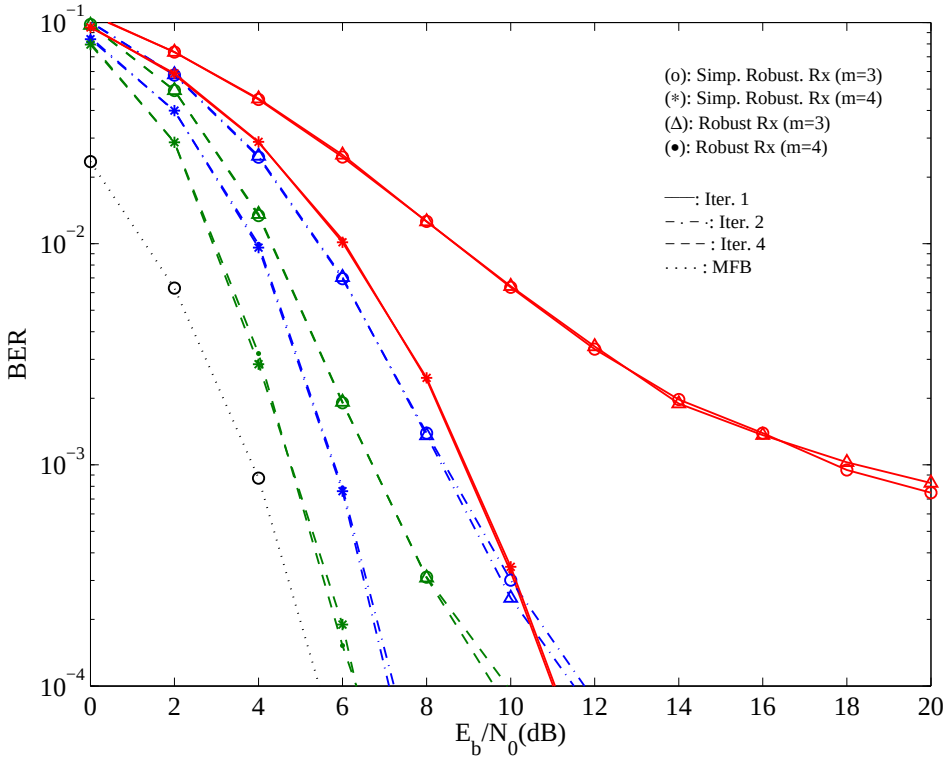

Figure 5.15: BER performance for a BS cooperation scenario with $P = 2$ MTs and $R = 2$ BSs. Comparison of results with quantization with $m = 3$ and 4 bits of resolution employing simplified robust and robust receivers (2^{nd} MT).

CHAPTER 6

Clustered Multiuser Detection with Base Station Cooperation Systems

In the previous chapters the concept of BS cooperation architecture was developed and evaluated, particularly in section 4. In chapter 6 the concept of BS cooperation is extended to clustered environments, such as C-RAN (Centralized-Radio Access Network). C-RAN architectures are expected to deal, with more efficiency, with the massive increase of mobile devices and provide higher data transmissions, spectral efficiency and high-speed mobility users. Therefore, BS cooperation schemes are suited to be enhanced by C-RAN-type systems, which are a fundamental approach to deal with high interference levels associated to reduced frequency reuse factors. This chapter presents different clustered scenarios and provides performance results that can evaluate such cases.

Chapter 6 is organized as follows: Section 6.1 contextualizes the BS cooperation system in a clustered scenario based on the C-RAN approach. In section 6.2 several multi-user detection techniques framed in a clustered scenario are presented. Section 6.3 shows the performance results where the several detection techniques explained in section 6.2 are evaluated.

6.1 C-RAN Contextualization

5G cellular communications can deal with the massive explosion of mobile devices, the need for higher data transmissions, spectral efficiency and high-speed mobility users [9]. This will be achieved mainly by combining massive MIMO techniques, small cells and employing reduced frequency reuse factors, ideally aiming at a universal frequency reuse [42]. Moreover, one can consider C-RAN (Centralized-Radio Access Network) architectures as one of the optimal approaches to enhance the potential of BS cooperation schemes [43–

45], which are critical to cope with high interference levels associated to reduced frequency reuse factors.

6.2 Multi-User Clustered Detection Techniques

Fig. 6.1 illustrates the adopted cellular scenario where the BS cooperation scheme is inserted in a clustered approach, suitable for C-RAN architectures. The system is char-

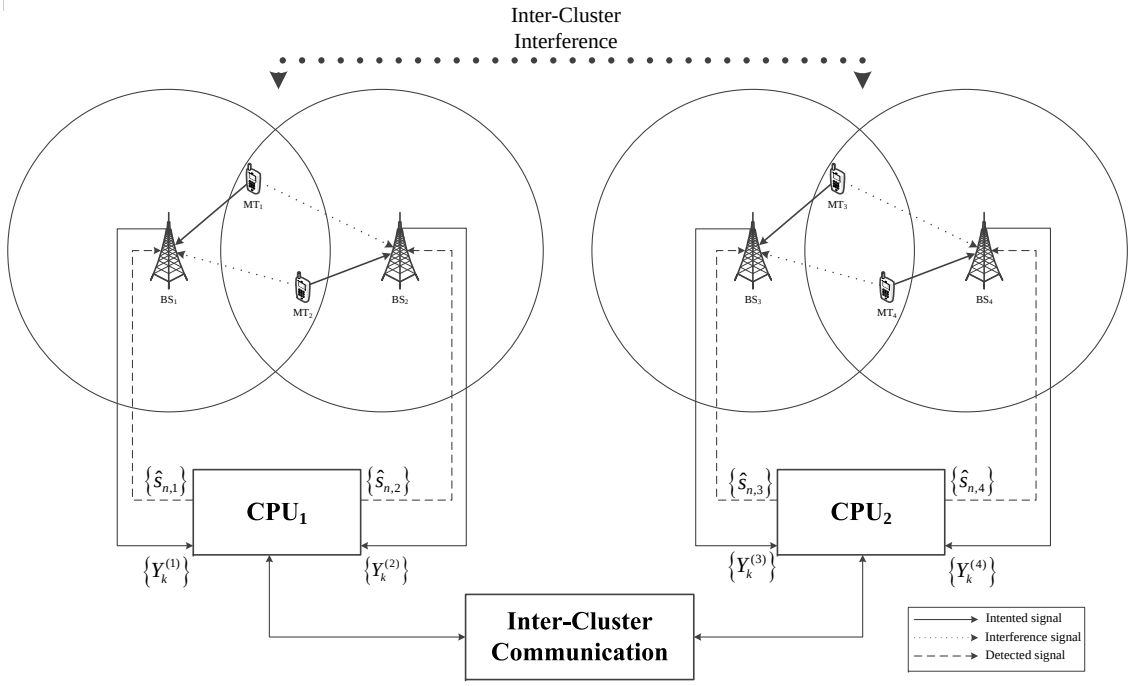

Figure 6.1: Adopted clustered cellular scenario.

acterized by two clusters employing BS cooperation-based wireless architectures. Both clusters can communicate through a backhaul network in a C-RAN structure. Inter-cluster interference is considered, being accounted for at each BS. For the clustered architecture presented in Fig. 6.1, the frequency-domain detector output for the p^{th}th MT and i^{th} iteration is given by

$$Y_k^{(r)} = \sum_{p \in C}^{P} S_{k,p} H_{k,p}^{ep(r)} + \sum_{p \notin C}^{P} S_{k,p} H_{k,p}^{ep(r)} + N_k^{(r)}, \tag{6.1}$$

with C denoting the set of BSs in the cluster, e.g., for the cluster with BSs 1 and 2 we have $C = \{1,2\}$. Moreover, two scenarios are considered, one with a fixed separation between clusters and one with a linear set of cells, which correspond to a more realistic scenario.

6.2.1 Fixed Separation Between Clusters

Fig. 6.2 illustrate a 2 cells scenario with limited inter-cell links, where β indicates the interference from a given MT to the remaining BSs in the other cluster. We assume that

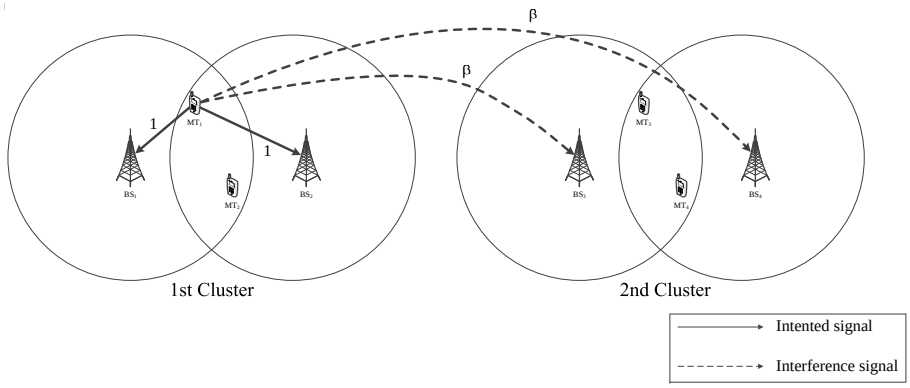

Figure 6.2: 1st MT transmission contributions

the links belonging to a given cluster have a transmission reference value, i.e., the main link of 1 or 0 dB. Moreover, β indicates the average power below the main link. For simplicity purposes, only the β effect from the 1$^{\text{st}}$ MT is shown. The case for the remaining MTs can easily be extended.

6.2.1.1 SCD (Single Cluster Detection)

SCD corresponds to a localized detection with no sharing of information between clusters. It provides the lowermost system requirements, in which for detection purposes and despite the β interference, the system is composed of $P = 2$ MTs and $R = 2$ BSs. The power associated with the different links $\xi_{p,r}$ is given by

$$\mathbf{\Xi}_C = \begin{bmatrix} \xi_{1,1} & \xi_{1,2} \\ \xi_{2,1} & \xi_{2,2} \end{bmatrix} = \begin{bmatrix} 1 & 1 \\ 1 & 1 \end{bmatrix}. \tag{6.2}$$

Nevertheless, the interference originated from the remaining MTs for detection purposes is also taken into account. For localized detections in clusters scenarios, $\mathbf{H}_k$, firstly defined in (4.7), is written according to the cluster that is being considered. So, for the case in (6.2) we only consider $\mathbf{H}_C$ from the complete $\mathbf{H}_k$ matrix form. Therefore, the $\mathbf{F}$ and $\mathbf{B}$ coefficients are given by

$$\mathbf{F}_C = \kappa \mathbf{\Lambda}_C \mathbf{H}_C^H \mathbf{e}_2 \tag{6.3}$$

and

$$\mathbf{B}_C = \mathbf{H}_C \mathbf{F}_C - \mathbf{e}_2, \tag{6.4}$$

with

$$\mathbf{\Lambda}_C = \left(\mathbf{H}_C^H \left(\mathbf{I}_2 - \mathbf{P}_2^2 \right) \mathbf{H}_C + f\left(SNR\right) \mathbf{I}_2 \right)^{-1}. \tag{6.5}$$

6.2.1.2 FD (Full Detection)

The FD (Full Detection) procedure is employed with total sharing of information. The system can be seen as a single cluster with $P = R = 4$ and it presents macro-diversity

effects inherent to BS cooperation architectures and the power associated with the different links $\xi_{p,r}$ can be written as

$$\mathbf{\Xi} = \begin{bmatrix} \xi_{1,1} & \xi_{1,2} & \xi_{1,3} & \xi_{1,4} \\ \xi_{2,1} & \xi_{2,2} & \xi_{2,3} & \xi_{2,4} \\ \xi_{3,1} & \xi_{3,2} & \xi_{3,3} & \xi_{3,4} \\ \xi_{4,1} & \xi_{4,2} & \xi_{4,3} & \xi_{4,4} \end{bmatrix} = \begin{bmatrix} 1 & 1 & \beta & \beta \\ 1 & 1 & \beta & \beta \\ \beta & \beta & 1 & 1 \\ \beta & \beta & 1 & 1 \end{bmatrix}. \tag{6.6}$$

6.2.1.3 HD (Hybrid Detection)

The HD (Hybrid Detection) method corresponds to an intermediate scheme for the detection procedure. By enabling the HD approach we can have higher interference values given by β. This increases the detection requirements in comparison with SCD and decreases them regarding FD. In this case, the power associated with the different links $\xi_{p,r}$ is given by

$$\mathbf{\Xi} = \begin{bmatrix} \xi_{1,1} & \xi_{1,2} & \xi_{1,3} & \xi_{1,4} \\ \xi_{2,1} & \xi_{2,2} & \xi_{2,3} & \xi_{2,4} \end{bmatrix} = \begin{bmatrix} 1 & 1 & \beta & \beta \\ 1 & 1 & \beta & \beta \end{bmatrix}. \tag{6.7}$$

6.2.2 Linear Set of Cells

Instead of a limited inter-cell link's scenario we can consider a more realistic scenario, shown in Fig. 6.3. For the sake of simplicity we only show the interference effect, represented

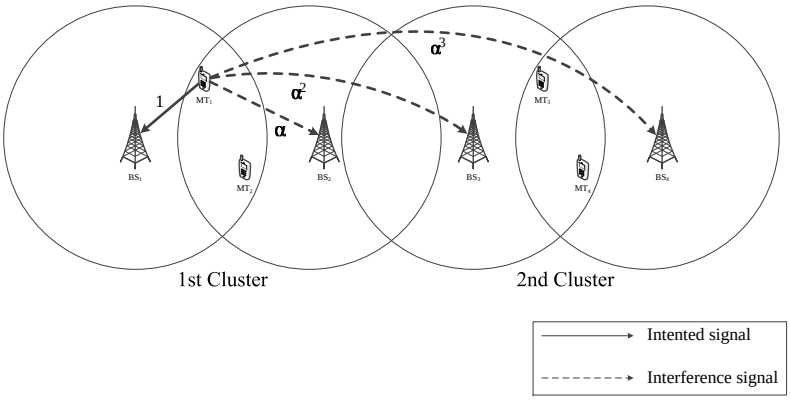

Figure 6.3: 1st MT transmission contributions

by the coefficient α, originated from the 1st MT. As previously described with the β parameter, α indicates the average power below the main link. BSs that are further away will receive lower interference levels when compared with the closest ones. Moreover, there is some overlapping between clusters. In this case, each cluster performs the detection in a localized method and they can iteratively share side information through the backhaul link in order to strategically compensate a higher or lower amount of information shared. Hence, we have an iterative receiving scheme in each cluster provided by the implementation of BS cooperation systems and an iterative detection strategy with the sharing of information in

a C-RAN type environment. Regarding Fig. 6.3, the power associated with the different links $\xi_{p,r}$ is given by

$$\mathbf{\Xi} = \begin{bmatrix} 1 & \alpha & \alpha^2 & \alpha^3 \\ \alpha & 1 & \alpha & \alpha^2 \\ \alpha^2 & \alpha & 1 & \alpha \\ \alpha^3 & \alpha^2 & \alpha & 1 \end{bmatrix}. \tag{6.8}$$

Moreover, for a SCD method, where each cluster detects its MTs, the power associated with the different links is given by

$$\mathbf{\Xi}_C = \begin{bmatrix} \xi_{1,1} & \xi_{1,2} \\ \xi_{2,1} & \xi_{2,2} \end{bmatrix} = \begin{bmatrix} 1 & \alpha \\ \alpha & 1 \end{bmatrix}. \tag{6.9}$$

Clearly, the complexity of each detection scheme is conditioned by the size of matrices to invert, which is done for each iteration and subcarrier, and the required overheads for exchanging received signals and data estimates. This is directly related with the iterative algorithm, where the received signals have size N and the data estimation, concerning each inter-cluster iteration, also have size N. For the Single Cluster Detection, this must be done for each cluster.

The complexity of the considered receiver is essentially conditioned by the size of the matrices to invert and the required overheads for exchanging received signals and data estimates, which is shown in Table 6.1. P and R indicate the total number of MTs and BSs, respectively, that are considered in the system. Moreover, P_c and R_c are the MTs and BSs, respectively, that belong only to a given cluster.

	Matrix inversion	Required overheads	
	Dimensions	Received signals	Data estimates
Full Detection	$R \times R$	R	0
Single Cluster Detection	$R_c \times R_c$	R_c	0
Hybrid Detection	$R \times R$	R	R

Table 6.1: Complexity and required overheads

When we consider clustered architectures, the complexity is conditioned by the fact that for each frequency and each iteration it is necessary to invert a matrix with the cluster dimension. Regarding FD approaches it is necessary to invert a matrix with dimension equal to the number of receiving BSs. For clustered systems, the global iterations required is related to the number of intra-cluster iterations times the number of inter-cluster iterations, i.e., 3 to 4 intra-cluster iterations times 1 to 3 inter-cluster iterations. Moreover, with the iterative algorithm the received signals have size N and the data estimation, concerning each inter-cluster iteration, also have size N. In the FD definition it is only necessary to

perform 3 or 4 iterations. When the Single Cluster Detection is enabled, this must be considered to each cluster.

6.3 Performance Results

The previous section described different detection techniques in a clustered context, where the interference levels are related with two scenarios, mainely a two cells scenario with limited inter-cell links and a more realistic scenario. In this section we present a set of performance results to properly evaluate both cases previously explained.

The data blocks associated with each MT have $N = 256$ data symbols, selected from a QPSK constellation under a Gray mapping rule, plus an appropriate cyclic prefix. We considered a multipath channel with 64 symbols-spaced taps and uncorrelated Rayleigh fading on the different multipath components. Similar results were observed for other channels with rich multipath propagation. The channels between different transmitting and receiving antennas are assumed uncorrelated. Perfect synchronization and channel estimation is assumed and also that the useful part of the blocks transmitted by different MTs arrive at each BS simultaneously. In practice, this could be accomplished by employing extended cyclic prefixes, with duration longer than the maximum overall channel impulse response plus the difference between the maximum and minimum propagation delay between MTs and BSs, provided that we have accurate channel estimates.

Let us start by considering the limited inter-cell links scenario (illustrated in Fig. 6.2). Fig. 6.4 illustrates the case where we have a BS cooperation scenario employing a FD approach with the interference parameter β corresponding to 0 dB. It is clear that there is a significant performance improvement when the received signals associated to different BSs are combined. The performance improvement is higher for the 1^{st} iteration, that corresponds to the linear FDE, which is due to the higher residual ISI at the FDE output. Moreover, the performance of the iterative receiver is already close to the MFB just after 4 iterations and the macro-diversity also reduces the shadowing effects and improves overall coverage.

Fig. 6.5 considers the BER performance when the receiver is based on the clustered scenario described in [10]. BSs 1 and 2 are associated with one cluster and BSs 3 and 4 to the other, with interference $\beta = -15$ dB. From this figure it is clear that we can have relatively good separation for different MTs. However, the performance degrades for high SNR values, i.e., high values of E_b/N_0. This is due to the fact that our receiver assumptions does not consider the inter-cluster interference. For low SNR this is not a problem because the noise is much higher than the residual interference. But for high SNR this leads to a mismatched receiver, since $\mathbf{F}$ and $\mathbf{B}$ coefficients are designed assuming lower interference levels. To overcome this problem, we can modify (4.39) so as to preclude

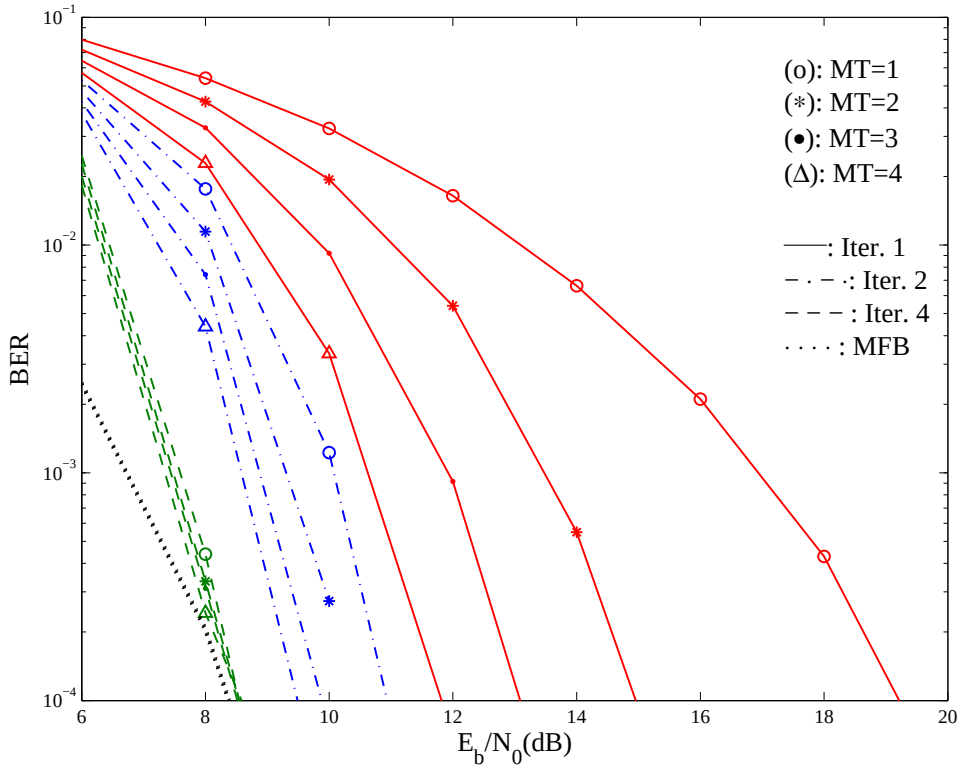

Figure 6.4: BS cooperation scenario with $C = 1$ clusters, $P = 4$ MTs, $R = 4$ BSs and $\beta = 0$ dB.

$\sigma_n^2/\sigma_s^2 = 1/SNR$ taking values too small. This can be done by using $f(SNR)$ as

$$f(SNR) = \begin{cases} 1/SNR & \text{if } SNR < SNR_0 \\ 1/SNR_0 & \text{if } SNR \geq SNR_0 \end{cases} \tag{6.10}$$

instead of the initially $f(SNR) = 1/SNR$ in (4.39), i.e., by performing a kind of clipping on SNR when we are computing the receiver parameters. We verified $SNR_0 = 13$ dB leads to relatively good results. The corresponding BER performance is depicted in Fig. 6.6. This value of SNR_0 was employed in the remaining of this thesis. Additionally, the performance results are compared with the case where FD is employed, i.e., a full BS cooperation detection scheme, since there is not a single definition of MFB for clustered scenarios.

Fig. 6.7 and 6.8 show the average BER performance for all MTs, regarding the detection types described in (6.2) and (6.7), respectively. Each figure shows the performance results for β values of -20 and -15 dB. Both figures demonstrate that less transmitted power for the interference links induces better performance results. Moreover, it can be seen that there is not a significant difference between the two detection approaches, and in this case the detection type regarding the cluster only can be considered, which requires less processing.

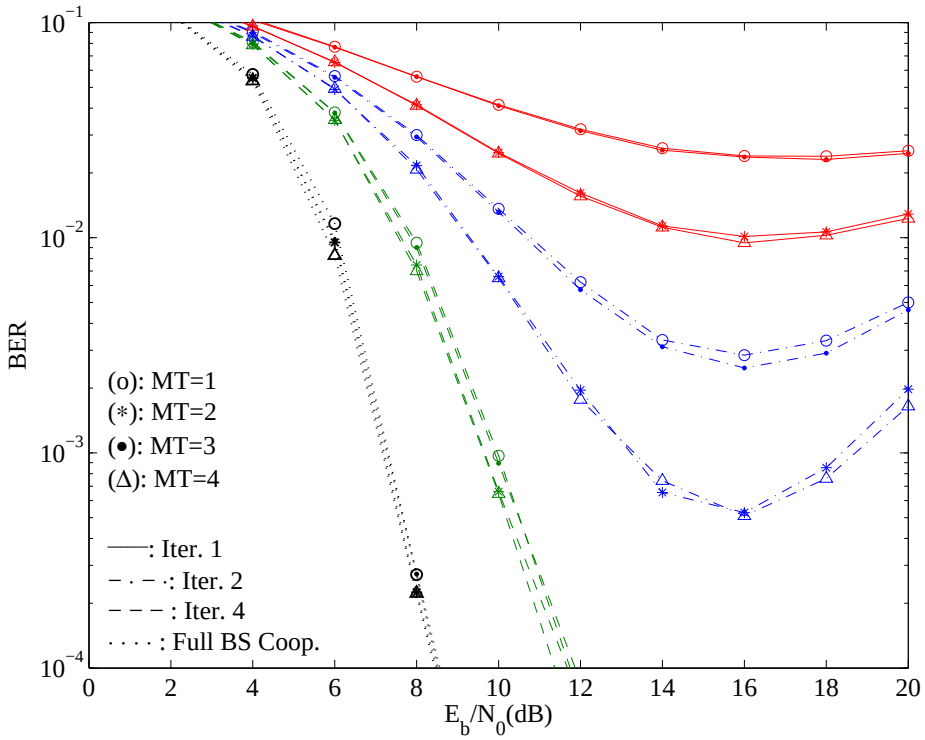

Figure 6.5: BER performance for the receiver of [10] in the clustered scenario (one cluster associated to BSs 1 and 2 and the other associated to BSs 3 and 4), when $\beta = -15$ dB.

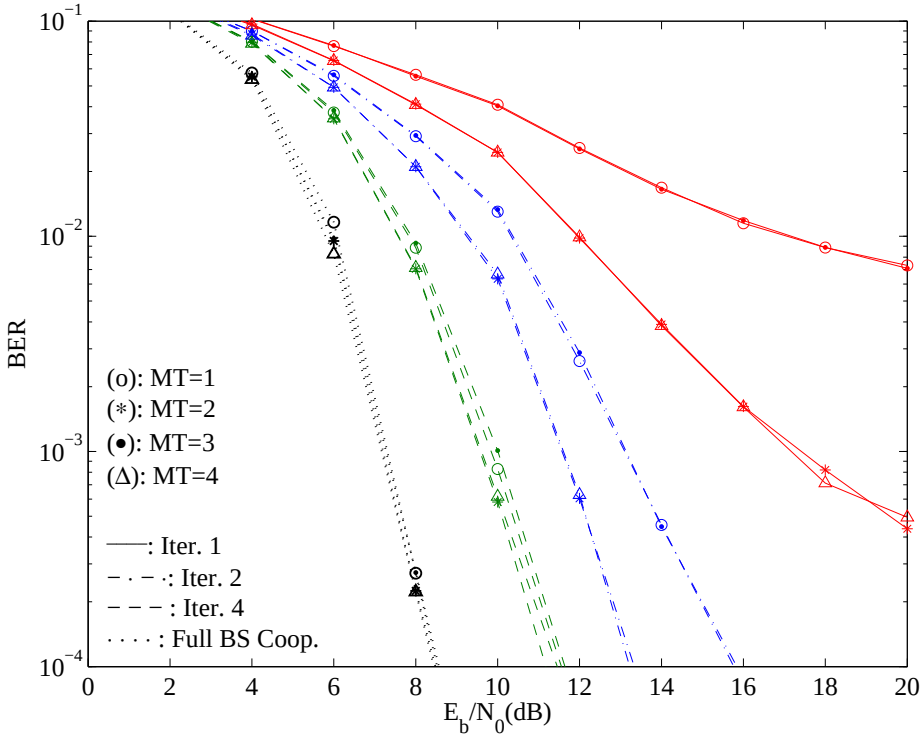

Figure 6.6: As in Fig. 6.5, but setting a limit on the SNR with $SNR_0 = 13$ dB in (6.10).

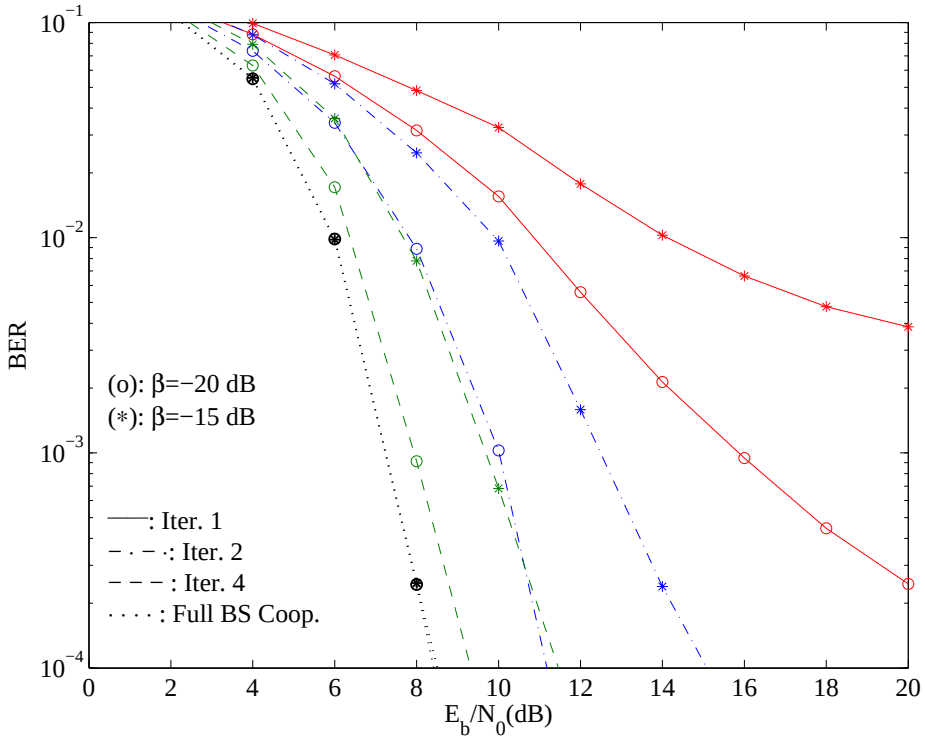

Figure 6.7: BS cooperation scenario with $C = 2$ clusters, each cluster with $P = 2$ MTs and $R = 2$ BSs. Detection type based on the SCD approach.

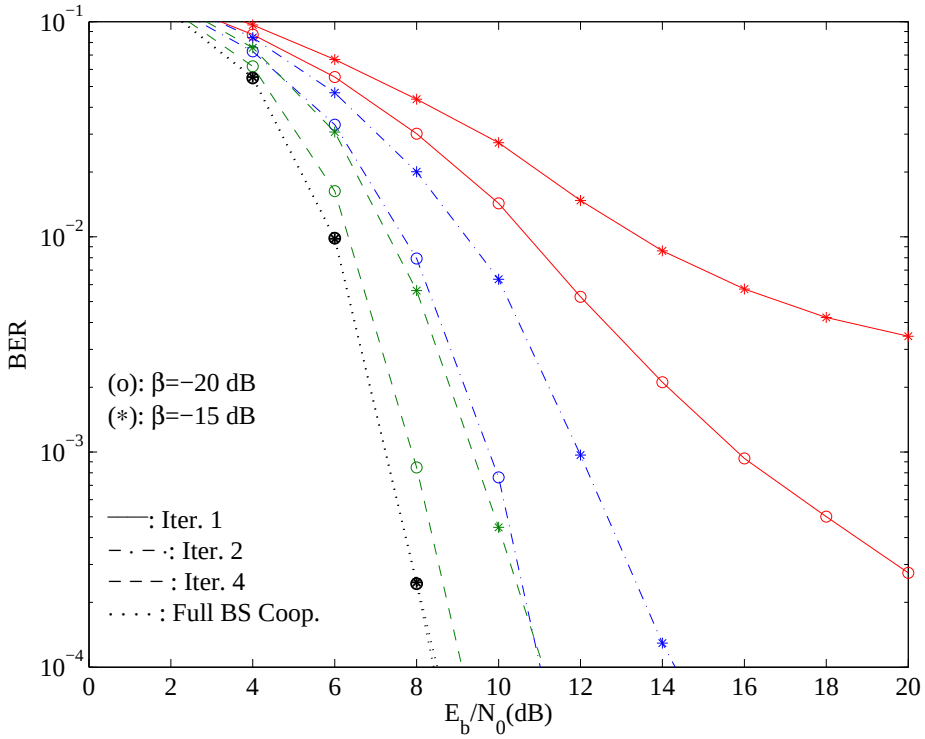

Figure 6.8: BS cooperation scenario with $C = 2$ clusters, each cluster with $P = 2$ MTs and $R = 2$ BSs. Detection type based on the HD approach.

Let us now analyze the case where 2 clusters communicate to allow interference cancelation and to decrease the overall system's detection requirements. Fig. 6.9 illustrates the MTs average values for the BER performance results considering the detection based on the single cluster detection method. Clearly, it can be seen that with inter-cluster

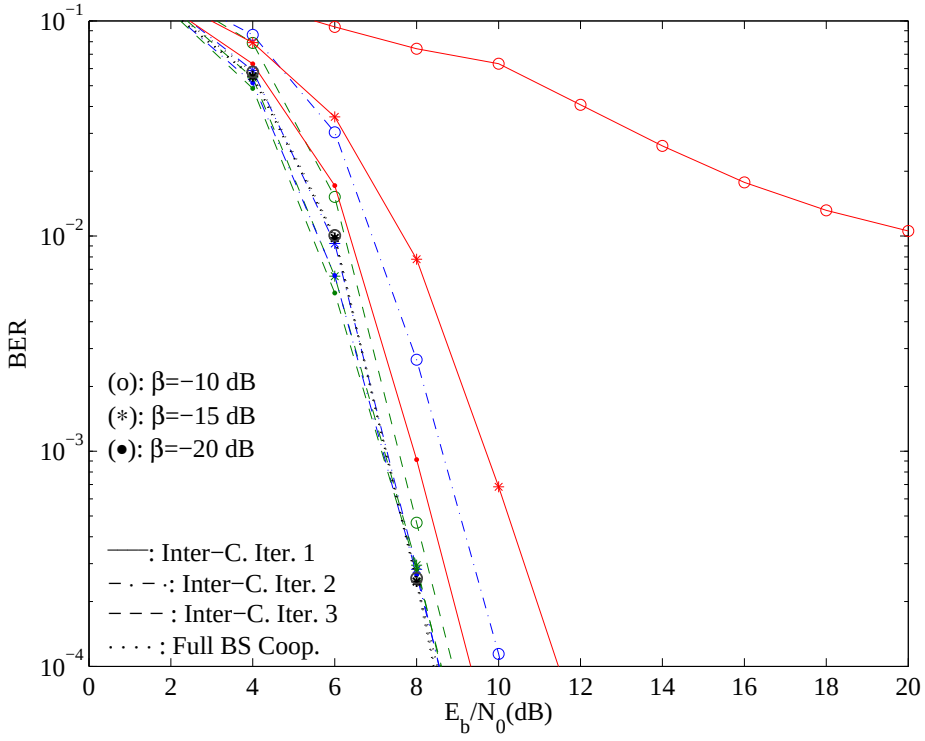

Figure 6.9: BS cooperation scenario with $C = 2$ clusters, each cluster with $P = 2$ MTs and $R = 2$ BSs. Detection type based on the SCD approach with inter-cluster communication.

iterations the BER performance is nearly the same of the full BS cooperation case after just 3 iterations. Furthermore, with this approach we can detect the MTs with significant accuracy and decrease the detection requirements, especially when comparing to the results shown in Fig. 6.4.

Regarding the study of a cellular system based on a more realistic scenario (see Fig. 6.3), Fig. 6.10 illustrates the average BER performance from all MTs for each iteration when α corresponds to -20, -15 and -10 dB. As with the scenario previously studied, these results show the impact of higher interference values ($\alpha = -10$ dB) on the performance of the considered receiver, when compared with lower values such as $\alpha = -20$ dB. When considering $\alpha = -20$ dB, at the fourth iteration, it is already possible to have performance results close to the Full BS cooperation scenario. Considering the scenario presented in Fig. 6.10, Fig. 6.11 shows the average iterations that are required for the receiver to perform a successfully detection of a given detected block. Moreover, we also show the PER (Packet Error Rate) associated with the same case. It is possible to see that for high values of E_b/N_0 and considering $\alpha = -20$ dB only one iteration is required, greatly decreasing the process involved to perform the detection. For low values of E_b/N_0 the receiver has to

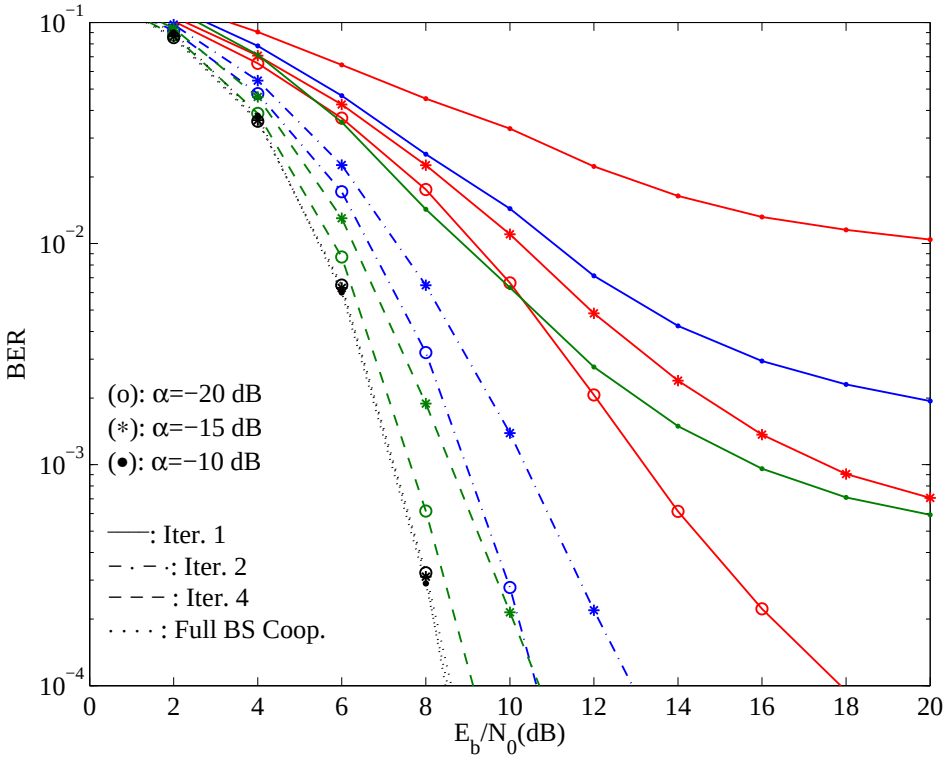

Figure 6.10: Average BER performance of all MTs for each iteration, when $\alpha = -20$, -15 and -10 dB.

perform 4 iterations, even though it is not sufficient to successfully detect the majority of the blocks, as we can conclude from the PER performance. Nevertheless, it is possible to practically achieve the performance provided by the Full BS cooperation case.

Enabling the sharing of information between clusters in a iterative methodology, Fig. 6.12 shows the 4^{th} iteration of the average BER performance for all MTs considering the possibility of having inter-cluster iterations. The α values considered are -10, -5 and -3 dB. Similarly to the case where we have limited inter-cell links, by increasing the number of inter-cluster iterations the performance results can be very close to the Full BS cooperation scenario, even for high values of α such as -5 dB. Nevertheless, for $\alpha = -3$ dB the performance is largely degraded. So, it is possible to sustain high interference environments by increasing the processing of the iteration method. Taking into account the same scenario presented in Fig. 6.12 let us consider the average inter-cluster iterations required to perform a successfully detection in a given block and the PER performance regarding that case. These results are depicted in Fig. 6.13, where we consider α values of -10, -5 and -3 dB. As expected, for $\alpha = -10$ dB we only need approximately 1 iteration for a high E_b/N_0. For lower values of E_b/N_0, regardless of the α interference we need 3 inter-cluster iterations, which requires an overload of backhaul information shared between clusters. Moreover, even with 3 iterations the detector was not able to successfully perform the detection, as confirmed by the PER performance.

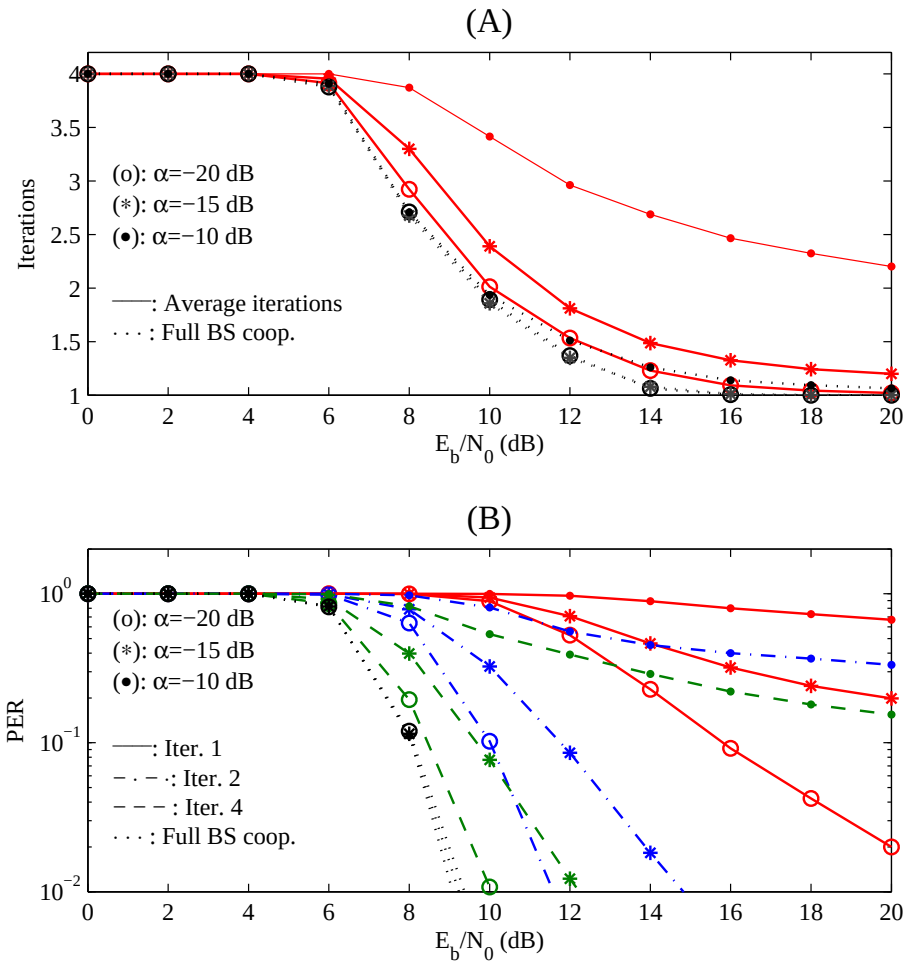

Figure 6.11: Average iterations required for successfully detect a given block (A) and average PER (B) performance, in the conditions of Fig. 6.10.

It should be pointed out that for very large systems the use of the FD technique is too complex, and our clustered techniques can be a very interesting alternative. However, if the interference levels are still significative, then it must be necessary to combine our techniques with other techniques, for reducing the number of interfering cells. On the other hand, if the system is operating at very high frequencies, e.g., for mm-wave communications, physical obstacles such as walls can be enough to reduce the number of cells with strong interfering levels, allowing the direct employment of our clustered detection schemes.

The proposed methods depend on the interference level and from our results it can be concluded that, in the uplink transmission, it is possible to accurately detect the MTs with low detection requirements. When enabling an inter-cluster communication methodology, one can allow the flexibility of increasing the interference value and maintaining a low overall system's detection requirements without sacrificing the performance.

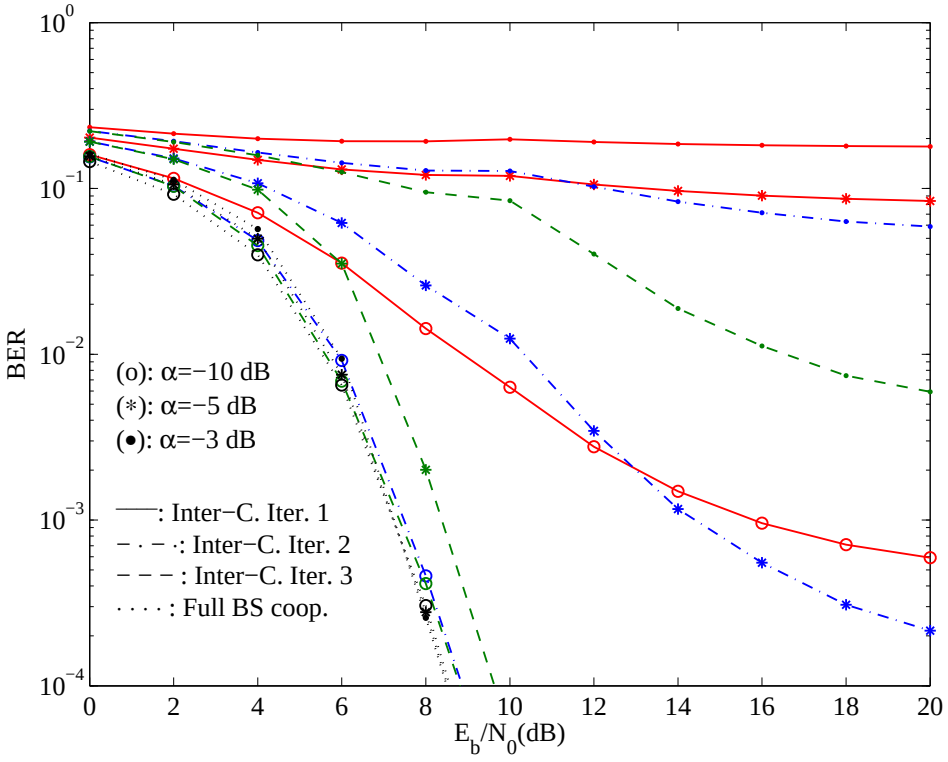

Figure 6.12: 4^{th} iteration of average BER performance for all MTs, when $\alpha = -10$, -5 and -3 dB and up to 3 inter-cluster iterations.

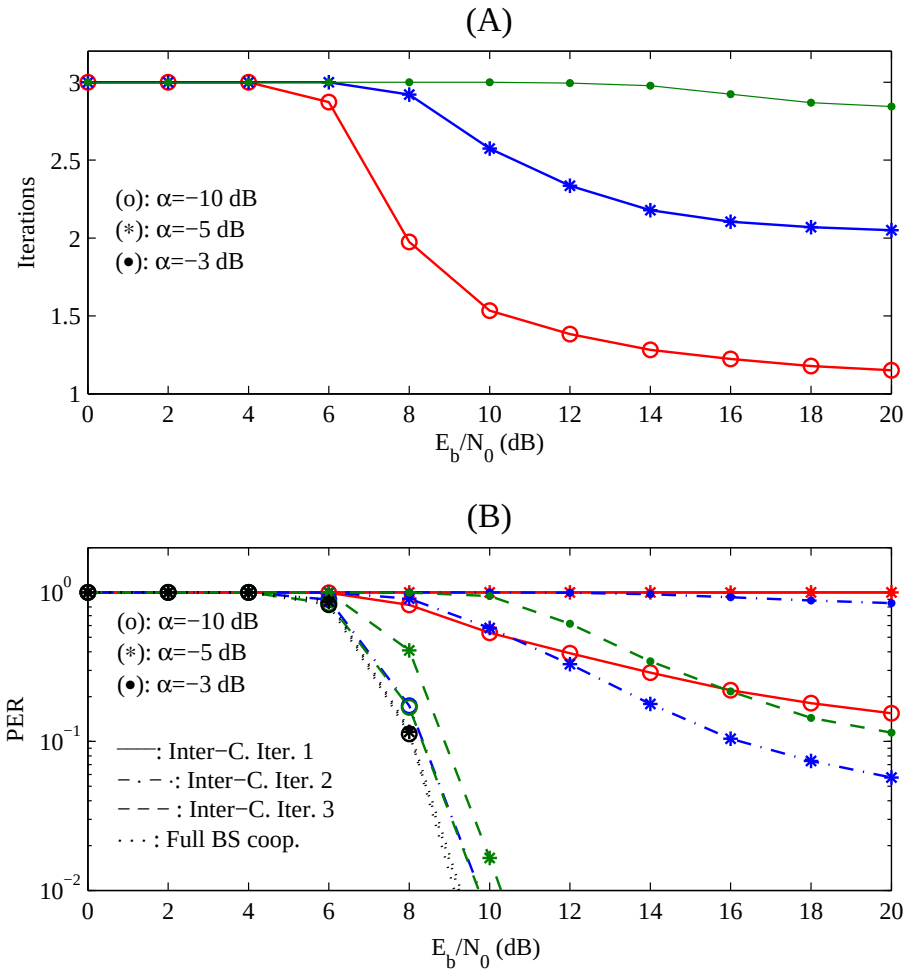

Figure 6.13: Average inter-cluster iterations required for successfully detect a given block (A) and average PER performance (B), for each inter-cluster iteration, in the conditions of Fig. 6.12.

CHAPTER 7

Conclusions and Future Work

7.1 Conclusions

The main objective of this thesis is focused on the study and development of efficient techniques for the uplink of BS cooperation systems, with receivers based on the IB-DFE concept, and with SC-FDE schemes as a modulation choice. The developed work is related with the signal's transmission and user's detection, that contribute to achieve better performance, while maintaining a low system complexity. Chapter 2 introduced a set of basic concepts in digital transmission systems, such as interference, frequency-reuse techniques and multipath-based communication channels. Moreover, chapter 2 described the modeling of the transmitted and received signals in a channel highly affected by multipath and introduced the concept of multi-cell cooperation techniques. Chapter 3 introduced basic principles of MC and SC modulations. It was shown how SC modulations could benefit from FDE techniques by taking advantage of the CP-assisted block transmission approach and be a valid alternative to MC-based OFDM modulations, particulary in the uplink transmission. These schemes are especially interesting for high data rate CP-assisted block transmissions over severely time-dispersive channels, with much lower complexity then the optimum receivers. Also, in chapter 3 it was shown that FDE receivers considering the MMSE criteria have better performance results, since They do not attempt to fully invert the channel effects. Chapter 3 demonstrated that iterative non-linear receivers, such as IB-DFE are optimal when compared to the linear ones, where it was shown that the system's performance is closer to the MFB just after 4 iterations. With these iterative receivers, the result for the first iteration corresponds to those of conventional linear MMSE-FDE technique; the subsequent iterations provide a performance enhancement, thanks to the iterative cancelation of residual interference. Chapter 4 presented the MIMO receiver structure for the uplink transmission of SC-FDE systems based on IB-DFE techniques.

In this chapter, the computation for the different parameters was provided and it was shown that users being detected in the fist place had worst BER performance than those detected when the system already has some information in the previously detected data. To complement the study on these architecture schemes, a simple and accurate analytical model for obtaining the BER performance was presented, and a comparison between both simulated and theoretical approaches was performed. Furthermore, a simple method for improving the achievement of theoretical BER performance was proposed. The work related with the MUD detection in this chapter was partially published in [10–12]. Chapter 5 was dedicated to adding the quantization proceeding into the conventional BS cooperations schemes with SC-FDE schemes for the uplink and iterative receivers based on the IB-DFE concept. Even though sampling and quantization introduces distortion, it is an essential process to decrease the transmission requirements in the backhaul link. In this thesis, the quantization process was studied by comparing receivers that did not consider quantization effects and receivers that considered uniform quantization. Furthermore, this chapter presented robust receivers that take into account the spectral characterization of the quantization noise. The performance results demonstrated that it is possible to have robust, yet simple, receivers that can have a good agreement with the performance values which are quite acceptable when the quantization employs $m = 4$ bits of resolution. Similarly to chapter 4, a relatively simple and accurate analytical approach for obtaining the performance of the proposed receivers employing quantization was presented. The work presented in this chapter was published in [13–15]. In chapter 6 BS cooperation system with clustered environments such as C-RAN was extended. In C-RAN systems, a cloud-based scheme is a promising approach for designing transmission schemes for future cellular networks. The BS cooperation scheme in C-RAN systems was characterized in this chapter and it was shown that BS cooperation architectures can be related to future wireless networks. Chapter 6 proposed several multi-user detection techniques that are suitable for cloud-based schemes. The work presented was this chapter is published in [16–18].

7.2 Future Work

Telecommunication's engineering is an area with the most significant development in the last years, with endless research possibilities that can provide a direct impact in our present lives. Despite the relevant contribution of the developed study of this thesis work there are various issues that can and must be taken into account for future developments. Therefore, as enrichment to the work elaborated in this thesis, additional future research may include:

- **Channel Estimation**
  It was assumed that the channel state is well know. However, in real applications the channel estimation must be performed. Since it is a very important topic, its study will be a valuable contribution to this work.

- **Channel Synchronization**
  Perfect time and frequency synchronization was assumed. It is well known that accurate synchronization is fundamental for a communication system to guarantee good performance. Thus, ensuring an effective time and frequency synchronization, while maintaining a good complexity/performance tradeoff, will be a valuable contribution to this work.

- **OFDM and SC-FDE comparison**
  In spite of the basic principles of MC and SC modulations have been introduced in chapter 2, all the research performed in this thesis was focused on the SC-FDE modulation combined with iterative (turbo) FDE schemes, since they have excellent performance in severely time-dispersive channels, making it a promising candidate for future broadband wireless systems. For that reason, a comparison study concerning the performance results obtained with OFDM modulation for the same scenarios, will be a significant contribution to this work.

- **Interference mitigation**
  When considering the interference issues and techniques that allow its mitigation two main approaches can be considered, Multiuser Detection (MUD) methods and Interference Alignment (IA) techniques [46]. When compared with multiuser detection, interference alignment has half the capacity, at most, but the detection is simpler since performed locally, and there is no need to share transmitted/detected data, although the global channel knowledge is still required. IA techniques are a promising approach concerning interference mitigation, and they deserve a solid study and a performance comparison with MUD systems.

APPENDIX A

Minimum Mean Squared Error Analytical Computation: SISO Linear FDE

This appendix explains all the mathematical manipulations regarding the Mean Square Error (MSE) computation, considering SC with linear FDE in a Single-Input Single-Output System (SISO) system.

At the receiver, the samples Y_k are characterized by

$$Y_k = H_k S_k + N_k, \tag{A.1}$$

where S_k is the frequency-domain of the transmitted data symbol s_n. H_k denotes the overall channel frequency response for the k^{th} frequency and N_k indicates the channel noise term in the frequency-domain. The output samples of the linear FDE block are expressed by

$$\tilde{S}_k = F_k Y_k. \tag{A.2}$$

It is assumed that the global channel frequency response is given by

$$F_k H_k \tag{A.3}$$

and the average overall channel frequency response corresponds to

$$\gamma = \frac{1}{N} \sum_{k=0}^{N-1} F_k H_k. \tag{A.4}$$

Moreover, $\tilde{S}_k$ can be expressed as

$$\tilde{S}_k = \gamma S_k + \varepsilon_k, \tag{A.5}$$

where ε_k represents the global error consisting of the residual ISI plus the channel noise and a SINR can be defined by

$$\text{SINR} = \frac{|\gamma|^2 \, \mathbb{E}\left[|S_k|^2\right]}{\mathbb{E}\left[|\varepsilon_k|^2\right]}. \tag{A.6}$$

Maximizing SINR corresponds to minimizing the error associated to ε_k, hence the MSE on the received data samples can be defined as

$$\theta(k) = \frac{1}{N^2} \sum_{k=0}^{N-1} \theta_k, \tag{A.7}$$

where

$$\theta_k = \mathbb{E}\left[\left|\tilde{S}_k - \gamma S_k\right|^2\right] = \mathbb{E}\left[\left|Y_k F_k - \gamma S_k\right|^2\right] \tag{A.8}$$

corresponds to the MSE minimization for each k. One can notice that θ_k can be written as

$$\begin{aligned}
\theta_k &= \mathbb{E}\left[\left(\tilde{S}_k - \gamma S_k\right)^* \left(\tilde{S}_k - \gamma S_k\right)\right] \\
&= \mathbb{E}\left[\left(F_k Y_k - \gamma S_k\right)^* \left(F_k Y_k - \gamma S_k\right)\right] \\
&= \mathbb{E}\left[\left(F_k^* Y_k^* \gamma^* S_k^*\right) \left(F_k Y_k - \gamma S_k\right)\right] \\
&= \mathbb{E}\left[F_k^* Y_k^* F_k Y_k - F_k^* Y_k^* \gamma S_k - \gamma^* S_k^* F_k Y_k + \gamma^* \gamma S_k^* S_k\right] \\
&= \mathbb{E}\left[F_k^* Y_k^* Y_k F_k\right] - \mathbb{E}\left[\gamma F_k Y_k S_k^*\right] - \mathbb{E}\left[\gamma F_k^* Y_k^* S_k\right] + \mathbb{E}\left[\gamma^* \gamma S_k^* S_k\right] \\
&= \left|F_k\right|^2 \mathbb{E}\left[Y_k^* Y_k\right] - \gamma F_k \mathbb{E}\left[Y_k S_k^*\right] - \gamma F_k^* \mathbb{E}\left[Y_k^* S_k\right] + \left|\gamma\right|^2 \mathbb{E}\left[S_k^* S_k\right].
\end{aligned} \tag{A.9}$$

Furthermore,

$$\begin{aligned}
\mathbb{E}\left[Y_k^* Y_k\right] &= \mathbb{E}\left[\left(H_k^* S_k^* + N_k^*\right)\left(H_k S_k + N_k\right)\right] \\
&= \mathbb{E}\left[H_k^* S_k^* H_k S_k + H_k^* S_k^* N_k + N_k^* H_k S_k + N_k^* N_k\right] \\
&= \left|H_k\right|^2 \mathbb{E}\left[\left|S_k\right|^2\right] + \mathbb{E}\left[\left|N_k\right|^2\right],
\end{aligned} \tag{A.10}$$

since

$$\mathbb{E}\left[\left|N_k S_k\right|^2\right] = 0, \tag{A.11}$$

$$\mathbb{E}\left[\left|S_k\right|^2\right] = 2\sigma_S^2, \tag{A.12}$$

and

$$\mathbb{E}\left[\left|N_k\right|^2\right] = 2\sigma_N^2. \tag{A.13}$$

Moreover,

$$\mathbb{E}\left[Y_k S_k^*\right] = \mathbb{E}\left[\left(H_k S_k + N_k\right) S_k^*\right] = H_k \mathbb{E}\left[\left|S_k\right|^2\right] = 2H_k \sigma_S^2 \tag{A.14}$$

and

$$\mathbb{E}\left[Y_k^* S_k\right] = \mathbb{E}\left[Y_k S_k^*\right]^* = 2H_k^* \sigma_S^2. \tag{A.15}$$

Taking these deductions into account, (A.9) can be written as

$$\begin{aligned}
\theta_k &= \left|F_k\right|^2 \left(\left|H_k\right|^2 2\sigma_S^2 + 2\sigma_N^2\right) - \gamma F_k H_k 2\sigma_S^2 - \gamma S_k^* H_k^* 2\sigma_S^2 + \left|\gamma\right|^2 2\sigma_S^2 \\
&= 2\left|F_k\right|^2 \left(\left|H_k\right|^2 \sigma_S^2 + \sigma_N^2\right) - 4\gamma \mathrm{Re}\{F_k H_k\}\sigma_S^2 + 2\left|\gamma\right|^2 \sigma_S^2.
\end{aligned} \tag{A.16}$$

The minimization of the MSE provides the optimum F_k at each subcarrier θ_k. Defining the Lagrange function

$$J = \mathbb{E}\left[\left|\Theta_k\right|^2\right] + \lambda\left(\gamma - 1\right), \tag{A.17}$$

where λ corresponds to the Lagrange multipliers and assuming the condition

$$\gamma = 1, \tag{A.18}$$

the optimum coefficients F_k are obtained by solving the system of equations

$$\begin{cases} \nabla_{F_k} J = 0 \\ \nabla_{\lambda} J = 0. \end{cases} \tag{A.19}$$

Knowing that the following rules can be applied

$$\nabla_x \left(x^H R x \right) = 2Rx \tag{A.20a}$$

$$\nabla_x \left(x^H p \right) = \nabla_x \left(p^T x^* \right) = 2p \tag{A.20b}$$

$$\nabla_x \left(p^H x \right) = \nabla_x \left(x^T p^* \right) = 0 \tag{A.20c}$$

$$\nabla_x \left(2\mathrm{Re}\{p^H x\} \right) = \nabla_x \left(p^H x + p^T x^* \right) = \nabla_x \left(\mathrm{Re}\{x^H p\} \right) = 2p, \tag{A.20d}$$

the optimum coefficient F_k is expressed as

$$F_k = \frac{H_k^*}{NSR + |H_k|^2}, \tag{A.21}$$

where

$$NSR = \frac{1}{SNR} = \frac{\sigma_N^2}{\sigma_S^2}. \tag{A.22}$$

APPENDIX B

Minimum Mean Squared Error Analytical Computation: SISO IB-DFE

This appendix presents all the mathematical manipulations regarding the MSE computation, considering a SC-FDE modulation with IB-DFE in a SISO system.

Considering the i^{th} iteration and the k^{th} frequency, the frequency-domain block at the output of the equalizer is expressed by

$$\tilde{S}_k^{(i)} = F_k^{(i)} Y_k - B_k^{(i)} \hat{S}_k^{(i-1)}, \tag{B.1}$$

where $F_k^{(i)}$ and $B_k^{(i)}$ are the feedforward and feedback coefficients from the DFE block, respectively. $\hat{S}_k^{(i-1)}$ corresponds to the DFT of the "hard-decision"of the time-domain data block $\hat{s}_n^{(i-1)}$ from the previous iteration, in relation to the transmitted time-domain block s_n.

One can assume an average overall channel frequency response denoted by $\gamma^{(i)}$ expressed by

$$\gamma^{(i)} = \frac{1}{N} \sum_{k=0}^{N-1} F_k^{(i)} H_k. \tag{B.2}$$

If the estimates of the transmitted block are reliable, the feedback filter can be employed to eliminate the residual ISI. The equalized samples related to each iteration, in the frequency-domain, are then given by

$$\tilde{S}_k^{(i)} = \gamma^{(i)} S_k + \varepsilon_k^{(i)}, \tag{B.3}$$

where $\varepsilon_k^{(i)}$ represents the global error consisting of the residual ISI plus the channel noise. The feedforward and feedback IB-DFE coefficients are chosen in order to maximize the SINR, as

$$\text{SINR} = \frac{\left|\gamma^{(i)}\right|^2 \mathbb{E}\left[|S_k|^2\right]}{\mathbb{E}\left[\left|\varepsilon_k^{(i)}\right|^2\right]}. \tag{B.4}$$

The DFE estimated frequency-domain data samples $\hat{S}_k^{(i)}$ can be expressed as

$$\hat{S}_k^{(i)} = \rho^{(i)} S_k + \Delta_k^{(i)}, \tag{B.5}$$

where ρ corresponds to a correlation coefficient and is defined as

$$\rho^{(i-1)} = \frac{\mathbb{E}\left[\hat{S}_k^{(i-1)} S_k^*\right]}{\mathbb{E}\left[|S_k|^2\right]} = \frac{\mathbb{E}\left[\hat{s}_n^{(i-1)} s_n^*\right]}{\mathbb{E}\left[|s_n|^2\right]}. \tag{B.6}$$

The maximization of the SINR corresponds to minimizing the error associated to ε_k. Therefore, the MSE on the received data samples can be defined as

$$\theta(k) = \frac{1}{N^2} \sum_{k=0}^{N-1} \theta_k, \tag{B.7}$$

where

$$\theta_k = \mathbb{E}\left[\left|\tilde{S}_k - \gamma S_k\right|^2\right] \tag{B.8}$$

corresponds to the MSE minimization for each k. Assuming that $\gamma^{(i)} = 1$ and taking equation B.5 into account, then the MSE, at a given iteration, can be written as

$$\begin{aligned}
\theta_k &= \mathbb{E}\left[\left(\tilde{S}_k - S_k\right)^* \left(\tilde{S}_k - S_k\right)\right] \\
&= \mathbb{E}\left[\left(F_k Y_k - B_k \hat{S}_k - S_k\right)^* \left(F_k Y_k - B_k \hat{S}_k - S_k\right)\right] \\
&= \mathbb{E}\left[\left(F_k Y_k - B_k \rho S_k + B_k \Delta_k - S_k\right)^* \left(F_k Y_k - B_k \rho S_k + B_k \Delta_k - S_k\right)\right],
\end{aligned} \tag{B.9}$$

where Δ_k denotes a zero-mean error term for the k^{th} frequency-domain hard decision estimate. Knowing that

$$\mathbb{E}\left[\Delta_k^{(i)}\right] = 0 \tag{B.10}$$

and

$$\mathbb{E}\left[\Delta_k S_{k'}^*\right] \approx 0 \tag{B.11}$$

for $k' \neq k$, then

$$\mathbb{E}\left[|\Delta_k|^2\right] \approx \left(1 - \rho^2 \mathbb{E}\left[|S_k|^2\right]\right). \tag{B.12}$$

Moreover, after a few mathematical straightforward manipulations, B.13 can be written as

$$\begin{aligned}
\theta_k = {} & F_k^* R_Y F_k - 2\mathrm{Re}\{F_k^* \rho R_{Y^* S} B_k\} - 2\mathrm{Re} F_k^* R_{Y^* S} \\
& + B_k^* |\rho|^2 R_S B_k + B_k^* R_{\Delta_k} B_k - 2\mathrm{Re}\{B_k^* \rho^* R_S\} + R_S,
\end{aligned} \tag{B.13}$$

where the different correlation matrices correspond to

$$R_y = |H_k|^2 R_S + R_N, \tag{B.14a}$$

$$R_{Y^* S} = H_k R_S, \tag{B.14b}$$

$$R_\Delta \approx \left(1 - \rho^2 \mathbb{E}\left[|S_k|^2\right]\right), \tag{B.14c}$$

with

$$R_S = 2\sigma_S^2, \tag{B.14d}$$

and

$$R_N = 2\sigma_N^2. \tag{B.14e}$$

The minimization of MSE leads to the optimum F_k and B_k coefficients, at each subcarrier θ_k. Defining the Lagrange function

$$J = \mathbb{E}\left[|\Theta_k|^2\right] + \lambda(\gamma - 1), \tag{B.15}$$

where λ corresponds to the Lagrange multipliers. Assuming the condition

$$\gamma = 1, \tag{B.16}$$

the optimum F_k and B_k coefficients are obtained by solving the system of equations

$$\begin{cases} \nabla_{F_k} J = 0 \\ \nabla_{B_k} J = 0 \\ \nabla_{\lambda} J = 0. \end{cases} \tag{B.17}$$

Knowing that the following rules can be applied

$$\nabla_x \left(x^H R x\right) = 2Rx \tag{B.18a}$$

$$\nabla_x \left(x^H p\right) = \nabla_x \left(p^T x^*\right) = 2p \tag{B.18b}$$

$$\nabla_x \left(p^H x\right) = \nabla_x \left(x^T p^*\right) = 0 \tag{B.18c}$$

$$\nabla_x \left(2\mathrm{Re}\{p^H x\}\right) = \nabla_x \left(p^H x + p^T x^*\right) = \nabla_x \left(\mathrm{Re}\{x^H p\}\right) = 2p, \tag{B.18d}$$

the optimum coefficients F_k and B_k are given by

$$F_k^{(i)} = \frac{\kappa^{(i)} H_k^*}{NSR + (1 - (\rho^{(i-1)})^2)\,|H_k|^2} \tag{B.19}$$

and

$$B_k^{(i)} = \rho^{(i-1)}(F_k^{(i)} H_k - \gamma^{(i)}), \tag{B.20}$$

respectively, where $\kappa^{(i)}$ is selected to ensure that $\gamma^{(i)} = 1$. Also,

$$NSR = \frac{1}{SNR} = \frac{\sigma_N^2}{\sigma_S^2}. \tag{B.21}$$

APPENDIX C

Minimum Mean Squared Error Analytical Computation: MIMO IB-DFE

This appendix explains all the mathematical manipulations regarding the MSE computation, for the p^{th} user and k^{th} frequency, of the estimated $\tilde{S}_{k,p}$ samples. The MSE is given by

$$MSE_{k,p} = \mathbb{E}\left[\left|\tilde{S}_{k,p} - S_{k,p}\right|^2\right] = \mathbb{E}\left[\left|\mathbf{F}_k^T\mathbf{Y}_k - \mathbf{B}_k^T\bar{\mathbf{S}}_k - \mathbf{S}_k\right|^2\right]. \tag{C.1}$$

Moreover, for a given iteration i

$$\bar{\mathbf{S}}_k^{(i-1)} \simeq \mathbf{P}^{(i-1)}\hat{\mathbf{S}}_k^{(i-1)}, \tag{C.2}$$

where

$$\mathbf{P}^{(i-1)} = \text{diag}\left(\rho_1^{(i-1)}, ..., \rho_P^{(i-1)}\right), \tag{C.3}$$

with the correlation coefficient defined as

$$\rho^{(i-1)} = \frac{\mathbb{E}\left[\hat{S}_k^{(i-1)}S_k^*\right]}{\mathbb{E}\left[\left|S_k\right|^2\right]} = \frac{\mathbb{E}\left[\hat{s}_n^{(i-1)}s_n^*\right]}{\mathbb{E}\left[\left|s_n\right|^2\right]}. \tag{C.4}$$

In (C.2), $\hat{\mathbf{S}}_k^{(i-1)}$ corresponds to

$$\hat{\mathbf{S}}_k^{(i-1)} \approx \mathbf{P}^{(i-1)}\mathbf{S}_k + \mathbf{\Delta}_k, \tag{C.5}$$

where

$$\mathbf{\Delta}_k = \left[\Delta_{k,1}, ..., \Delta_{k,P}\right]^T \tag{C.6}$$

has a zero mean and is uncorrelated with $\mathbf{P}^{(i-1)}$.

Knowing that the definition of the expected value can be written as

$$\mathbb{E}\left[\left|\tilde{S}_{k,p}\right|^2\right] = \mathbb{E}\left[\left|\tilde{S}_{k,p}\tilde{S}_{k,p}^*\right|^2\right] \tag{C.7}$$

and that the following matrix manipulations are possible

$$a^T b = b^T a, \tag{C.8}$$

$$a^H b = b^T a^* \tag{C.9}$$

and

$$a^H = (a^*)^T, \tag{C.10}$$

then the MSE can be written as

$$MSE_{k,p} = \mathbb{E}\left[\left(\mathbf{F}^H\mathbf{Y}^* - \mathbf{B}^H\bar{\mathbf{S}}^*\right)\left(\mathbf{Y}^T\mathbf{F} - \bar{\mathbf{S}}^T\mathbf{B} - S_p\right)\right]. \tag{C.11}$$

For simplicity purposes the dependence on the k^{th} carrier index was dropped in the previous definitions.

One can notice that

$$\sigma_S^2 = \mathbb{E}\left[|S_p|^2\right], \tag{C.12a}$$

$$\sigma_N^2 = \mathbb{E}\left[|N|^2\right], \tag{C.12b}$$

$$\mathbf{R}_S = \mathbb{E}\left[\mathbf{S}^*\mathbf{S}^T\right] = \sigma_S^2\mathbf{I}_P, \tag{C.12c}$$

$$\mathbf{R}_N = \mathbb{E}\left[\mathbf{N}^*\mathbf{N}^T\right] = \sigma_N^2\mathbf{I}_R, \tag{C.12d}$$

$$\mathbf{R}_Y = \mathbb{E}\left[\mathbf{Y}^*\mathbf{Y}^T\right] = \mathbf{H}^H\mathbf{R}_S\mathbf{H} + \mathbf{R}_N, \tag{C.12e}$$

$$\mathbf{R}_{\bar{\mathbf{S}}} = \mathbb{E}\left[\bar{\mathbf{S}}^*\bar{\mathbf{S}}^T\right] = \mathbf{P}^2\mathbf{R}_S, \tag{C.12f}$$

$$\mathbf{R}_{\bar{\mathbf{S}},\mathbf{Y}} = \mathbb{E}\left[\bar{\mathbf{S}}^*\mathbf{Y}^T\right] = \mathbf{P}^2\mathbf{R}_S\mathbf{H}, \tag{C.12g}$$

$$\mathbf{R}_{\mathbf{Y},S_p} = \mathbb{E}\left[\mathbf{Y}^*S_p\right] = \mathbf{H}^H\mathbf{R}_S\mathbf{e}_p, \tag{C.12h}$$

$$\mathbf{R}_{\bar{\mathbf{S}},S_p} = \mathbb{E}\left[\bar{\mathbf{S}}^*S_p\right] = \mathbf{P}^2\mathbf{R}_S\mathbf{e}_p, \tag{C.12i}$$

where σ_S^2 and σ_N^2 denote the symbol and noise variances, respectively. $\mathbf{I}_P$ is a $P \times P$ identity matrix and $\mathbf{e}_p$ is a column vector of size P with 0 in all positions except the p^{th} position that is 1. Hence,

$$\begin{aligned} MSE_{k,p} = \mathbf{F}^H\mathbf{R}_Y\mathbf{F} + \mathbf{B}^H\mathbf{P}^2\mathbf{R}_S\mathbf{B} + \sigma_S^2 - \mathbf{B}^H\mathbb{E}\left[\bar{\mathbf{S}}^*\mathbf{Y}^T\right]\mathbf{F} - \mathbf{F}^H\mathbb{E}\left[\mathbf{Y}^*\bar{\mathbf{S}}^T\right]\mathbf{B} - \\ -\mathbf{F}^H\mathbb{E}\left[\mathbf{Y}^*S_p\right] - \mathbf{F}^T\mathbb{E}\left[\mathbf{Y}S_p^*\right] - \mathbf{B}^H\mathbb{E}\left[\bar{\mathbf{S}}^*S_p\right] - \mathbf{B}^T\mathbb{E}\left[\bar{\mathbf{S}}S_p^*\right], \end{aligned} \tag{C.13}$$

which can be rearranged to

$$\begin{aligned} MSE_{k,p} = \mathbf{F}^H\mathbf{R}_Y\mathbf{F} + \mathbf{B}^H\mathbf{P}^2\mathbf{R}_S\mathbf{B} + \sigma_S^2 - \\ -2\mathrm{Re}\{\mathbf{F}^H\mathbb{E}\left[\mathbf{Y}^*S_p\right]\} + 2\mathrm{Re}\{\mathbf{B}^H\mathbb{E}\left[\bar{\mathbf{S}}^*S_p\right]\} - \\ -2\mathrm{Re}\{\mathbf{B}^H\mathbb{E}\left[\bar{\mathbf{S}}^*\mathbf{Y}^T\right]\mathbf{F}\}, \end{aligned} \tag{C.14}$$

since

$$\mathrm{Re}\{a^H b\} = \mathrm{Re}\{b^T a^*\} = \mathrm{Re}\{b^H a\} \tag{C.15a}$$

and

$$\mathrm{Re}\{a^*\} = \mathrm{Re}\{a\}. \tag{C.15b}$$

Ultimately, the MSE can be written as

$$\begin{aligned} MSE_{k,p} = \mathbf{F}^H \mathbf{R}_Y \mathbf{F} + \mathbf{B}^H \mathbf{R}_{\bar{\mathbf{S}}\bar{\mathbf{S}}} \mathbf{B} + \mathbf{R}_S - 2\mathrm{Re}\{\mathbf{F}^H \mathbf{R}_{\mathbf{Y}S_p}\} + \\ + 2\mathrm{Re}\{\mathbf{B}^H \mathbf{R}_{\bar{\mathbf{S}}S_p}\} - 2\mathrm{Re}\{\mathbf{B}^H \mathbf{R}_{\bar{\mathbf{S}}Y} \mathbf{F}\}. \end{aligned} \tag{C.16}$$

The minimization of the mean squared error is possible with the knowledge of the following rules for the gradient of matrix products

$$\nabla_x \left(x^H R x \right) = 2Rx \tag{C.17a}$$

$$\nabla_x \left(x^H p \right) = \nabla_x \left(p^T x^* \right) = 2p \tag{C.17b}$$

$$\nabla_x \left(p^H x \right) = \nabla_x \left(x^T p^* \right) = 0 \tag{C.17c}$$

$$\nabla_x \left(2\mathrm{Re}\{p^H x\} \right) = \nabla_x \left(p^H x + p^T x^* \right) = \nabla_x \left(\mathrm{Re}\{x^H p\} \right) = 2p. \tag{C.17d}$$

The minimization of the MSE provides the optimum $\mathbf{F}_{k,p}$ and $\mathbf{B}_{k,p}$ coefficients at each subcarrier $\Theta_{k,p}$. Defining the Lagrange function

$$J = \mathbb{E}\left[\left| \Theta_{k,p} \right|^2 \right] + \lambda_p \left(\gamma_p - 1 \right), \tag{C.18}$$

where $\{\lambda_p; p = 1, ..., P\}$ corresponds to the Lagrange multipliers and assuming the condition

$$\gamma_p = \frac{1}{N} \sum_{k=0}^{N-1} \sum_{r=1}^{R} F_{k,p}^{(r)} H_{k,p}^{eq(r)} = 1, \tag{C.19}$$

the optimum coefficients $\mathbf{F}_k$ and $\mathbf{B}_k$ can be obtained by solving the system of equations

$$\begin{cases} \nabla_{\mathbf{F}} J = 0 \\ \nabla_{\mathbf{B}} J = 0 \\ \nabla_{\lambda} J = 0. \end{cases} \tag{C.20}$$

Therefore, the optimum coefficients are given by

$$\mathbf{F} = \kappa \mathbf{\Lambda} \mathbf{H}^H \mathbf{e}_p \tag{C.21}$$

and

$$\mathbf{B} = \mathbf{H}\mathbf{F} - \mathbf{e}_p, \tag{C.22}$$

with

$$\mathbf{\Lambda} = \left(\mathbf{H}^H \left(\mathbf{I}_P - \mathbf{P}^2 \right) \mathbf{H} + \frac{1}{SNR} \mathbf{I}_R \right)^{-1}, \tag{C.23}$$

κ is selected to ensure that $\gamma_p = 1$, in order to have a normalized FDE with $\mathbb{E}\left[\tilde{s}_{n,p}\right] = s_{n,p}$.

Bibliography

[1] J. Proakis and M. Salehi, *Digital Communications*, 5th. Mc-Graw Hill, 2007.

[2] M. Dohler, R. Heath, A. Lozano, C. Papadias, and R. Valenzuela, "Is the PHY Layer Dead?", *IEEE, Communications Magazine*, vol. 49, no. 4, pp. 159 –165, 2011.

[3] D. Falconer, S. Ariyavisitakul, A. Benyamin-Seeyar, and B. Eidson, "Frequency Domain Equalization for Single-Carrier Broadband Wireless Systems", *IEEE, Communications Magazine*, vol. 40, no. 4, pp. 58–66, 2002.

[4] J. Cimini L., "Analysis and Simulation of a Digital Mobile Channel Using Orthogonal Frequency Division Multiplexing", *IEEE Transactions on, Communications*, vol. 33, no. 7, pp. 665 –675, 1985.

[5] N. Benvenuto, R. Dinis, D. Falconer, and S. Tomasin, "Single Carrier Modulation With Nonlinear Frequency Domain Equalization: An Idea Whose Time Has Come Again", *Proceedings of the IEEE*, vol. 98, no. 1, pp. 69 –96, 2010.

[6] A. Gusmão, R. Dinis, J. Conceicão, and N. Esteves, "Comparison of Two Modulation Choices for Broadband Wireless Communications", in *Vehicular Technology Conference Proceedings, 2000. VTC 2000-Spring Tokyo. 2000 IEEE 51st*, vol. 2, 2000, 1300 –1305 vol.2.

[7] R. Dinis, A. Gusmão, and N. Esteves, "On Broadband Block Transmission over Strongly Frequency-Selective Fading Channels", in *Proc. Wireless*, 2003.

[8] N. Benvenuto and S. Tomasin, "Block Iterative DFE for Single Carrier Modulation", *Electronics Letters*, vol. 38, no. 19, pp. 1144 –1145, 2002.

[9] C.-X. Wang, F. Haider, X. Gao, X.-H. You, Y. Yang, D. Yuan, H. Aggoune, H. Haas, S. Fletcher, and E. Hepsaydir, "Cellular Architecture and Key Technologies for 5G Wireless Communication Networks", *Communications Magazine, IEEE*, vol. 52, no. 2, pp. 122–130, 2014.

[10] F. C. Ribeiro, R. Dinis, F. Cercas, and A. Silva, "Receiver Design for the Uplink of Base Station Cooperation Systems employing SC-FDE Modulations", *EURASIP Journal on Wireless Communications and Networking*, vol. 2015, no. 1, 2015.

[11] F. Ribeiro, R. Dinis, F. Cercas, and A. Silva, "On the Theoretical BER Performance of SC-FDE Schemes with IB-DFE Receivers", in *IEEE Vehicular Technology Conf. - VTC-Spring*, vol. 1, 2015, pp. 1–5.

[12] F. C. Ribeiro, R. Dinis, F. Cercas, and A. Silva, "Improved BER Performance Evaluation of Base Station Cooperation Systems Employing SC-FDE Modulation with IB-DFE Receivers", in *IASTED International Conf. on Modelling, Identification and Control - MIC*, vol. 1, 2015, pp. 1–8.

[13] F. C. Ribeiro, J. Guerreiro, R. Dinis, F. Cercas, and A. Silva, "Robust Receivers for Base Station Cooperation Systems", *Digital Signal Processing*, vol. 64, pp. 8 –16, 2017, ISSN: 1051-2004.

[14] J. Guerreiro, F. Ribeiro, and R. Dinis, "An Accurate Low Complexity Method for Studying Quantization Effects in Base Station Cooperation Systems", in *IEEE Vehicular Technology Conf. - VTC-Fall*, vol. 1, 2015, pp. 1–5.

[15] F. Ribeiro, J. Guerreiro, R. Dinis, F. Cercas, and A. Silva, "On the Design of Robust Multi-User Receivers for Base Station Cooperation Systems", in *IEEE Vehicular Technology Conf. - VTC-Fall*, vol. 1, 2016, pp. 1–7.

[16] F. C. Ribeiro, R. Dinis, F. Cercas, and A. Silva, "Multiuser Detection for the Uplink of Clustered 5G Systems with Universal Frequency Reuse", *Physical Communication*, vol. 23, pp. 29 –36, 2017, ISSN: 1874-4907.

[17] F. C. Ribeiro, R. Dinis, F. Cercas, and A. Silva, "Clustered Multiuser Detection for the Uplink of 5G Systems", in *IEEE Vehicular Technology Conf. - VTC-Spring*, vol. 1, 2016, pp. 1–5.

[18] F. Ribeiro, R. Dinis, F. Cercas, and A. Silva, "Efficient Clustered Detection for the Uplink of Cellular Systems with Universal Frequency Reuse", in *International Conf. for Telecommunication and Multi-Media(TEMU),*, vol. 1, 2016, pp. 1–6.

[19] M. Haenggi and R. K. Ganti, "Interference in Large Wireless Networks", *Found. Trends Netw.*, vol. 3, no. 2, pp. 127–248, Feb. 2009, ISSN: 1554-057X.

[20] X. Yang and A. P. Petropulu, "Co-channel Interference Modeling and Analysis in a Poisson Field of Interferers in Wireless Communications", in *Classical, Semi-classical and Quantum Noise*, L. Cohen, H. V. Poor, and M. O. Scully, Eds. Boston, MA: Springer US, 2012, pp. 271–282.

[21] T. Rappaport, *Wireless Communications: Principles and Practice*, 2nd. Upper Saddle River, NJ, USA: Prentice Hall PTR, 2001, ISBN: 0130422320.

[22] B. Sklar and C. E. Services, "Rayleigh Fading Channels in Mobile Digital Communication Systems Part I: Characterization", *IEEE Communications Magazine*, pp. 90–100, 1997.

[23] A. Goldsmith, *Wireless Communications*. New York, NY, USA: Cambridge University Press, 2005, ISBN: 0521837162.

[24] D. Gesbert, M. Shafi, D. shan Shiu, P. J. Smith, and A. Naguib, "From Theory to Practice: An Overview of MIMO Space-Time Coded Wireless Systems", *IEEE Journal on Selected Areas in Communications*, vol. 21, no. 3, pp. 281–302, 2003.

[25] A. J. Viterbi, *CDMA: Principles of Spread Spectrum Communication*. Redwood City, CA, USA: Addison Wesley Longman Publishing Co., Inc., 1995, ISBN: 0-201-63374-4.

[26] G. Kramer, I. Marić, and R. D. Yates, "Cooperative Communications", *Foundations and Trends in Networking*, vol. 1, no. 3-4, pp. 271–425, 2007, ISSN: 1554-057X.

[27] D. Gesbert, S. G. Kiani, A. Gjendemsjo, and G. E. Oien, "Adaptation, Coordination, and Distributed Resource Allocation in Interference-Limited Wireless Networks", *Proceedings of the IEEE*, vol. 95, no. 12, pp. 2393–2409, 2007.

[28] R. Zakhour, Z. K. M. Ho, and D. Gesbert, "Distributed Beamforming Coordination in Multicell MIMO Channels", in *VTC Spring 2009 - IEEE 69th Vehicular Technology Conference*, 2009, pp. 1–5.

[29] H. Dahrouj and W. Yu, "Coordinated Beamforming for the Multicell Multi-Antenna Wireless System", *IEEE Transactions on Wireless Communications*, vol. 9, no. 5, pp. 1748–1759, 2010.

[30] L. Cimini, "Analysis and Simulation of a Digital Mobile Channel Using Orthogonal Frequency Division Multiplexing", *Communications, IEEE Transactions on*, vol. 33, no. 7, pp. 665–675, 1985.

[31] H. Sari, G. Karam, and I. Jeanclaude, "An analysis of orthogonal frequency-division multiplexing for mobile radio applications", in *Vehicular Technology Conference, 1994 IEEE 44th*, 1994, 1635–1639 vol.3.

[32] O. Somekh, B. Zaidel, and S. Shamai, "Sum Rate Characterization of Joint Multiple Cell-Site Processing", *IEEE Transactions on, Information Theory*, vol. 53, no. 12, pp. 4473 –4497, 2007.

[33] E. Bjo Andrnson, R. Zakhour, D. Gesbert, and B. Ottersten, "Cooperative Multicell Precoding: Rate Region Characterization and Distributed Strategies With Instantaneous and Statistical CSI", *IEEE Transactions on, Signal Processing*, vol. 58, no. 8, pp. 4298–4310, 2010.

[34] R. Gray and D. Neuhoff, "Quantization", *Information Theory, IEEE Transactions on*, vol. 44, no. 6, pp. 2325–2383, 1998.

[35] W. Stallings, "Digital Signaling Techniques", *Communications Magazine, IEEE*, vol. 22, no. 12, pp. 21–25, 1984.

[36] B. Widrow, I. Kollar, and M.-C. Liu, "Statistical Theory of Quantization", *Instrumentation and Measurement, IEEE Transactions on*, vol. 45, no. 2, pp. 353–361, 1996.

[37] C. Shannon, "Communication in the Presence of Noise", *Proceedings of the IRE*, vol. 37, no. 1, pp. 10–21, 1949.

[38] H. E. Rowe, "Memoryless nonlinearities with gaussian inputs: elementary results", *The Bell System Technical Journal*, vol. 61, no. 7, pp. 1519–1525, 1982.

[39] J. J. Bussgang, "Crosscorrelation functions of amplitude-distorted gaussian signals", 1952.

[40] T. Araujo and R. Dinis, "Performance Evaluation of Quantization Effects on Multicarrier Modulated Signals", *IEEE Transactions on, Vehicular Technology*, vol. 56, no. 5, pp. 2922–2930, 2007.

[41] P. M. João Guerreiro Rui Dinis, "Use of equivalent nonlinearities for studying quantisation effects on sampled multicarrier signals", *Electronics Letters*, vol. 51, 151–153(2), 2015.

[42] E. Larsson, O. Edfors, F. Tufvesson, and T. Marzetta, "Massive MIMO for Next Generation Wireless Systems", *Communications Magazine, IEEE*, vol. 52, no. 2, pp. 186–195, 2014.

[43] K. Balachandran, J. H. Kang, K. Karakayali, and K. M. Rege, "NICE: A Network Interference Cancellation Engine for Opportunistic Uplink Cooperation in Wireless Networks", *IEEE Transactions on Wireless Communications*, vol. 10, no. 2, pp. 540–549, 2011.

[44] K. Maruta, A. Ohta, M. Iizuka, and T. Sugiyama, "Iterative Inter-Cluster Interference Cancellation for Cooperative Base Station Systems", in *Vehicular Technology Conference (VTC Spring), 2012 IEEE 75th*, 2012, pp. 1–5.

[45] K. Balachandran, J. H. Kang, M. K. Karakayali, and K. M. Rege, "Base Station Cooperation with Non-Ideal Backhaul and Non-Full Buffer Traffic", in *2014 IEEE 80th Vehicular Technology Conference (VTC2014-Fall)*, 2014, pp. 1–5.

[46] V. R. Cadambe and S. A. Jafar, "Interference Alignment and Degrees of Freedom of the K-User Interference Channel", *IEEE Transactions on Information Theory*, vol. 54, no. 8, pp. 3425–3441, 2008.